Extending the CRISPR-Cas9-based imaging toolbox to improve the detection of chromosomal DNA

Dissertation

zur Erlangung des

Doktorgrades der Naturwissenschaften (Dr. rer. nat.)

der

Naturwissenschaftlichen Fakultät III

Agrar- und Ernährungswissenschaften,

Geowissenschaften und Informatik

Martin-Luther-Universität Halle-Wittenberg

vorgelegt von

Herr Bhanu Prakash Potlapalli

geboren am 26.05.1993 in Tanikella, India

Gutachter:

1. Prof. Dr. Andreas Houben
2. Prof. Dr. Tony Heitkam

Acknowledgment

Table of Contents

Abbreviations

ANOVA	One-way analysis of variance
AP	Alkaline phosphatase
BSA	Bovine serum albumin
CASFISH	Cas9-mediated fluorescence in situ hybridization
CCD	Cooled charge-coupled device
CCD	chromatin contact domains
CMP	Chromatin-modulating peptides
COMBO-FISH	Combinatorial Oligonucleotide Fluorescence in situ Hybridization
CRISPR	Clustered Regularly Interspaced Palindromic Repeats
CRISPR-CID	CRISPR-Cas9 mediated chromogenic *in situ* detection
CRISPR-FISH	CRISPR-Cas9-based *in situ* labeling
crRNA	CRISPR RNA
CTD	C-terminal domain
DAPI	4',6-diamidino-2-phenylindole
DBS	Double-strand breaks
dCas9	Dead Cas9
eGFP	Enhanced GFP
EM	Electron microscope
EMISH	Electron microscope with *in situ* hybridization
fCRISPR	fluorogenic CRISPR
FISH	Fluorescence *in situ* hybridization
FRET	Fluorescence Resonance Energy Transfer
FROS	Fluorescent repressor operator system
GCN4	General control nonderepressible 4 peptides
GFP	Green fluorescent proteins
GISH	Genomic in situ hybridization
GMO	Genetically modified organism
GOLD-FISH	Genome oligopaint via local denaturation fluorescence in situ hybridization
gRNA	Guide RNA
HBC	4-((2-hydroxyethyl) (methyl)amino)-benzylidene)-cyanophenyl-acetonitrile
HDR	Homology-directed repair
HRP	Horseradish peroxidase
IgG	Immunoglobulin G

IPTG	Isopropyl-β-D-1-thiogalactopyranoside
ISH	*In situ* hybridization
MCP	MS2 coat protein
NHEJ	Nonhomologous end joining
NLS	Nuclear localization signals
NUC	Nuclease domain
PAM	Proximal adjacent motif
PBS	Phosphate-buffered saline
PER	Primer exchange reaction
POI	Protein of interest
QD	Quantum dots
RASER-FISH	Resolution After Single-Strand Exonuclease Resection
REC	Recognition domain
RGEN-ISL	RNA-guided endonuclease - *in situ* labelling
RNP	Ribonucleoprotein
RPM	Revolutions per minute
RT	Room temperature
RVD	Repeat variable di-residue
Sa. Cas9	*Staphylococcus aureus Cas9*
scFv	Single-chain variable antibody fragments
sdAb	Single-domain antibody
SEM	Scanning electron microscopy
sgRNA	Single guide RNA
Sp. Cas9	*Streptococcus pyogenes* Cas9
SSC	Saline-sodium citrate
TAD	topologically associated domains
TALE	Transcription activator-like effector
TEM	Transmission electron microscopy
TMB	3,3',5,5'-Tetramethylbenzidine
tracrRNA	trans-activating crRNA
TRB1	Telomeric repeat binding protein
TSA	Tyramide signal amplification
Tyr-FISH	Tyramide- Fluorescence *in situ* hybridization
ZFP	Zinc finger proteins
3D	three-dimensional

1. Introduction

1.1 Chromatin organization

In eukaryotic cells, genomic DNA undergoes extensive folding facilitated by histones and non-histone proteins, forming intricate three-dimensional (3D) chromatin structures in the nucleus. The primary role of chromatin is to condense long DNA molecules into compact, denser structures, playing a pivotal role in all DNA-dependent transactions such as gene transcription (LI *et al.* 2012), DNA replication (POPE *et al.* 2014), repair and recombination (VERGARA AND GUTIERREZ 2017) across various developmental stages. The fundamental building block of chromatin organization is the nucleosome, where approximately 147 base pairs of nucleotides are wound around an octamer of histone proteins (LUGER *et al.* 1997; LI *et al.* 2002). The linear arrangement of nucleosomes is further compacted into more condensed chromatin fibers. These fibers then fold to create chromatin loops, which contribute to the formation of chromatin domains or topologically associated domains (TAD). These domains exhibit a tendency to organize into more complex higher-order chromatin compartments (MISTELI 2020). In interphase nuclei, this level of chromatin organization is evident through the separate positioning of heterochromatin and euchromatin.

Heterochromatin is characterized by its intense staining and compacted structure in interphase nuclei. These regions are repeat-rich and lacking in genes and transcriptionally silent, and tend to align towards the nuclear periphery (AVRAMOVA 2002; DE NOOIJER *et al.* 2009). In contrast, euchromatin is gene-rich, transcriptionally active, and located in the interior of the nucleus (DE NOOIJER *et al.* 2009). Initially, heterochromatin is categorized into two classes, constitutive and facultative heterochromatin (BROWN 1966). Constitutive heterochromatin includes satellite DNA such as centromeric repeats, whereas facultative heterochromatin exhibits variability in its state across different cell types (FRANSZ *et al.* 2002).

During the interphase, chromatin adopts a structurally loose configuration, facilitating access for RNA and DNA polymerase during DNA replication. Chromosomes, the primary units of genome organization, are organized into distinct territories during interphase, and this arrangement is non-randomly termed chromosome territories (SEXTON AND CAVALLI 2015; MISTELI 2020). This organization strategically places gene-poor chromosomes predominantly in the heterochromatin-rich periphery, while gene-rich regions occupy the euchromatic interior. Additionally, there is an observed correlation between the transcriptional activity of

specific genes and their nuclear positioning (PERIC-HUPKES *et al.* 2010). On the other hand, epigenetic marks play a crucial role in modifying the chromatin environment during development through various histone modifications (LI *et al.* 2002). This dynamic organization of 3D chromatin has sparked interest in studying its dynamic nature.

Two general approaches have been developed and applied to investigate the detailed structures of the 3D genome organization: sequencing-based mapping and microscopy-based imaging. Conventional methods for 3D genome mapping, such as Hi-C (LIEBERMAN-AIDEN *et al.* 2009; FENG *et al.* 2014) and ChIA-PET (DEKKER *et al.* 2013), identify pairwise long-range chromatin interactions through chromatin proximity ligation. This is succeeded by high-throughput sequencing and mapping to the reference genome, enabling the inference of long-range chromatin contacts and the reconstruction of the 3D configuration of the genome. Nevertheless, 3D genome mapping data, derived often from millions of cells, offer an average perspective of genome folding (GIORGETTI AND HEARD 2016). These techniques reveal smaller subunits of chromosome territories, topologically associated domains (TADs) and chromatin contact domains (CCDs). Despite providing clear contact probabilities, the mapping data lack a defined physical scale, such as in micrometers and nanometers. To address these limitations, *in situ* hybridization techniques can be utilized to observe the physical genome architecture at diverse spatiotemporal resolutions within individual nuclei or chromosomes using microscopy. This approach employs different DNA staining methods, offering a metric scale (KUBALOVÁ *et al.* 2023).

1.2 *In situ* hybridization (ISH)

In situ hybridization (ISH) stands as a versatile molecular cytogenetics tool, revolutionizing traditional cytogenetic methods by allowing the precise localization of specific genes or DNA sequences within cells and tissues during cytological preparations. In 1969, *in situ* hybridization (ISH) was first introduced to identify ribosomal genes in *Xenopus* toad oocytes (GALL AND PARDUE 1969) and HeLa cells (JOHN *et al.* 1969). In the ISH method, the genomic DNA needs to be denatured, and a labeled complementary single-stranded DNA/RNA probe is used to hybridize to specific genomic sequences visualized by light microscope (JIANG AND GILL 2006). Isotopic probes were successfully used to label the repetitive DNA sequences in various plant species (BEDBROOK *et al.* 1980; DENNIS *et al.* 1980; HUTCHINSON *et al.* 1981), providing crucial insights into the origin and evolution of repeated DNAs within cereal species genomes

(RAYBURN AND GILL 1985). ISH precisely locates DNA sequences, correlating physical location and DNA composition with sequence data. This technique maps targeted DNA sequences, providing insights into the distribution of repetitive, low copy, and single-copy sequences. Overall, ISH offers valuable information about genome organization and the spatial distribution of genomic sequences on both interphase and metaphase chromosomes. This pioneering technique initially used the sensitive radioactive probes for detecting the target DNA sequences and later hybridization sites are observed by autoradiography with X-ray film or liquid emulsion. This isotopic probe comes with limitations, including restricted resolution due to the emitted isotopic signal captured by an emulsion layer. Additionally, scoring and statistically analyzing silver grains on numerous metaphase cells are required (JIANG AND GILL 1994). The autoradiographic procedure for detecting hybridization sites demands an extended exposure time, often spanning several weeks or months, despite its short half-life (JOHN *et al.* 1969). Furthermore, the method involves exposure to radiation, posing biohazard risks (JIN AND LLOYD 1997).

To overcome these drawbacks, a series of non-isotopic-based ISH techniques using immunological methods were developed. This technique utilizes light or fluorescence microscopes to investigate the target DNA sequences. Initially, Rudkin and Stollar (1977) reported on labeling ribosomal RNA sequences on *Drosophila* polytene chromosomes, employing rabbit anti-hybrid antiserum against a poly(rA)-poly(dT) for detecting RNA-DNA hybrids, with hybridization sites detected using rhodamine-conjugated anti-rabbit Immunoglobulin G (IgG) and visualized with a fluorescence microscopy. In another approach, biotin-labeled DNA probes prepared via nick translation were used to label repetitive sequences on *Drosophila* polytene chromosomes (LANGER-SAFER *et al.* 1982) and mouse chromosomes (MANUELIDIS *et al.* 1982), as well as mRNA in chicken muscle tissues (SINGER AND WARD 1982). These methods use biotin-labeled DNA probes for hybridization with target DNA on cytological preparations. Detection involves rabbit anti-biotin antibodies. Later, the hybridization sites were detected either by fluorometrically using fluorescein labeled antibodies or by cytochemically with horseradish peroxidase-labeled goat anti-rabbit IgG antibodies. This biotin-labeled probes provided a superior resolution and lower background interference compared to conventional ISH using isotope labeling and autoradiography. A similar technique was employed to label repetitive sequences on metaphase chromosomes of wheat, employing enzymatic reporter molecules such as horseradish peroxidase or alkaline

phosphatase conjugated streptavidin (RAYBURN AND GILL 1985). On the other hand, digoxygenin-labeled DNA probes were used in combination with antibodies carrying fluorescent or enzymatic tags to detect the target DNA sequences. Moreover, similar indirect approaches were used for simultaneous labeling of double (HOPMAN *et al.* 1986) and triple (NEDERLOF *et al.* 1989) target DNA sequences in different species. Enzymatic detection methods have advantages over fluorescence methods, allowing for prolonged reactions to amplify signals without signal fading. However, these methods require indirect detection of the labeled DNA / RNA probes.

1.3   Fluorescence *in situ* hybridization (FISH)

The development of chemically modified nucleic acids capable of incorporating fluorophores or haptens, such as biotin or digoxigenin has played a crucial role in advancing *fluorescence in situ* hybridization (FISH) techniques. These haptens can be effectively detected through the use of fluorophore-labeled reporters linked to streptavidin or anti-digoxigenin molecules. Fluorescence *in situ* hybridization (FISH), employing fluorochromes for detection, is applicable for identifying target DNA sequences in both interphase nuclei and metaphase chromosomes. Initially, Bauman et al. (1980) pioneered the use of a 3'-end fluorochrome-labeled RNA probe to tag DNA sequences in human tissues and *Drosophila*. Subsequently, Pinkel et al. (1986) introduced an alternative approach involving biotin-labeled DNA probes for chromosome classification and the detection of chromosome aberrations through indirect FISH methods. Over time, researchers advanced the technique further by employing multi-color labeling, using differently colored DNA probes to tag various DNA sequences in both human and plant species, reviewed by Jiang and Gill (1994). Furthermore, recent advancements in sequencing technology and DNA sequence synthesis infrastructure have spurred the development of oligo FISH. This technique entails the computational design of oligo probes specific to target single copy DNA, directly labeled with fluorophores and haptens, simplifying the probe preparation process. Numerous studies have been reported in plants for labeling target DNA, and even entire chromosomes, as reviewed by Harun et al. (2023).

1.3.1　Principle of the FISH method

FISH involves the use of a microscopic slide onto which fixed interphase nuclei or metaphase chromosomes are attached, along with a labeled DNA probe. The probe can be directly labeled with a fluorochrome or with a hapten-like biotin. Subsequently, both the sample and the probe are denatured to render them single-stranded, a necessary step for FISH that facilitates the probe's access to the target DNA. The sample and probe DNA are then hybridized together on the slide and incubated at a lower temperature, typically around 37 °C. This temperature facilitates the binding of the probe to complementary DNA strands. Following hybridization, multiple washing steps are carried out to remove excess probes and reduce background noise. Finally, the signal from the probe DNA is examined using fluorescence microscopy. The FISH methodology is depicted in Figure 1.
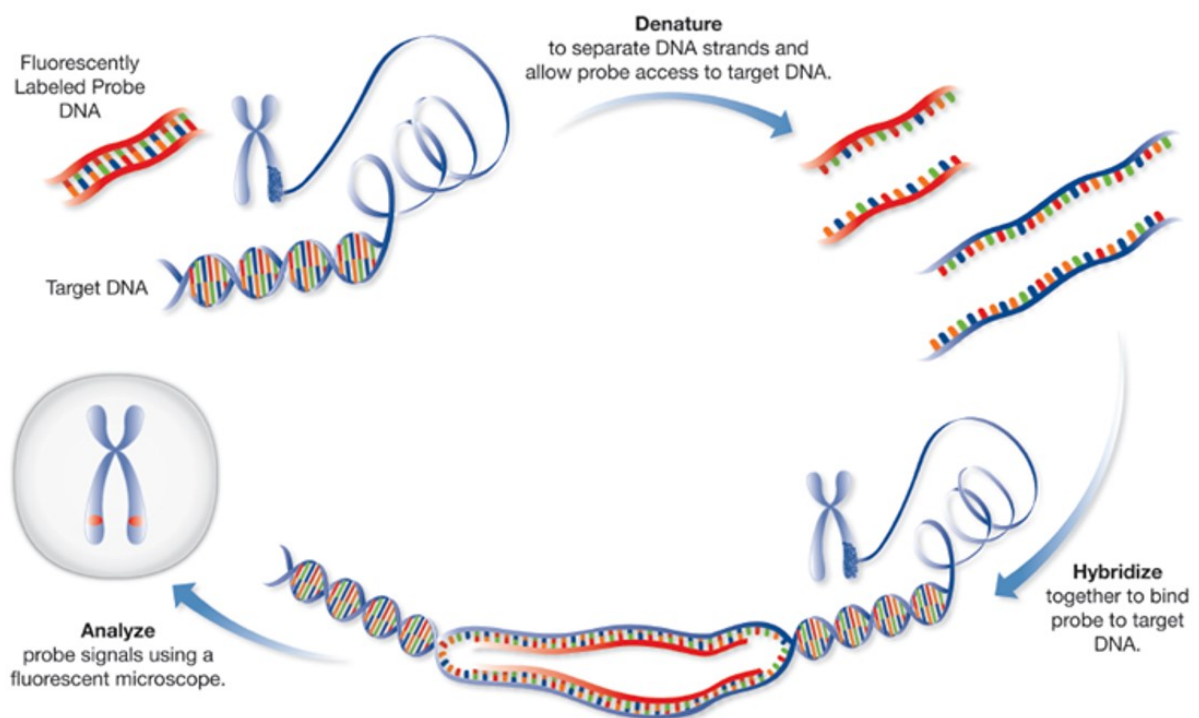
Fig 1: Schematic showing the FISH procedure. FISH utilizes fluorescently labeled complementary DNA sequences as probes. Initially, both genomic and probe DNA are denatured to render them single-stranded. Subsequently, they are hybridized together at a lower temperature to allow the probe to bind to the target DNA. Finally, using a fluorescence microscope, the probe DNA can be visualized. Figure modified from www.ogt.com.

1.3.2 Other FISH techniques

Additionally, numerous other techniques have been developed for various applications, employing similar FISH techniques. One such technique is genomic *in situ* hybridization (GISH). In contrast to FISH, which utilizes target-specific probes, GISH employs total genomic DNA from a specific species as a probe, and unlabeled DNA from other species as a blocking DNA, enabling the molecular-level distinction of foreign chromatin in interspecific hybrids. Initially developed by Schwarzacher et al. (1989) in plants, later many researchers used this technique to identify the parental genomes in natural allopolyploid species, reviewed by Silva and Souza (2013). On the other hand, the sensitivity of FISH has been increased significantly (10-100 times) by utilizing the signal amplification method called Tyramide-FISH (Tyr-FISH). In Tyr-FISH, a hapten-labeled oligo is employed as a probe and then detected using peroxidase-conjugated streptavidin or avidin. Horseradish peroxidase (HRP) facilitates the deposition of multiple fluorochrome- or biotin-labeled tyramide molecules near a target nucleic acid sequence *in situ* (RAAP *et al.* 1995). This approach has been successfully applied in plants to identify DNA fragments that are less than 1 kb in size (JIANG AND GILL 2006). Similarly, FISH techniques for labeling DNA on stretched DNA fibers and chromosomes, as well as immuno-FISH for combining immunoassaying and FISH, have been developed and successfully utilized in plant science, reviewed by Jiang and Gill (2006). These techniques have been successfully employed for chromosome identification, karyotyping, phylogenetic analysis, chromosome-specific painting, and physical mapping in both plants and humans, reviewed by Jiang and Gill (2006). Furthermore, they are utilized for diagnostic approaches to detect chromosomal abnormalities and identify infectious diseases, reviewed by Cui et al. (2016).

1.3.3 The major drawback of standard FISH

While FISH is a powerful technique for understanding chromatin structure and function, the denaturation step required for probe labeling invariably disrupts the native chromatin structure (MONGELARD *et al.* 1999; SOLOVEI *et al.* 2002; MARKAKI *et al.* 2012). In general, there are two different denaturation methods: thermal denaturation involves heating the DNA up to 95 °C, while alkaline denaturation uses sodium hydroxide (NaOH) to unwind the double-stranded DNA into single strands at room temperature simply by adjusting the pH (AGENO *et al.* 1969). Several reports have demonstrated the effects of denaturation on chromatin structure. Initially, Raap et al. (1986) found nearly 40% of DNA loss post-heat denaturation of

nuclei fixed in methanol/acetic acid, indicating inconsistencies in denaturation effects. Later, Mongelard et al. (1999) demonstrated through DAPI analysis that increasing the denaturation step intensified the impact on the DAPI staining pattern, which was similarly observed in FISH signals. This phenomenon could be attributed to the loss of chromatin-associated proteins, potentially leading to changes in chromatin modification. Furthermore, Solovei et al. (2002) observed that while chromatin domains appeared well-preserved after 3D-FISH when visualized with a light microscope, electron microscopy revealed dispersed chromatin domains and alteration of nuclear ultrastructure post-heat denaturation, suggesting it to be the most damaging step to nuclear morphology. Supportingly, Markaki et al. (2012) observed swelling or dispersal of chromatin, particularly due to heat denaturation, when observed by super-resolution microscopy. Additionally, formamide, commonly used to lower the melting and annealing temperature of DNA, is often combined with thermal denaturation method (VESELINYOVÁ *et al.* 2021). However, recent reports have indicated significant alterations in chromatin structure resulting from formamide-based denaturation (SHIM *et al.* 2024). All these reports indicate that denaturation-induced chromatin changes cannot be excluded in DNA FISH experiments (MARKAKI *et al.* 2012; SHIM *et al.* 2024). Moreover, these denaturation-induced artifacts can lead to biased interpretations of detailed 3D chromatin organization when viewed at high structural resolution. However, the development of microscopy technology has resulted in various microscopes and techniques, such as SIM, PALM, STORM, STED, with enhanced lateral resolution (approximately 100 nm). This has fueled a growing interest in studying the 3D chromatin structure at high resolution. Furthermore, it emphasizes the importance of developing alternative methods for labeling target DNA while minimizing disruption to chromatin structure.

1.3.4 Non-denaturing FISH methods

Alternative approaches have been developed to address the limitations of heat denaturation in FISH methods. One such method is low-temperature FISH, where only the DNA probe is denatured at 94°C, followed by hybridization between 52 °C and 72 °C for 30 min to label α satellites of human chromosomes (DURM *et al.* 1997). Another innovative approach is Combinatorial Oligonucleotide Fluorescence *in situ* Hybridization (COMBO-FISH), which utilizes homopurine/homopyrimidine DNA oligonucleotide probes to form triplex formations with intact DNA duplexes, based on Hoogsteen base pairs (HAUSMANN *et al.* 2003). This

eliminates the need for prior denaturation of the target DNA. However, both methods are limited to labeling specific sequences and cannot be applied to all genomic sequences (BROWN *et al.* 2022). On the other hand, non-denaturing FISH (ND-FISH) utilizes short oligos to label simple sequence repeats (SSRs) on fixed nuclei and chromosomes in various species, eliminating the need for genomic DNA denaturation (CUADRADO *et al.* 2009; ZHU *et al.* 2017). SSRs comprise DNA tracts where a short base-pair motif is repeated multiple times in tandem. Despite its effectiveness, the mechanism by which short oligos label SSRs remains unclear (ZHU *et al.* 2017). Moreover, while ND-FISH is proficient in labeling SSRs, its application is presently limited to this type of sequence and does not encompass unique sequences. A recent advancement in FISH techniques is RASER-FISH (Resolution After Single-Strand Exonuclease Resection). This method involves incorporating a mixture of BrdU and BrdC into genomic DNA, either in cell culture or in vivo. Subsequently, the DNA is stained with DAPI and exposed to UV light to induce DNA breaks. An exonuclease is then used to create stretches of single-stranded DNA, which are subsequently utilized for binding labeled single-stranded DNA probes (BROWN *et al.* 2022). It's important to note that the use of UV light may lead to alterations in the nanoscale chromatin organization at specific loci (SHIM *et al.* 2024). Additionally, the incorporation of BrdU/C in this method can make it laborious.

1.4 Methods for live imaging of DNA

1.4.1 Fluorescent repressor operator system (FROS)

FROS is a method developed for visualizing genomic regions in living cells (ROBINETT *et al.* 1996; LAU *et al.* 2003), based on the *Lac* operator/ repressor system. In this method, operator sequences are first inserted near the target region. Subsequently, these operator sequences are detected using a fluorescent protein fused with the repressor protein, allowing binding to the specific inserted operator sequence. This system has been successfully applied across various organisms to investigate the localization, replication, and segregation of chromosomes at the individual cell level (MILBREDT AND WALDMINGHAUS 2017). A similar approach has been employed to study chromatin dynamics (KATO AND LAM 2001), and dual labeling systems have been established using two different operator systems with different fluorescent proteins attached in *Arabidopsis thaliana* (MATZKE *et al.* 2005). However, it's important to note that this system requires the prior insertion of operators near the target

region. Additionally, *de novo* methylation of the operator sequence and alterations in chromatin dynamics have been observed, as reviewed by Khosravi et al. (2020a).

1.4.2   ANCHOR

ANCHOR is the DNA labeling tool derived from the bacterial ParABS chromosome segregation machinery (MARIAMÉ *et al.* 2018). It consists of a bipartite system where the ParB protein (OR) can specifically bind to a short, non-repetitive DNA target sequence known as *parS* (ANCH), and subsequently spreads onto neighboring sequences through protein oligomerization. By inserting the *parS* sequences upstream of the target region and employing fluorescently fused ParB protein, accumulation occurs, leading to the formation of a site-specific fluorescent focus. This method was successfully applied to study human cytomegalovirus (HCMV) infection and replication in living human cells (MARIAMÉ *et al.* 2018). In a recent development, the random insertion of *parS* sequences into the *A. thaliana* genome facilitated the tracking of chromatin mobility during cell differentiation in root epidermal cells (MESCHICHI *et al.* 2021). Similarly, to FROS, ANCHOR faces the limitation of untargeted labeling of the genome and demands a laborious process for inserting the *parS* sequence within the target region.

1.4.3   Zinc finger proteins (ZFP)

ZFPs recognize DNA binding motifs found in eukaryotes, with the Cys2-His2 motif being the most commonly used, first discovered in TFIIIA, a transcription factor (MILLER *et al.* 1985). This motif typically consists of 30 amino acids folded into a ββα structure, where the α-helix domain is responsible for interacting with three nucleotides. Engineering amino acids within the α-helix domain can modify the recognition site of the ZFPs. Lindhout et al. (2007), first demonstrated the visualization of centromeres in living root meristems of *A. thaliana* and major satellites in mouse cells using engineered ZFPs fused with green fluorescent proteins (GFP). Despite this success, they encountered difficulties in visualizing sequences with moderate to low copy numbers. Recently, a successful application involved the use of a 6-array of ZFPs-GFP to label repetitive sequences on chromosome 14 in human cells (ICHIKAWA *et al.* 2023). However, the binding of ZFPs depends on both the target sequence and the chromatin context, which consequently limits their applicability (KHOSRAVI *et al.* 2020a).

1.4.4 Transcription activator-like effector (TALE)

The plant pathogenic bacteria genus Xanthomonas secretes TALE proteins, which bind to host plant promoter sequences, activating genes that aid in bacterial infection. TALE proteins feature a central repeat domain composed of 33-35 conserved amino acids, where amino acids 12 and 13 are variable and termed repeat variable di-residue (RVD) (BOCH *et al.* 2009). Modifying the amino acids in the RVD allows binding to all four DNA bases (MAK *et al.* 2012). Initially, multiple engineered TALEs fused with fluorescent proteins were successfully engineered to label repetitive sequences in live human (MA *et al.* 2013), and mouse cells (MIYANARI *et al.* 2013). Later, Fujimoto et al. (2016) successfully applied TALEs to label various repetitive DNA sequences in different tissues of *A. thaliana*. Similarly, to all the aforementioned methods, the utilization of TALEs was restricted by the laborious and time-consuming process of re-engineering them to bind to different sequences. Recently, advancements in live imaging techniques have led to the adoption of more user-friendly CRISPR-Cas9-based methods.

1.5 Clustered Regularly Interspaced Palindromic Repeats (CRISPR-Cas)

First discovered in 1987 by Japanese researchers in *Escherichia coli* (ISHINO *et al.* 1987), CRISPRs have since been identified in numerous bacteria and archaea species (MOJICA *et al.* 2000). CRISPR sequences, as a family of repeats, form distinctive genetic loci and confer RNA-guided, adaptive, and inheritable immunity against viruses and plasmids in prokaryotes by targeting nucleic acids (BARRANGOU *et al.* 2007). These loci consist of an array of direct repetitive sequences, non-coding RNAs, and CRISPR-associated Cas genes, collectively forming the CRISPR-Cas system. CRISPR, along with Cas genes, stores unique DNA sequences known as protospacers acquired from invading phages between CRISPR direct repeats, serving as a memory mechanism to prevent phage infection (BOLOTIN *et al.* 2005; GARNEAU *et al.* 2010; MARRAFFINI AND SONTHEIMER 2010). These Cas genes encode a diverse array of proteins, each possessing distinct functional domains (HORVATH AND BARRANGOU 2010). The combination of CRISPR-Cas, and spacers forms the CRISPR RNA (crRNA) array. Depending on the sequence composition and mechanism of Cas genes within the CRISPR-Cas system, they are categorized into two major classes, six types, and 33 subtypes (MAKAROVA *et al.* 2020). Type I, III, and IV fall under Class 1 of the CRISPR-Cas system. In this class, RNA-mediated cleavage of phages is executed by a large complex comprising several effector proteins. In contrast, Type II, V, and

VI belong to Class 2 of the CRISPR-Cas system. In this class, only a single RNA-guided endonuclease is required for the cleavage of invading genetic materials, reviewed by Wang et al. (2016).

The molecular mechanism involved in the CRISPR-Cas-mediated immunity in prokaryotes is based on RNA-guided DNA targeting and carried out in three phases, in the first acquisition phase, spacer sequences are selected from the incoming phage genome and inserted between the CRISPR repeats to serve as genetic memory. During the second expression phase, Cas proteins are expressed, and the CRISPR array containing spacers is transcribed to form pre-crRNA, which is then processed into small mature crRNA molecules by Cas proteins. Finally, in the interference phase, Cas proteins form complexes with the crRNAs and recognize incoming phages based on complementary sequences. Once recognized, the complex cleaves the phage DNA, effectively inactivating it. In type I and II CRISPR systems, during the interference phase, recognition of a 2- 5 base pairs long specific motif called the proximal adjacent motif (PAM) is required (MOJICA *et al.* 2009). This motif is positioned adjacent to the crRNA target site within the invading phage genomes. The presence of the PAM sequence enables the CRISPR system to differentiate between the host genome and the invading genome, thereby preventing self-cleavage of the genome (HSU *et al.* 2014). However, each CRISPR system requires a unique PAM sequence, indicating that PAM specificity is organism-dependent and CRISPR system-specific (SHAH *et al.* 2013). Despite the variety of CRISPR systems, type II has received the most attention due to its unique characteristic of requiring only a single protein, Cas9, for RNA-guided DNA recognition and cleavage, making it particularly powerful for genome engineering applications (GASIUNAS *et al.* 2012; JINEK *et al.* 2012; RAN *et al.* 2013; WANG *et al.* 2016; JIANG AND DOUDNA 2017).

1.5.1 Cas9: an RNA-guided nuclease for genome editing

CRISPR-Cas9 is characterized by a single DNA endonuclease, Cas9, which utilizes dual nuclease domains—HNH and RuvC—to cleave each DNA strand (SAPRANAUSKAS *et al.* 2011; GASIUNAS *et al.* 2012; JINEK *et al.* 2012). In contrast to other CRISPR systems, which utilize a single crRNA for conferring immunity, the type II Cas9 employs both trans-activating crRNA (tracrRNA) and crRNA duplex to confer immunity against phages (Fig. 2). The tracrRNA plays a vital role in crRNA processing, Cas9 binding, and Cas9-mediated cleavage. With the assistance of ribonuclease III and Cas9, tracrRNA aids in the maturation of crRNA, which specifies target

specificity during the later stages of interference (Fig. 2) (DELTCHEVA *et al.* 2011). This configuration renders Cas9 as a dual-RNA-guided DNA endonuclease system. The crRNA consists of a 5' 20 bp guide sequence along with a segment of the direct repeat, which pairs with the tracrRNA. This pairing guides Cas9 to cleave the target complementary DNA via Watson-Crick base pairing and cleaves the DNA 3 bp upstream of the PAM with HNH or the RuvC-like domain (Fig. 2). The HNH domain cleaves the DNA strand that is complementary to the 20 bp of the crRNA, while the RuvC domain cleaves the non-target DNA strand (GASIUNAS *et al.* 2012; JINEK *et al.* 2012) (Fig. 3A). Mutating one nuclease resulted in the cleavage of a single DNA strand (Cas9 nickase), whereas mutating both nucleases (dead Cas9 or dCas9) resulted in a complete loss of cleavage ability, although the Cas9 protein can still bind to the target DNA (Fig. 3B). For efficient DNA cleavage Cas9 relies on base pairing between the 20 bp sequence of crRNA and target DNA, along with the presence of a PAM sequence adjacent to the target sequence, for recognition of the target sequence. Whereas any mutation in the PAM site further greatly reduced the cleavage efficiency considering the importance of the PAM requirement for efficient Cas9 cleavage. Additionally, the fusion of both tracrRNA and crRNA into a chimeric single guide RNA (sgRNA) exhibited similar cleavage efficiency (JINEK *et al.* 2012), simplifying the process of programming the 20 bp region of the sgRNA to target any DNA sequence along with the adjacent PAM. This makes it an easily programmable platform for specific genomic editing and other applications in eukaryotes.
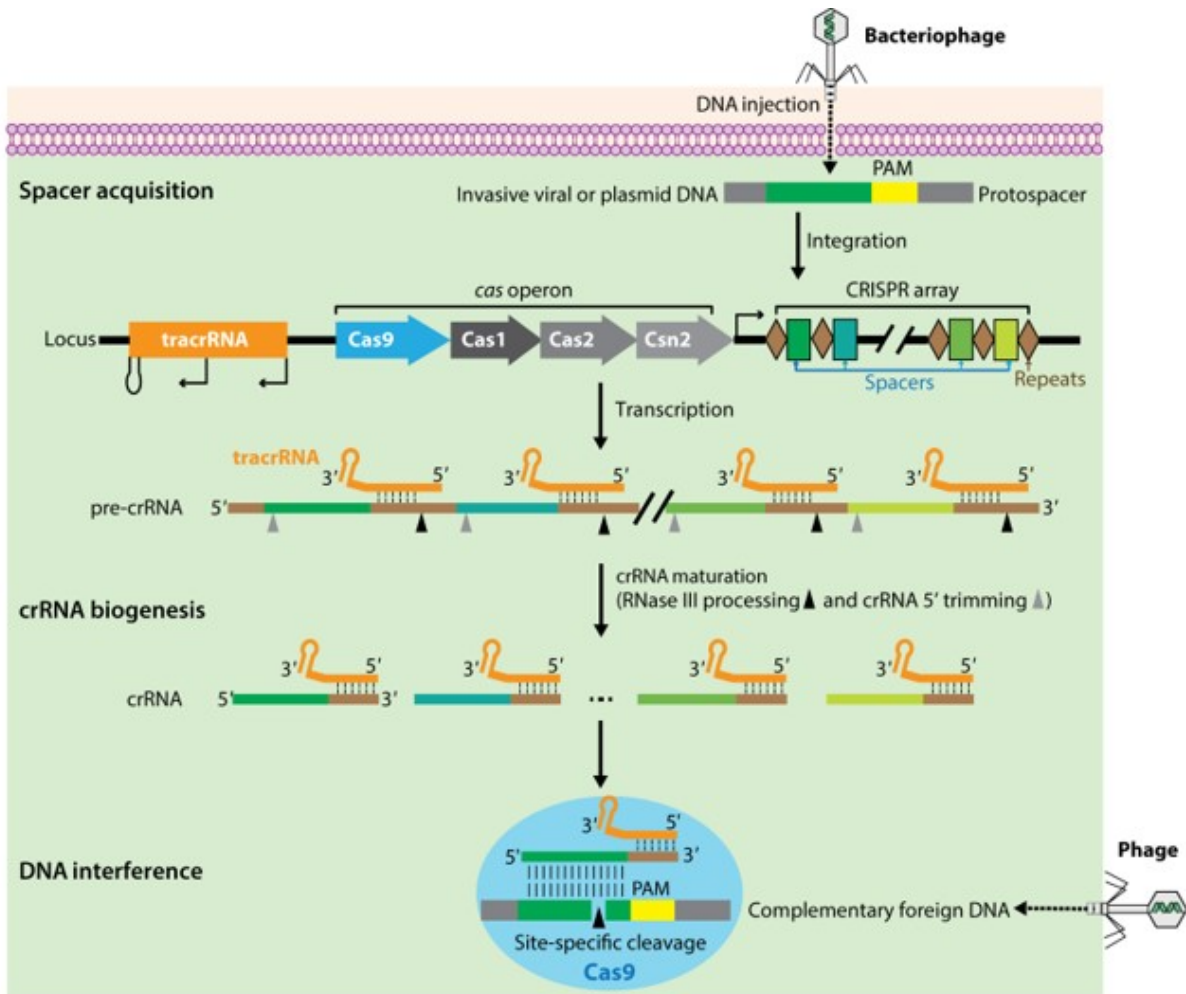
Fig 2: CRISPR–Cas9-mediated DNA interference in bacterial adaptive immunity. (a) A typical CRISPR locus in a type II CRISPR–Cas system comprises an array of repetitive sequences (repeats, brown diamonds) interspaced by short stretches of nonrepetitive sequences (spacers, colored boxes), as well as a set of CRISPR-associated (cas) genes (colored arrows). Preceding the cas operon is the trans-activating CRISPR RNA (tracrRNA) gene, which encodes a unique noncoding RNA with homology to the repeat sequences. Upon phage infection, a new spacer (dark green) derived from the invasive genetic elements is incorporated into the CRISPR array by the acquisition machinery (Cas1, Cas2, and Csn2). Once integrated, the new spacer is co transcribed with all other spacers into a long precursor CRISPR RNA (pre-crRNA) containing repeats (brown lines) and spacers (dark green, blue, light green, and yellow lines). The tracrRNA is transcribed separately and then anneals to the pre-crRNA repeats for crRNA maturation by RNase III cleavage. Further trimming of the 5` ends of the crRNA (gray arrowheads) by unknown nucleases reduces the length of the guide sequence to 20 nt. During interference, the mature crRNA–tracrRNA structure engages Cas9 endonuclease and further directs it to cleave foreign DNA containing a 20-nt crRNA complementary sequence preceding the PAM sequence. Figure modified from Jiang and Doudna (2017).

Among the diverse Cas9 variants originating from different organisms, Cas9 from *Streptococcus pyogenes* (Sp. Cas9) is a large multidomain and multifunctional DNA endonuclease, consisting of 1368 amino acids. It is the most commonly utilized for genome engineering, primarily due to its requirement for a simple PAM sequence (NGG, where N

represents any nucleotide) reviewed by Wang et al. (2016); Jiang and Doudna (2017). Although Cas9 from *Staphylococcus aureus* (Sa. Cas9) is relatively smaller, comprising 1053 amino acids compared to Sp. Cas9, it requires a larger PAM sequence (NNGRRT, where R represents an A or G) (NISHIMASU *et al.* 2015; RAN *et al.* 2015). Despite this discrepancy, Sa. Cas9 has shown comparable genome editing efficiency to Sp. Cas9 (RAN *et al.* 2015). Similarly, in addition to differences in the PAM sequence, these Cas9 variants also display variations in the crRNA and tracrRNA sequences (NISHIMASU *et al.* 2015). This feature enables Cas9 variants to be employed orthogonally, allowing them to be used simultaneously for genome engineering and targeting purposes (ESVELT *et al.* 2013; MA *et al.* 2015; DREISSIG *et al.* 2017).
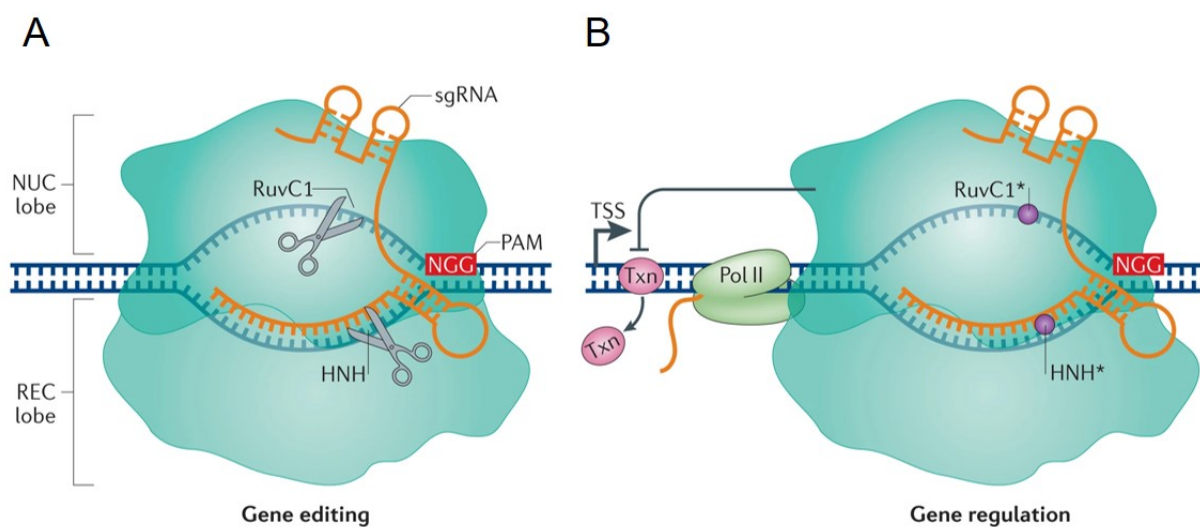
Fig 3: (A) The S. pyogenes Cas9 endonuclease consists of a nuclease (NUC) lobe and a recognition (REC) lobe. Cas9 is targeted to specific DNA sequences by direct pairing of the chimeric single guide RNA (sgRNA) with the target DNA. This targeting relies on the presence of a 5' protospacer-adjacent motif (PAM) in the DNA, which in S. pyogenes is usually NGG. Binding mediates cleavage of the target sequence by two nuclease domains, RuvC1 and HNH. (B) The Sp. dCas9 protein contains mutations in its RuvC1 (D10A) and HNH (H841A) domains, which inactivate its nuclease function (circles). dCas9 retains the ability to target specific sequences through the sgRNA and PAM. Figure modified from Dominguez et al. (2016).

1.5.2   Structure and mechanism of the Cas9 protein

Structural examination of the apo Sp. Cas9 revealed the presence of dual lobes. In one lobe, the nuclease domain (NUC) and variable C-terminal domain (CTD) are located, while the other lobe contains a large alpha-helical recognition domain (REC) (JINEK *et al.* 2014). To interrogate the DNA, Cas9 utilizes a 20 bp spacer sequence on the crRNA or the 5' end of the sgRNA, which confers target specificity. Conversely, the tracrRNA or the 3' end of the sgRNA is necessary for

the recruitment of Cas9 (Doudna and Charpentier 2014). The Cas9-mediated DNA cleavage methodology is illustrated in Figure 4. In the apo state, Cas9 remains inactive. However, upon binding with guide RNA, a conformational rearrangement of Cas9 occurs, transitioning it into an active state for DNA interrogation (Jiang et al. 2015). At this stage, the 10-nt RNA seed sequence of the crRNA adopts a preordered A-form conformation, which is necessary for the initial DNA interrogation and strand invasion process. Additionally, the PAM interaction sites are positioned for PAM interrogation. After binding to the appropriate PAM, Cas9 begins interrogating the adjacent DNA sequences for target sequences. If the DNA complementarity within the crRNA seed sequences is not found, Cas9 will dissociate from the DNA and continue surveying for the next PAM. Upon finding the target DNA that is complementary to the seed sequence, Cas9 initiates DNA melting at the nucleation site near the PAM interaction region. The phosphate lock loop in the CTD domain stabilizes the RNA-DNA duplex and flips the first base of the target DNA, rotating the DNA and facilitating base pairing. Then, Cas9 unwinds the non-target strand. After finding the complementarity of the guide seed sequence and target DNA, this results in a conformational change in Cas9, which further proceeds with the base pairing of the 5` of the guide sequences. Completing the binding of the guide with target DNA further changes the Cas9 conformation to activate the HNH and result in cleavage of the target DNA strand. This conformational change further directs the non-target strand to the RuvC for cleavage (Sternberg et al. 2015; Jiang et al. 2016). This process induces double-stranded breaks (DSBs) close to the PAM sequence. In eukaryotes, these DSBs can be repaired by triggering cellular DNA repair mechanisms, such as nonhomologous end joining (NHEJ) or homology-directed repair (HDR) (Wang et al. 2016). These mechanisms can be utilized for precise gene insertion, knockout, deletions, or corrections (Choulika et al. 1995; Lieber 2010).
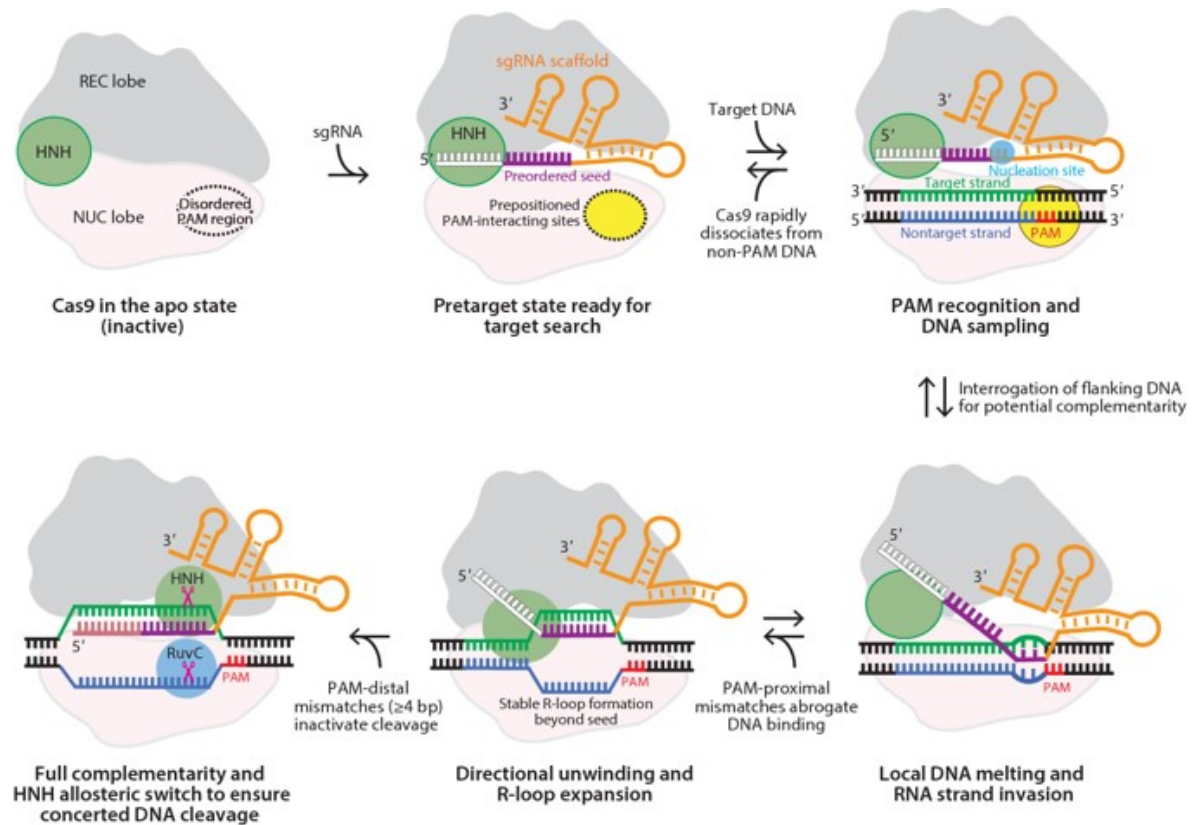
Fig 4: Schematic representations of the proposed mechanisms of CRISPR–Cas9-mediated target DNA recognition and cleavage. Upon sgRNA loading, Cas9 undergoes a large conformational rearrangement to reach a target-recognition mode, in which the PAM-interacting cleft (dotted circle) that is largely disordered in apo–Cas9 becomes prestructured for PAM sampling, and the guide RNA seed is preorganized in an A-form helical conformation for interrogation of adjacent DNA for guide RNA complementarity. Dotted white boxes denote the disordered nonseed RNA nucleotides. Cas9 is further activated through coordinated multiple steps starting with PAM recognition, followed by local DNA melting, RNA strand invasion, and stepwise R-loop formation, as well as allosteric regulation of the RuvC domain by conformational change of the HNH domain to ensure concerted DNA cleavage. Abbreviations: bp, base pair; NUC, nuclease lobe; PAM, protospacer adjacent motif; REC, recognition lobe; sgRNA, single-guide RNA. Figure modified from Jiang and Doudna (2017).

Compared to other genome editing techniques such as zinc finger nucleases (ZFNs), transcription activator-like effector nucleases (TALEs), and homing mega nucleases, the CRISPR-Cas9 system stands out due to its flexibility as an RNA-guided DNA nuclease. Its efficiency in site-specific genome editing is attributed to the Watson-Crick base pairing mechanism. Moreover, CRISPR-Cas9 is cost-effective, robust, and easily engineered, making it the preferred choice for genome editing. This has made Cas9 a versatile tool for precisely editing the genome, simply by swapping the 20 bp crRNA or sgRNA sequence to targetedly manipulate the genome in animals, mammals, and plants, reviewed by Nidhi et al. (2021);

Wang and Doudna (2023). Beyond genome editing, CRISPR-Cas9 has been harnessed for gene regulation, epigenome engineering, and genome imaging, utilizing the nuclease-deficient Cas9 (dead Cas9 or dCas9). This variant can only bind target DNA without cutting it (Qi *et al.* 2013), opening up avenues for various applications reviewed by Wang et al. (2016).

1.5.3 Applications of CRISPR-Cas9 for live imaging in humans and animals

The first demonstration of harnessing Cas9 for genome imaging was given by Chen et al. in 2013. They achieved this by fusing one copy of Enhanced GFP (eGFP)to the dead (d)Cas9 to label the telomere and other repetitive sequences in live human cells (CHEN *et al.* 2013a). Additionally, they reported on the optimization of sgRNA design, which significantly increased the signal-to-noise ratios of CRISPR labeling of repeat sequences. Later, this strategy was further enhanced for signal amplification by fusing three copies of fluorescent proteins to dCas9. This modification successfully enabled the simultaneous labeling of different repetitive sequences using various Cas9 variants with their cognate sgRNA in human cells (MA *et al.* 2015). Recently, (WANG *et al.* 2019), utilized a preassembled ribonucleoprotein (RNP) composed of dCas9 and a fluorophore-labeled sgRNA (LiveFISH) to detect chromosomal disorders in live human T cells. Additionally, they tracked the dynamics of CRISPR-Cas9-induced double-strand breaks (DSBs) (WANG *et al.* 2019).

To further advance CRISPR labeling techniques, various strategies have been developed to enhance the signal intensities of CRISPR-dCas9-based systems by engineering either the dCas9 proteins or the sgRNA. Initially, Chen et al. (2018) introduced the CRISPR-tag concept, involving the integration of a DNA-tag adjacent to the target gene using CRISPR editing. This tag comprised a mCherry encoding region and intronic repeat regions containing multiple CRISPR-Cas9 target sites. These sites enabled the binding of dCas9 fused with 14 copies of GFP, resulting in signal amplification and successful visualization of human genes across different cell stages. Similarly, dCas9 was engineered to incorporate the previously developed SunTag signal amplification system (TANENBAUM *et al.* 2014). In the CRISPR-SunTag system, dCas9 is fused with 24 copies of general control nonderepressible 4 (GCN4) peptides. These peptides can be specifically detected with fluorescent single-chain variable antibody fragments (scFv), resulting in signal amplification. This system was successfully utilized for labeling both repetitive (YE *et al.* 2017), and low-copy DNA sequences and also single-copy sequences (NEGUEMBOR *et al.* 2017), in human and mouse live cells.

Alternatively, several methods have been developed by engineering sgRNA to incorporate different RNA aptamer sequences. One such approach is CRISPR-Casilio, where sgRNA is modified to incorporate Pumilio/fem-3 binding factor (FBF) RNA-binding domains of Pumilio proteins. The 8-mer RNA sequence on PUF binding sites (PBS) can be detected by the PUF domain fused with a fluorescent protein for signal amplification (CHENG *et al.* 2016). This system successfully labeled repetitive sequences (CHENG *et al.* 2016), and has been further developed to enable the successful labeling of non-repetitive sequences such as MUC4 with just a single sgRNA (CLOW *et al.* 2022). Recently, it has been applied in studying cancer biology and the dynamics of extrachromosomal DNA (YI *et al.* 2022). In parallel, (MA *et al.* 2016) developed the CRISPRainbow system, where sgRNA was engineered to independently incorporate three distinct RNA aptamers (PUF, MS2, or PP7). These aptamers were detected with the target protein fused with fluorescent proteins, enabling the labeling of six chromosome-specific repeat sequences (MA *et al.* 2016). Later (QIN *et al.* 2017), introduced the CRISPR-16xMS2-MCP system, incorporating 16 copies of MS2 aptamers into the sgRNA and using MS2 coat protein (MCP) fused to fluorescent proteins for signal amplification. This system successfully labeled low-copy sequences and the single-copy MUC4 gene using 8 sgRNAs, outperforming previous methods such as CRISPR-Casilio and CRISPRainbow (VAN TRICHT *et al.* 2023). Subsequently, the CRISPR-Sirius system was developed, achieving superior imaging of repetitive sequences through sgRNA optimization, albeit using only 8 copies of MS2 compared to the 16 used in the CRISPR-16xMS2-MCP system (MA *et al.* 2018). However, except for CRISPR-Sirius, all other methods have been successfully used for labeling low and single-copy sequences, either using multiple or single sgRNAs, as reviewed by (VAN TRICHT *et al.* 2023).

Alternately, CRISPR-MB was developed by engineering sgRNA with a molecular beacon targeting sequence (sgRNA-MTS). This modified sgRNA was paired with a molecular beacon fused with a fluorophore-quencher pair, enabling multiplexing of repetitive sequences in human cells (WU *et al.* 2018). Later, this method evolved into CRISPR/dual-FRET, where sgRNA-MTS was enhanced to include additional targeting sequences for hybridizing two molecular beacons with a FRET (Fluorescence Resonance Energy Transfer) pair. With this advancement, non-repetitive sequences of MUC4 genes were visualized using only three sgRNAs, demonstrating a superior signal-to-noise ratio compared to CRISPR-MB (MAO *et al.* 2019).

In contrast to CRISPR methods employing fluorescence proteins, CRISPR-QD introduces a unique approach by utilizing Quantum dots (QD) for signal generation (MA *et al.* 2017). Quantum dots are semiconductor nanocrystals known for their broad excitation and narrow emission spectra, along with long fluorescence lifetimes (BARROSO 2011). Remarkably, it successfully labeled single-copy sequences in live U1 cells using only two unique sgRNAs (MA *et al.* 2017).

Recently, (ZHANG *et al.* 2024), introduced fluorogenic CRISPR (fCRISPR) to address background noise concerns in CRISPR-based live imaging techniques. This method utilizes an engineered sgRNA containing the Pepper aptamer, and TdTomato fused with tDeg, a degron. The fluorescent proteins are inherently unstable and degrade quickly unless stabilized by binding to the Pepper RNA aptamer. This approach efficiently labeled low-copy sequences without the need for signal amplification and demonstrated a lower signal-to-noise ratio compared to the dCas9-MC2 system (ZHANG *et al.* 2024).

Additionally, several strategies were reported for labeling repetitive sequences in live humans and mammalian cells, reviewed by (VAN TRICHT *et al.* 2023). Subsequently, several researchers independently reported on labeling of single copy sequences using multiple sgRNAs targeting non-overlapping DNA regions (VAN TRICHT *et al.* 2023) and also visualized the entire chromosome 9 to study cell cycle dynamics in humans (ZHOU *et al.* 2017).

1.5.4   Applications of CRISPR-Cas9 for live imaging in plants

In plants, Dreissig et al. (2017) demonstrated the successful application of CRISPR labeling for telomeres in live cells of transiently transformed *Nicotiana benthamiana*. They employed two Cas9 orthologues from *Streptococcus pyogenes* and *Staphylococcus aureus*, fused with three copies of different fluorescent (eGFP or mRuby) reporters, demonstrating comparable efficiency. Independently, Fujimoto and Matsunaga (2017) reported similar telomere labeling in *N. tabacum* using Sp. dCas9-3x eGFP. These studies revealed that telomeres are localized on the nucleus periphery and exhibit dynamic positional changes of up to ± 2 μm while being tracked individually over a 30-minute period (DREISSIG *et al.* 2017). Moreover, when dCas9 targeting telomeres was co-transformed with a telomeric repeat binding protein (TRB1), the colocalization of both signals was observed. This illustrates the utility of this method for studying DNA/protein interactions (KHOSRAVI *et al.* 2020a). Later, the application of MS2 and PP7 aptamers in combination with dCas9 further improved the CRISPR labeling of telomeres

in *N. benthamiana* (Kʜᴏsʀᴀᴠɪ *et al.* 2020c). Aptamers are the short RNA oligo specially detected with the RNA binding proteins (Uʀʙᴀɴᴇᴋ *et al.* 2014). When these aptamers are inserted into the sgRNA, they can be detected using binding proteins fused with fluorescent proteins such as eGFP or mRuby. The application of sgRNA fused with 2x MS2 aptamers, in combination with dCas9, demonstrated an improved CRISPR labeling of *N. benthamiana* telomere number per nucleus, up to 1.7-fold compared to the previous method using dCas9: GFP (Kʜᴏsʀᴀᴠɪ *et al.* 2020c). However, both methods failed to label repetitive sequences in stable transformed *N. benthamiana*, *Arabidopsis thaliana* or *Daucus carota*.

1.5.5 Applications of CRISPR-Cas9 for imaging fixed human and animal specimens

CRISPR-Cas9 not only aids in labeling specific genomic sequences in live cells but also allows for precise DNA detection in fixed samples. With the progress in super-resolution microscopy and growing interest in studying native chromatin structure and its modifications throughout the cell cycle, there's a noticeable need for more sensitive chromatin labeling techniques. Unlike DNA FISH, which necessitates global DNA denaturation, CRISPR-Cas9 doesn't require such treatment, thereby preserving the chromatin structure. This encouraged Deng and his colleagues (2015), to develop a CRISPR-Cas9-based tool known as Cas9-mediated fluorescence *in situ* hybridization (CASFISH) method. CASFISH uses fluorophore-coupled sgRNA along with dCas9 protein holding a Halo-tag on C-terminus, which can be covalently detected with Halo ligands conjugated with an organic dye (Janelia Fluor) (Fig 5A). Using this approach, they successfully labeled telomeres and pericentromeric repeats on fixed cells and tissue sections of mouse. Additionally, they were able to label both high and low- repetitive sequences of MUC gene in fixed human cells (Dᴇɴɢ *et al.* 2015). Recently, Wang et al. (2021) developed a CRISPR based labeling method on fixed samples using a Cas9 nickase, called GOLD-FISH (genome oligopaint via local denaturation fluorescence *in situ* hybridization). In this approach, a Cas9 nickase first cleaves the non-target strand, resulting in a 3'-ssDNA overhang. Subsequently, Rep-X, a DNA helicase with 3'–5' helicase activity, is loaded onto the non-target strand to unwind the dsDNA until it encounters a blockade. Fluorescently labeled oligo probes are then used to hybridize the ssDNA without the need for heat denaturation (Wᴀɴɢ *et al.* 2021) (Fig 5B). This method was successfully used for labeling of both repetitive and single copy sequences in human cells and human breast cancer tissue sections. Additionally, GOLD-

FISH successfully labeled the p-arm and q-arm of chromosomes X using thousands of sgRNA and labeled oligo probes.
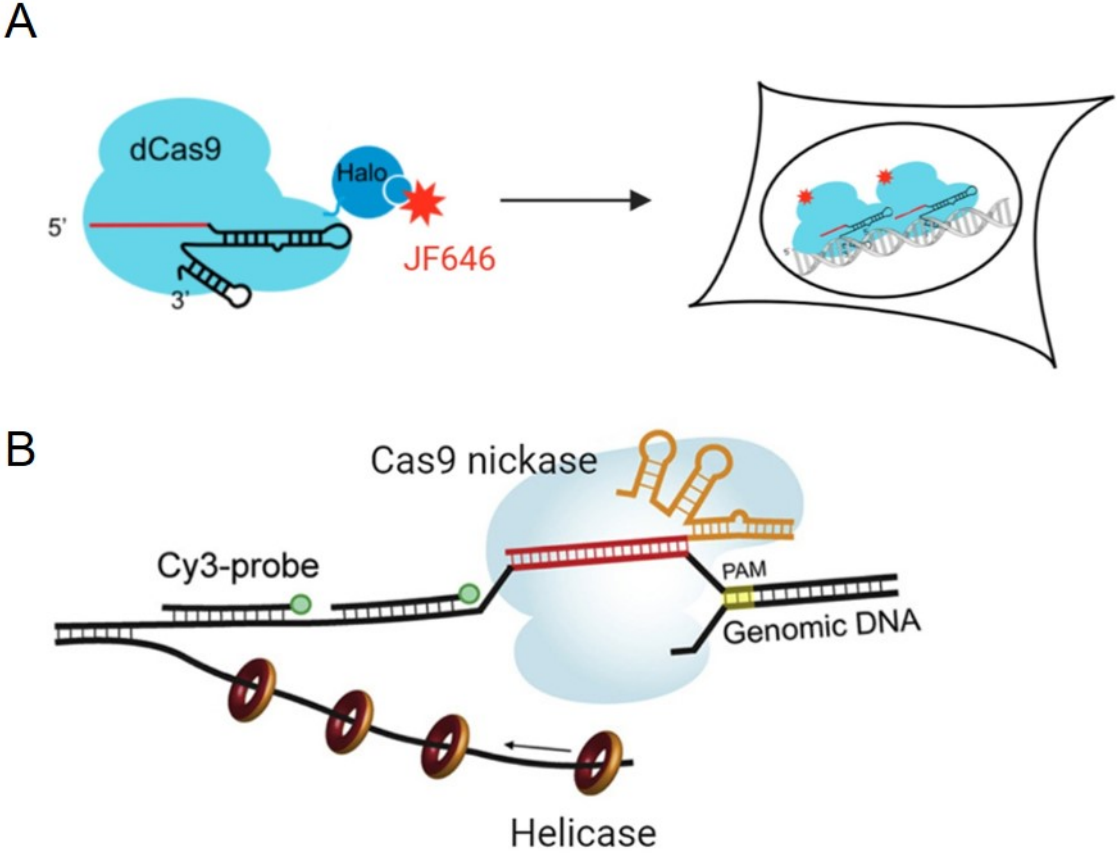
Fig 5: Schematic overview of CRISPR based genome labeling tools on fixed samples. (A) Schematic of the CASFISH strategy, using CRISPR dCas9 ribonucleoprotein (RNP) contains a Halo tag for binding its fluorophore (F)-labeled Halo ligand. (B) GOLD FISH relies on cleavage activity of Cas9 nickase and the local DNA-unwinding activity of helicase for subsequent fluorescence in situ hybridization (FISH) probe hybridization. Figure modified from Van Tricht et al. (2023).

1.5.6 Application of CRISPR-Cas9 for imaging fixed samples in plants

A simpler CRISPR-based DNA labeling method, termed CRISPR-FISH (also known as RGEN-ISL), was developed by Ishii et al. (2019). Unlike CASFISH, this method does not require laborious *in vitro* synthesis of sgRNA or engineering of dCas9 protein. Instead, CRISPR-FISH utilizes a bipartite guide RNA, a single ATTO™ 550 fluorescent-labeled tracrRNA, a target-specific crRNA, along with Sp. dCas9 protein to label the target sequence. The CRISPR-FISH methodology is depicted in Figure 6.
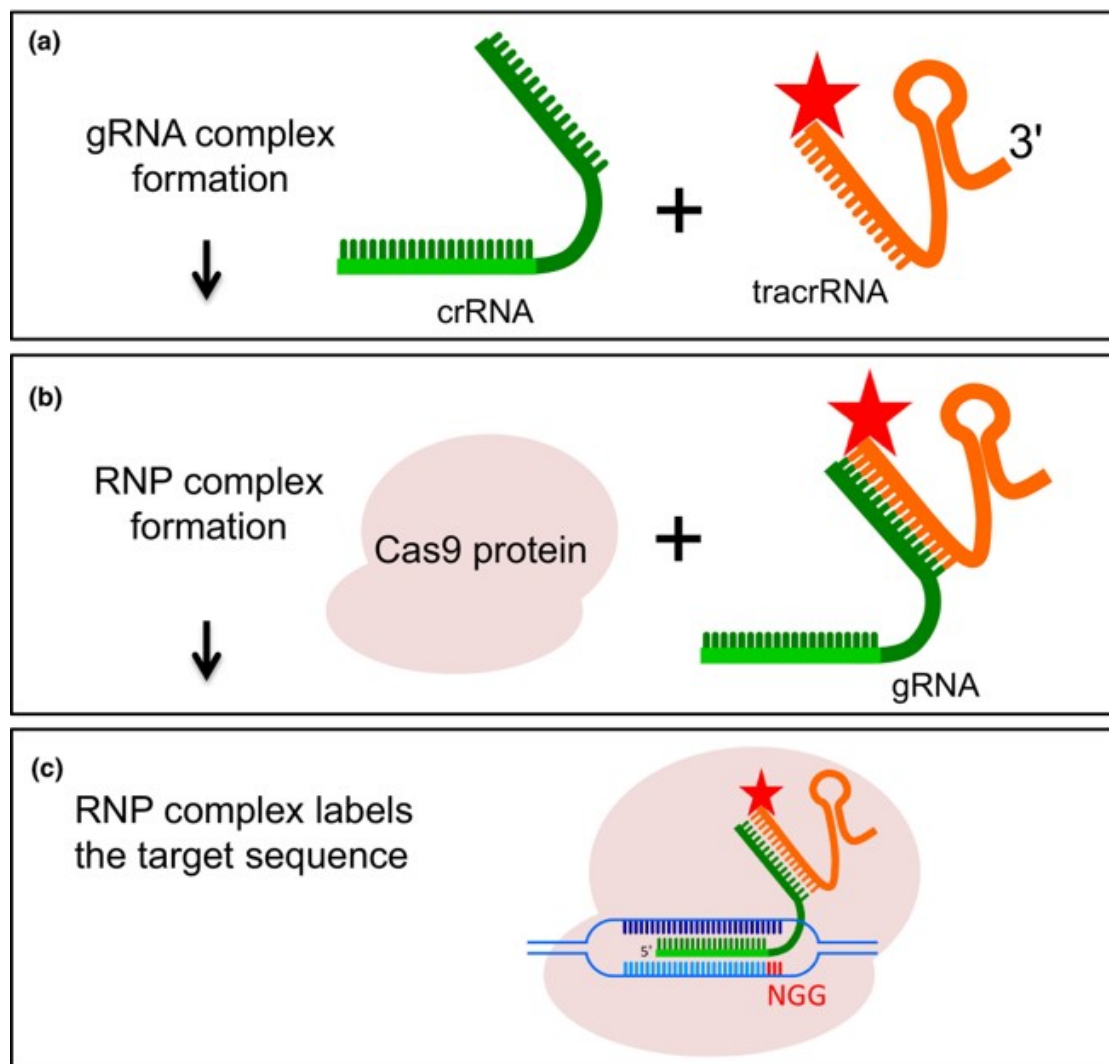
Fig 6: Schemata of the CRISPR-FISH method. (a) Guide RNA (gRNA) complex formation after hybridization of CRISPR RNA (crRNA) and 5 0 ATTO 550 (star) labelled trans-activating crRNA (tracrRNA). (b) Ribonucleoprotein (RNP) complex formation after combination of the recombinant Cas9 protein with gRNA. (c) Components of the RGEN-ISL system to label genomic targets. The crRNA: tracrRNA complex uses optimized Alt-R crRNA and ATTO 550labelled tracrRNA sequences that hybridize, and then form a complex with Cas9 endonuclease to guide targeted binding to genomic DNA. The binding site is specified by the protospacer element of the crRNA (light green bar). The crRNA protospacer element recognizes 19 or 20 nt on the opposite strand of the NGG protospacer adjacent motif (PAM) site. The PAM site (red) must be present immediately downstream of the protospacer element for binding to occur. Figure modified from Ishii et al. (2019).

CRISPR-FISH allows the simultaneous labeling of multiple DNA repetitive sequences via differently labeled tracrRNAs and target-specific crRNAs, serving as a multiplexing DNA labeling platform. Moreover, this method can be readily combined with immunostaining and EdU labeling, enabling the study of DNA-protein interactions and replication sites simultaneously (Ishii *et al.* 2019; Němečková *et al.* 2019). CRISPR-FISH is a versatile tool that can label genomic DNA on both formaldehyde and (3:1) ethanol: acetic acid fixed chromosomes and can label the target sequence at different temperatures (26 °C, 4 °C, and 37 °C). Hence better preservation of cell morphology, and chromatin structure is achieved for studying the three-dimensional genome organization with super-resolution imaging (Ishii *et al.* 2019; Potlapalli *et al.* 2020). Furthermore, CRISPR-FISH can be used to label specific DNA sequences in fixed plant tissue sections and plant organs (Nagaki and Yamaji 2020). 3D-SIM analysis of CRISPR-FISH knob labeling in *Zea mays* nuclei revealed compact and minimally altered chromatin. Subsequent DNA-FISH labeling on the same nuclei, followed by SIM analysis, confirmed impaired and flattened chromatin, likely due to denaturation. Therefore, CRISPR-FISH emerges as the preferred method for visualizing repeats when the ultrastructure of chromatin is of interest. Furthermore, real-time visualization of CRISPR-FISH labeling showcased the rapid kinetics of the reaction, with telomere labeling detected just 20 seconds after the addition of the RNP complex (Ishii *et al.* 2019). The extensive adaptability of CRISPR-FISH to diverse temperatures and method combinations has the potential to drive progress in chromosome biology. However, broader implementation of the method faces challenges in less-funded educational institutions and science outreach settings that lack expensive fluorescence microscopes. Additionally, the current method is limited to labeling repetitive sequences in fixed samples and cannot be applied to low-copy sequences. Therefore, further development of CRISPR-FISH is needed to address this issue.

2. Aims

Analyzing the three-dimensional organization of genomes using microscopic techniques aids in understanding how the spatial arrangement of chromatin influences gene regulation and activity. Recent advancements in this field have led to DNA visualization methods that utilize CRISPR-dCas9-based labeling techniques tailored for animal and plant genomes, reviewed by Khosravi et al. (2020a). One such innovative method is CRISPR-FISH, a rapid and straightforward method that fluorescently labels repetitive DNA sequences in fixed samples (ISHII *et al.* 2019; POTLAPALLI *et al.* 2020). Unlike FISH, CRISPR-FISH doesn't need global DNA denaturation and ensures a better preservation of the chromatin structure (ISHII *et al.* 2019; NĚMEČKOVÁ *et al.* 2019; POTLAPALLI *et al.* 2020).

Laboratory-based education has become an integral component of the school curriculum. Demonstrating CRISPR-FISH in schools can enhance students' understanding of CRISPR-Cas and chromatin organization, fostering early interest in biology. However, broader implementation of the method faces challenges in less-funded educational institutions and science outreach settings that lack expensive fluorescence microscopes. To overcome this limitation, a non-fluorescent CRISPR-ISH method must be developed.

Labeling low-copy or single-gene sequences with CRISPR-FISH is challenging due to the limited availability of fluorescently labeled RNP complexes, making detection difficult. Increasing the number of gRNAs can enhance detection but also raises costs and off-target risks. To overcome this, novel approaches to amplify signal intensity in combination with CRISPR-FISH should be developed.

Artifacts in electron microscopy (EM) studies are frequently linked to standard FISH protocols, mainly because of formamide and high-temperature treatment of chromatin. Developing less damaging approaches to studying chromatin will play a pivotal role in understanding chromatin structure at high structural resolution.

Hence, the aims of my study are:

1. Development of a non-fluorescent CRISPR-ISH method to label repetitive sequences on fixed nuclei and chromosomes.

2. Development of CRISPR-FISH method with enhanced signal intensity by harnessing novel approaches such as ALFA-tag, tyramide signal amplification (TSA), fluorescent

RNA pepper aptamers, and quantum dots (QD) in combination with CRISPR-FISH. In addition, pooled sgRNAs targeting specific DNA sequences will be tested in combination with CRISPR-FISH to visualize single-copy sequences.

3. Development of CRISPR-ISH for electron microscope-based signal detection to study the chromatin structure at the highest resolution.

3. Materials and Methods

3.1 Material and plant growth conditions

For isolation of leaf nuclei and somatic chromosomes, *Arabidopsis thaliana* (Col-0, Pro-0), *Nicotiana benthamiana*, maize (*Zea mays*-B73), Welsh onion (*Allium fistulosum*), onion (*Allium cepa*), broad bean (*Vicia faba*), and rapeseed (*Brassica napus*) plants were used. Chromosome suspension of the house mouse (*Mus musculus forma domestica*) was kindly provided by Prof. Dr. Thomas Liehr (Institute of Human Genetics, University, Jena, Germany).

A. thaliana seeds were sown in soil and germinated under short-day conditions (16h dark/8h light, 18-20 °C) and then transferred to long-day conditions (16 h light/ 8 h dark, 18- 20 °C) before bolting. For leaf material, plants were grown in the green house in pots. For meristematic root tips, seeds were germinated on wet filter paper in a petri dish at 26 °C, and meristematic roots were collected from 3 – 5 days old seedlings. For transient transformation, *N. benthamiana* seedlings were grown in a greenhouse under 16/8 hours light/dark conditions and 22 °C temperature for 2-4 weeks.

3.2 Preparation of leaf nuclei

For isolation of interphase nuclei, young leaf tissue was fixed in 4% formaldehyde (freshly made from a 37% stock solution) for all species except *Z. mays*, which was fixed in 2% formaldehyde (Němečková *et al.* 2019). The fixation was carried out in ice-cold Tris buffer (10 mM Tris-HCl (pH 7.5), 10 mM Na2-EDTA, 100 mM NaCl, 0.1% Triton X-100, and adjusted pH 7.5 with NaOH) for 5 min under vacuum in a concentrator (5301, Eppendorf) and followed by incubation for 25 min on ice without vacuum. Then, the tissue was rinsed twice in ice-cold Tris buffer for 5 min each on ice. After, the tissue was chopped in a drop of ice-cold chromosome isolation buffer (LB01 buffer: 15 mM Tris-HCl (pH 7.5), 2 mM Na2-EDTA, 0.5 mM spermin, 80 mM KCl, 20 mM NaCl, 15 mM β-mercaptoethanol and 0.1% Triton X-100 (Doležel *et al.* 1989)) using a fresh razor blade in a petri dish. Subsequently, 450 µl of chromosome isolation buffer was added to the homogenate, and the suspension was filtered through a 50 µM pore size mesh into a tube. After, 100 µl of nuclei suspension was spun on the glass slides using a cytocentrifuge (Cytospin3, Shandon) with 700 revolutions per min (rpm) for 5 min. Later the slides were kept in 1x phosphate buffer solution (PBS: 137 mM NaCl, 2.7 mM KCl, 10 mM Na2HPO4, 1.8 mM KH2PO4, pH 7.4) on ice until used.

3.3   Preparation of chromosomes

To prepare chromosome spreads, root tips were collected from germinated seeds of *Z. mays*, *V. faba*, *A. cepa, and A. fistulosum* 2 to 5 days after germination. To arrest mitosis at metaphase, the roots were pretreated and fixed according to the conditions outlined in Table 1. Then, the roots were washed twice in ddH2O and 1x citric buffer (0.01 M Na-citrate, citric acid pH 4.8) respectively for 5 min each on ice. Subsequently, 3-5 meristematic root tips were incubated in a 1.5 ml Eppendorf tube containing 30 - 50 µl of enzyme mixture (0.7% cellulase R10, 0.7% cellulase, 1% pectolyase, and 1% cytohelicase dissolved in 0.01 M citric buffer) and digested for different time points depending on the species, as indicated in Table 1.

Table 1 : Conditions for metaphase arresting, fixation, and enzyme treatment.

Species	Pretreatment and conditions	Fixation	Incubation time in enzyme
Z. mays	0.1% colchicine: ddH2O (2:1) for 3 hours at room temperature	3:1 (ethanol: acetic acid) for 24 h at room temperature	60 min at 37 °C
Vicia faba	2 mM 8 hydroxyquinoline at 15° C for 3 h		50 min at 37 °C
Allium cepa	Cold water for 24 hours	3:1 for 1 h	50 min at 37 °C
Allium fistulosum	Cold water for 24 hours		50 min at 37 °C

Chromosome cell suspension was prepared as described by Kirov et al. (2014). In brief, after digestion, the tubes containing digested meristems were vortexed for a few seconds to obtain a cell suspension. Then, 600 µl of ddH2O was added to the tube and centrifuged at 10,000 rpm for 45 seconds. The supernatant was discarded using a Pasteur pipette without disturbing the pellet. Subsequently, 600 µl of 96% ethanol was added to the tube and mixed. At this

stage, the suspension can be stored for 6 months at -20 °C. Alternatively, the tube was centrifuged at 11,000 rpm for 30 seconds, and the supernatant was discarded by inverting the tube. Finally, the pellet was resuspended in 50 - 100 µl of freshly prepared 3:1 (3 parts ethanol & 1-part acetic acid) fixative, depending on the cell concentration. At this stage, the suspension can be used directly for chromosome preparation or stored at -20 °C.

To drop the cell suspension, the hot plate was heated to 55 °C. Subsequently, 2-3 layers of moist tissue papers were placed on the hot plate to adjust the humidity to 50 - 55 grams of water vapor per cubic meter, ensuring optimal chromosome spreading. Meanwhile, the slides were placed on ice for 10 min. Subsequently, the slides were transferred to a humid chamber containing the moist tissue papers placed on the hot plate. Then, 8 µl of cell suspension was carefully dropped onto the pre-cooled slide within the humid chamber from a distance of 15 cm using a pipette. After the formation of granule-like structures on the slide, 20 - 30 µl of 3:1 ethanol acetic acid solution was added to the slides to remove the residual cytoplasm surrounding the chromosomes. The slides were allowed to sit in the humid chamber until the surface became granular. Steam was then applied to the slides from the water bath by holding the slide upside down over the water bath for 5 seconds. Subsequently, the slides were immediately dried with cold wind generated by a hairdryer. Following this, slides with well-spread mitotic chromosomes were selected using a phase-contrast light microscope. These selected slides were used immediately or stored in 96% ethanol in a Coplin jar at -20 °C.

A. thaliana chromosomes were prepared from young flower buds as described in (Mandáková and Lysak 2016). Whole inflorescences containing mainly closed flower buds were collected and fixed in freshly prepared 3:1 (3 parts ethanol & 1-part acetic acid) fixative for 24 hours at room temperature (RT). The fixative was changed several times within 24 hours until the flower buds remained white and the fixative remained clear. After fixation, the flower buds were washed twice in ddH2O for 5 min each in a staining block placed on ice. Buds containing yellow anthers with pollen were then carefully removed under a stereomicroscope. The remaining ddH2O was replaced with 0.01 M citrate buffer, and the buds were washed twice for 5 min each on ice. Then, the flower buds were digested in a staining block containing a 50% enzyme mixture in 0.01 M citrate buffer at 37 °C for 60 min. Afterwards, the enzyme mixture was replaced with 0.01 M citrate buffer and the staining block was placed on ice until further use. For the preparation of chromosome slides, a single flower bud was transferred

onto a glass slide using a dissecting needle. Then, 0.2 µl of 0.01 M citrate buffer was added, and the flower bud was tapped with a dissection needle under a stereomicroscope until a fine cell suspension was formed. Then 10 - 20 µl of 60% acetic acid was added to the cell suspension and placed the slide on hot plate at 50 °C and the suspension was spread on the slide by circular stirring with a paper clip for 30 seconds without touching the slide surface (Ross *et al.* 1996; MANDÁKOVÁ AND LYSAK 2016). Later, 100 µl of freshly prepared 3:1 (3 parts ethanol & 1-part acetic acid) fixative was added around the suspension on the glass slide and administrating the last drop of the fixative in the middle of the suspension. Then, the extra fixative was discarded by tilting the slide and immediately dried with cold wind generated by a hairdryer. Following this, slides with well-spread mitotic chromosomes were selected using a phase-contrast light microscope. These selected slides were either used immediately or stored in 96% ethanol in a Coplin jar at -20 °C.

Murine chromosomes were obtained from the skin of a laboratory house mouse strain C57Bl6/J. Chromosome slide preparation was done as described in (POTLAPALLI *et al.* 2020).

3.4   Preparation of recombinant dCas9 protein

To obtain recombinant dCas9 protein, the *Streptococcus pyogenes* dead version of the Cas9 gene, with double nuclease mutations (D10A and H840A), was amplified using PCR primers with overhangs containing *Nco*I and *Hind*III restriction sites from the dCas9:3xPP7: GFP vector (KHOSRAVI *et al.* 2020c). All the primers used in this study were summarized in Appendix Table 1. Subsequently, the amplicon was cloned into pET22b+ (Invitrogen), a bacterial expression vector containing a C-terminal hexahistidine affinity tag (pET22b-dCas9-6xHis) using restriction-based cloning. For the construction of the dCas9-HRP vector, the HRP sequence was amplified using specific primers containing overhangs containing *Hind*III and *Not*I restriction sites from the vector pOCC30-dCas9-linker-HRP. This vector was kindly provided by the Dresden University of Technology (TU Dresden) (Dip gene project). The amplified sequences were cloned on the C terminus of dCas9 present in pET22b vector using restriction-based cloning. For the construction of ALFA-fused dCas9 vectors, various copies of the ALFA-tags were amplified from a synthetic DNA fragment (Eurofins genomics) (Table 2) that contained ALFA-tag sequences as a PCR template using specific primers featured overhangs containing either *Nco*I or *Hind*III and *Not*I restriction sites. These amplified ALFA-tag sequences were then cloned either at the N- or C-terminus of the dCas9 protein present in pET22b-dCas9-

6xHis vector using restriction-based cloning. The vector encoding for eGFP-NbALFA was obtained from Addgene (136626) (FARRANTS *et al.* 2020).

Plasmids were transformed into *Escherichia coli* Rosetta 2(DE3) using the heat shock transformation and plated on the LB plate (tryptone 10 g/l, yeast extract 5 g/l and NaCl 10 g/l, pH 7.0) supplemented with ampicillin 100 mg/L and chloramphenicol 30 mg/L. After selection of single colonies, they were inoculated into liquid LB medium and incubated overnight at 37 °C with shaking at 200 rpm. The following day, the overnight cultures were diluted 1:50 into fresh 2x TY media (tryptone 16 g/l, yeast extract 10 g/l and NaCl 5 g/l, pH 7.5) and grown at 37 °C until reaching an OD600 of 0.5. The cultures were then shifted to 18 °C and incubated for 1 h with shaking at 180 rpm. Protein expression was induced by adding isopropyl-β-D-1-thiogalactopyranoside (IPTG) to a final concentration of 0.5 mM, and the cells were grown at 18 °C with shaking at 180 rpm for 16 hours. Then, the cells were harvested by centrifugation at 6500 rpm for 20 min at 4 °C, and the resulting pellet was either used for protein purification on the same day or stored at -80 °C for future use.

The pellet was thawed on ice for 20 min, and then resuspended in lysis buffer (50 mM NaH_2PO_4, 500 mM NaCl, 10% glycerol, 10 mM imidazole, pH 8.0) containing 1 mg/ml lysozyme and Roche complete Protease inhibitor tablet (EDTA free). The suspension was transferred into a new 50 ml Falcon tube and lysed for 30 min on ice, with the cells stirred every 5 min using a glass rod. Subsequently, the cells were flash-frozen in liquid nitrogen and immediately thawed in water at RT. This was followed by sonication on ice for four cycles of 30 seconds each at 50% intensity using a Vibra-Cell Model VC60, Sonics & Materials, Inc. The lysate was then incubated on ice after adding Benzonase (Merck Millipore, 70746) to a final concentration of 1 μl/ml for 30 min, with stirring once every 5 min using a glass rod. Then, the lysate was centrifuged at 7000 rpm for 20 min at 4 °C, and the supernatant was transferred to a new 50 ml Falcon tube containing 1 ml of PureCube 100 Ni-NTA Agarose (Cube Biotech, 31103). The mixture was rotated at 4 °C for 90 min. Subsequently, the His-tagged proteins from the lysate were purified by gravity flow chromatography by passing the lysate through disposable polypropylene columns (Qiagen, 34924) and discarding the flow-through. Then, the column was washed twice with wash buffer (50 mM NaH_2PO_4, 500 mM NaCl, 10% glycerol, 20 mM imidazole, pH 8.0), and finally, the protein was eluted with elution buffer (50 mM NaH_2PO_4, 500 mM NaCl, 10% glycerol, 250 mM imidazole, pH 8.0) in 10 x 1 ml fractions

collected in 1.5 ml Eppendorf tubes. Next, the purified fractions were run on SDS-PAGE gel, and the fractions with higher protein concentration were pooled. The concentration of the purified proteins was determined using the Bradford assay, and then the proteins were stored at -20 °C for further use.

Table 2: List of synthetic ALFA-tag DNA fragment sequences

Name	Synthetic DNA sequences
1x ALFA-tag	CCATCACGTTTGGAAGAGGAACTGAGACGCCGCTTAACTGAACCT
3x ALFA-tags	CCCTCACGATTAGAAGAGGAACTAAGGAGACGCTTAACGGAACCGCCGAGCCGTCTCGAAGAAGAGCTCAGGAGACGCCTGACAGAACCACCGTCCAGATTGGAAGAGGAGCTGCGTCGTCGTTTGACCGAGCCG
6x ALFA-tags	CCCTCACGATTAGAAGAGGAACTAAGGAGACGCTTAACGGAACCGCCGAGCCGTCTCGAAGAAGAGCTCAGGAGACGCCTGACAGAACCACCGTCCAGATTGGAAGAGGAGCTGCGTCGTCGTTTGACCGAGCCGCCATCTCGCTTAGAGGAGGAACTGCGCAGGAGACTCACTGAACCGCCGTCAAGACTCGAGGAAGAACTCCGCAGAAGGTTAACTGAGCCACCCAGCAGATTAGAGGAGGAACTCCGTAGGCGTCTGACCGAACCT
12x ALFA-tags	CCCTCACGATTAGAAGAGGAACTAAGGAGACGCTTAACGGAACCGCCGAGCCGTCTCGAAGAAGAGCTCAGGAGACGCCTGACAGAACCACCGTCCAGATTGGAAGAGGAGCTGCGTCGTCGTTTGACCGAGCCGCCATCTCGCTTAGAGGAGGAACTGCGCAGGAGACTCACTGAACCGCCGTCAAGACTCGAGGAAGAACTCCGCAGAAGGTTAACTGAGCCACCCAGCAGATTAGAGGAGGAACTCCGTAGGCGTCTGACCGAACCTCCGTCTAGACTCGAAGAGGAGCTAAGGCGCAGGCTGACGGAGCCCCCTTCACGTTTGGAGGAAGAGTTACGTAGGCGCTTGACTGAACCCCCGTCTCGTTTAGAAGAAGAGCTACGTAGAAGATTGACGGAGCCGCCCTCTCGTCTTGAGGAAGAACTTAGGCGTAGATTAACCGAACCACCATCCCGTCTGGAAGAAGAGTTAAGGCGTAGATTGACTGAGCCACCCAGCCGACTCGAGGAAGAGCTTCGTAGGCGTTTAACCGAGCCG
6x ALFA-tags separated by linkers	GGTGGCGGAGGGTCTCCCTCACGATTAGAAGAGGAACTAAGGAGACGCTTAACGGAACCG GGCGGTGGAGGTTCCCCGAGCCGTCTCGAAGAAGAGCTCAGGAGACGCCTGACAGAACCA GGAGGTGGCGGGTCACCGTCCAGATTGGAAGAGGAGCTGCGTCGTCGTTTGACCGAGCCG GGGGGTGGCGGATCGCCATCTCGCTTAGAGGAGGAACTGCGCAGGAGACTCACTGAACCG GGGGGAGGCGGTAGTCCGTCAAGACTCGAGGAAGAACTCCGCAGAAGGTTAACTGAGCCA GGGGGAGGCGGTAGTCCCAGCAGATTAGAGGAGGAACTCCGTAGGCGTCTGACCGAACCT

3.5 Guide RNA and RNP complex preparation

To prepare functional guide RNA, we employed the bipartite guide RNA (crRNA and *trans*-activating crRNA (tracrRNA)) system (Alt-R CRISPR-Cas9) (JACOBI *et al.* 2017). To design the target-specific crRNA, 20-nucleotide-long target DNA sequences containing the corresponding PAM sequences of *S. pyogenes* Cas9 were selected, and the crRNAs were designed utilizing

the web-based tool CRISPRdirect (https://crispr.dbcls.jp/) (NAITO *et al.* 2014). Target-specific crRNA (Table 3) and 3' /5' labeled tracrRNAs were commercially produced and purchased from the company IDT (Integrated DNA Technologies, https://eu.idtdna.com). To prepare guide RNA, 20 µl of Nuclease-free duplex buffer (30 mM Hepes, pH 7.5; 100 mM CH_3CO_2K, provided by IDT) was added to 2 nmol of lyophilized crRNA and labeled tracrRNA to achieve a final concentration of 100 µM. The dissolved crRNA and tracrRNA were stored separately at -20°C. To prepare 10 µM guide RNA, 1 µl of 100 µM crRNA and 1 µl of 100 µM tracrRNA was mixed with 8 µl of nuclease-free duplex buffer. Both were hybridized in PCR tube and denatured for 5 min at 95 °C in a thermocycler and then stored at –20 °C. Then ribonucleoprotein complex (RNP) was assembled by mixing 1 µl (10 µM) of gRNA, 1 µl of dCas9 protein (1 µM), 10 µl of 10x Cas9 buffer (200 mM Hepes, pH 7.5, 1M KCl, 50 mM $MgCl_2$, 50% glycerol, 10% BSA, and 1% Tween 20), 10 µl of (10 mM) dithiothreitol (DTT), and 80 µl of ddH2O. The mixture was then incubated at 26 °C for 10 min and kept on ice until used. Prepared 100 µl of RNP complex was sufficient for 4 slides.

Table 3: List of crRNA sequences used

Species	probe name	crRNA sequence (5' – 3')	Target sequence, reference	CRISPR-FISH reference
Zea mays	Knob2	AAGGAAACATATGTGGGGTG	180 bp knob repeat, (ANANIEV *et al.* 1998)	(NĚMEČKOVÁ *et al.* 2019; POTLAPALLI *et al.* 2020)
Vicia faba	*Fok*1a	CGAGATTTTTGTTACTCCAA	*Fok*I repeat, (FUCHS *et al.* 1994a)	this study
Mus musculus	MS1a	CAGTTTTCTCGCCATATTCC	Major centromere satellite repeat, (Lehnertz et al., 2003)	(POTLAPALLI *et al.* 2020)

Allium fistulosum	AfiSat-375_1	TGACCGCTGTAAGCCGTCAA	Subtelomeric repeat (IRIFUNE *et al.* 1995)	this study
Allium fistulosum	AfiSat-375_2	GCCATAACCAGTCAAAACGA	Subtelomeric repeat (IRIFUNE *et al.* 1995)	this study
Allium cepa	AceSat-375_2	CTTCGGAGGGCCATAACTCT	Subtelomeric repeat (BARNES *et al.* 1985)	this study
Arabidopsis thaliana	Arabidopsis-type telomere	GGGTTTAGGGTTTAGGGTTT	Telomeric repeat (DREISSIG *et al.* 2017)	(ISHII *et al.* 2019)
Arabidopsis thaliana	Arabidopsis centromere	TTGAGAAGCAAGAAGAAGGT	Centromere repeat (MURATA *et al.* 1994)	(ISHII *et al.* 2019)

3.6 Standard CRISPR-FISH

The slides containing nuclei and chromosomes, fixed with a 3:1 solution of ethanol and acetic acid, as well as the formaldehyde-fixed *V. faba*, *A. fistulosum*, and *A. cepa* slides, were incubated in 0.2% Triton-X100 in 40 mM Tris-HCL (pH 9) at 37 °C for 30 min to enhance permeability. Subsequently, they were washed twice in 1x PBS for 5 min each at RT. Afterwards, 100 µl of 1x Cas9/1mM DTT in ddH2O was added to each slide and allowed to incubate for 5 min at RT. Subsequently, the buffer was removed by gently tilting the slides. Formaldehyde-fixed *A. thaliana* and *Z. mays* slides proceeded directly to the next step without incubating in Tris-HCL, following the previous step. Then, 25 µl of the RNP complex prepared using 5' Atto550 labeled tracrRNAs was added per slide and carefully covered with parafilm tape. The slides were then incubated at 37 °C for 1 hour or overnight at 4 °C in a humid chamber. After the incubation, the slides were washed in 1x PBS for 5 min and post-fixed with 4% formaldehyde in 1x PBS for 5 min. Subsequently, the slides were washed again with 1x

PBS. All the washing and post-fixation steps were performed at RT in the dark. Next, the slides were sequentially dehydrated in an ethanol series (70%, 90%, and 96%) for 2 min each at RT in the dark before being air-dried in the dark. Finally, 7 µl of VECTASHIELD solution containing (0.5 µg/ml) 4',6-diamidino-2-phenylindole (DAPI, Vector Laboratories, Burlingame, CA, USA) was applied to each slide, and they were stored at 4 °C for further microscopy.

3.7 Indirect CRISPR-FISH employing an anti-Cas9 antibody

After the standard CRISPR-FISH procedure and subsequent washing and post-fixation, the slides were blocked with 100 µl of 4% bovine serum albumin (BSA) in 1x PBS for 1 hour at RT in a humid chamber. Following this, the slides were washed in 1x PBS for 5 min at RT in dark. Then, 50 µl of a monoclonal anti-Cas9 mouse antibody (Santa Cruz Biotechnology, 7A9-3A3), diluted 1:300 in 2% BSA in 1x PBS, was added per slide and covered carefully with parafilm tape. The slides were incubated at 37 °C for 1 hour, followed by overnight incubation at 4 °C in a humid chamber. Subsequently, the slides were washed twice with 1x PBS for 5 min each on ice in the dark. Then, 50 µl of secondary anti-mouse Alexa 488 antibody (Thermo Fisher Scientific Inc. Massachusetts, USA, cat: A11001), diluted 1:200 in 2% BSA in 1x PBS, was applied per slide and covered with parafilm tape. The slides were then incubated at 37 °C for 1 hour in a humid chamber. Following this, the slides were washed twice with 1x PBS for 5 min each at RT in the dark. The subsequent steps of dehydration and counterstaining were performed as described for standard CRISPR-FISH.

3.8 Indirect CRISPR-FISH method with streptavidin FITC

The slides containing nuclei and chromosomes were incubated in 0.2% Triton-X100 in 40 mM Tris-HCL (pH 9) at 37 °C for 30 min to enhance permeability. Subsequently, they were washed twice in 1x PBS for 5 min each at RT. Afterwards, 100 µl of 1x Cas9/1mM DTT in ddH2O was added to each slide and allowed to incubate for 5 min at RT. Then, 25 µl of the RNP complex prepared using 3' biotin labeled tracrRNAs was added per slide and carefully covered with parafilm tape. The slides were then incubated at 37 °C for 1 hour or overnight at 4 °C in a humid chamber. After the incubation, the slides were washed in 1x PBS for 5 min and post-fixed with 4% formaldehyde in 1x PBS for 5 min. Subsequently, the slides were washed again with 1x PBS. All the washing and post-fixation steps were performed at RT. Then the slides were blocked with 100 µl of 4% BSA in 1x PBS for 1 hour at RT in a humid chamber. Following

this, the slides were washed in 1x PBS for 5 min at RT in the dark. Then, 50 µl of a streptavidin conjugated to FITC (Sigma-Aldrich, S3762) (1:100 diluted) in 1% BSA in 1x PBS, was added per slide and covered carefully with parafilm tape. The slides were then incubated at 37 °C for 1 hour in a humid chamber. Following this, the slides were washed twice with 1x PBS for 5 min each at RT in the dark. The subsequent steps of dehydration and counterstaining were performed as described for standard CRISPR-FISH.

3.9 Fluorescence *in situ* hybridization (FISH)

FISH using a labeled oligo probes specific for *A. thaliana* centromere (5`-biotin - ACACCATGAAAGCTTTGAGAAGCAAGAAGAAGGTTGGTTA) (MURATA *et al.* 1994) and telomere (5`-biotin -GGGTTTAGGGTTTAGGGTTTAGGGTTTAGGGTTT) (DREISSIG *et al.* 2017) (Table 1) was performed as described in (MA *et al.* 2008). The slides containing nuclei or chromosomes were prepared as described previously. The slides were washed with 2x saline sodium citrate (SSC: 0.30 M sodium citrate, 0.030 M NaCl, pH 7.0) for 5 min each at RT. This was followed by incubation in 45% acetic acid for 10 min, also at RT. Later, the slides were washed again in 2x SSC for 5 min each at RT. Subsequently, the slides were fixed in 4% formaldehyde in 1x PBS for 10 min at RT. To remove excess fixative, the slides were then rinsed twice with 2x SSC for 5 min each. Following this, the slides were sequentially dehydrated in an ethanol series (70%, 90%, and 96%) for 2 min each, before being air-dried. Then, 20 µl of hybridization buffer (50% (vol/vol) formamide, 10% (vol/vol) dextran sulfate in 2x SSC) containing 2 µl of oligo probe (10 µM) was added to each slide under a 22 x 22 coverslip. The DNA was denatured by baking the slides at 80 °C for 2 min on a hot plate. Subsequently, the slides were incubated overnight at 37 °C in a humid chamber. The next day, the coverslips were removed from the slides by washing them in 2x SSC for 5 min at RT. Subsequently, another 5-minute wash in 2x SSC was performed at RT. To prevent nonspecific probe binding, the slides were then incubated in 2x SSC at 58 °C in water bath for 20 min. Later the slides were transferred to 2x SSC at RT for 2 min. The blocking, streptavidin FITC detection, and washing steps were carried out as outlined for indirect CRISPR-FISH. Following these steps, dehydration and counterstaining were performed as described for standard CRISPR-FISH.

3.10 Counterstaining of specimens with nuclear dyes

Different non-fluorescent dyes were tested for nuclear staining, with the intention of combining them with the chromogenic detection method. Methyl green (Sigma, M8884-5G), methylene green, neutral red (Feinchemie K.-H. Kallies KG), naphthol green B (Waldeck, 1B-385), hematoxylin, and methylene blue (Merck, 115943) were tested on formaldehyde-fixed nuclei of *A. thaliana* and *V. faba*. For counterstaining, 300 µl of each dye was added to the respective slide.

3.11 CRISPR-CID - CRISPR Cas9 mediated chromogenic *in situ* detection

CRISPR-CID was conducted similarly to indirect CRISPR-FISH, employing biotinylated RNP complexes until post-fixation, washing, and blocking stages. Subsequently, the slides were washed twice in 1x PBS for 5 min each. Then 50 µl of streptavidin-conjugated alkaline phosphatase (AP) (ZytoChem Plus AP Kit, AP008RED) or horseradish peroxidases (HRP) (Permanent HRP Green Kit, ZUC070-100) was added per slide and carefully covered with parafilm tape. The slides were then incubated at 37 °C for 1 hour in a humid chamber. Subsequently, the slides were washed twice in 1x PBS at RT. In both cases, the area of the slide containing nuclei or chromosomes was marked by drawing a circle around the sample using a PAP pen to create a hydrophobic barrier. Later for AP detection, 50 µl of permanent red buffer with 0.8 µl of permanent red concentrate (ZytoChem Plus AP Kit, AP008RED) was added per slide. For HRP detection, 50 µl of HRP green substrate buffer with 4.5 µl of HRP green chromogen (Permanent HRP Green Kit, ZUC070-100) was added per slide. In both cases, the chromogenic substrate was incubated at RT in the dark in a humid chamber until the red/green color developed, typically over 10 min. The development of color intensity was monitored using a light microscope. The slides were subsequently washed in ddH2O for 2 min at RT. Following this, the slides were counterstained with a nuclear dye for 2 min. Subsequently, they were rinsed with tap water and air-dried. Finally, the slides were mounted with Entellan (Merck), allowed to air-dry, and analyzed using light microscopy.

3.12 Standard and indirect CRISPR-FISH and CRISPR-CID signal quantification

For quantification, nuclei were isolated from leaf tissues of *A. thaliana* and *Z. mays* fixed in 4% (Ishii *et al.* 2019) and 2% (Němečková *et al.* 2019) formaldehyde, respectively, following the method described above. After the nuclei were isolated, 2C nuclei were sorted using a BD

Influx cell sorter (BD Biosciences) by detecting DAPI fluorescence using laser excitation of 200 mW at 355 nm and a 450/40 bandpass filter. Next, microscopic slides were prepared from the sorted 2C nuclei using cytospin, following the method described above. These slides were utilized for standard and indirect CRISPR-FISH and CRISPR-CID labeling of repeats employing specific gRNAs. Following CRISPR labeling, signals of centromere and knob repeats from 50 flow-sorted 2C nuclei per analysis were quantified. Statistical analysis and Box plots were prepared using the ggplot2 library in RStudio's version 1.4.1717 (https://rstudio.com/).

3.13 CRISPR-FISH with ALFA-tagged dCas9

RNP complexes were prepared using dCas9 protein fused with ALFA-tags, target-specific crRNA, and Atto550 tracrRNA as described previously. CRISPR-FISH labeling with ALFA-tagged dCas9 was carried out following the standard CRISPR-FISH protocol until post-fixation and washing. Slides were then blocked with 100 µl of 4% BSA in 1x PBS for 1 hour at RT in a humid chamber. Subsequently, the slides were washed with 1x PBS for 5 min at RT in the dark. Next, 50 µl of NbALFA conjugated with ATTO488 (FluoTag®-X2 anti-ALFA, Cat No: N1502, NanoTag Biotechnologies GmbH) diluted 1:500 in 2% BSA in 1x PBS, or 50 µl of eGFP-NbALFA (1 µM) in 2% BSA in 1x PBS was added per slide and covered carefully with parafilm tape. The slides were then incubated at 37 °C for 1 hour in a humid chamber. Following this, the slides were washed twice with 1x PBS for 5 min each at RT in the dark. Subsequent steps of dehydration and counterstaining were performed as described in the standard CRISPR-FISH protocol.

In case of using a minibody (Recombinant sdAb anti-ALFA rabbit Fc-fusion, Cat No: N1583, NanoTag Biotechnologies GmbH) for detection of ALFA-tagged RNP complexes, after blocking and washing with 1x PBS in the dark, 50 µl of minibody diluted 1:500 in 2% BSA in 1x PBS was added per slide and covered carefully with parafilm tape. The slides were then incubated at 37 °C for 1 hour in a humid chamber. Following this, slides were washed twice in 1x PBS for 5 min each at RT in the dark. Then probed with 50 µl of anti-rabbit Alexa 488 antibody diluted 1:100 in 2% BSA in 1x PBS was added per slide and covered carefully with parafilm tape. The slides were then incubated at 37 °C for 1 hour in a humid chamber. Following this, the slides were washed and dehydrated and counterstained as described for standard CRISPR-FISH.

3.14   Preparation vectors suitable for CRISPR live imaging

CRISPR imaging vectors were prepared using Golden Gate cloning with type IIS enzymes (*Bpi*I and *Bsa*I) and the MoClo Toolkit (The MoClo Toolkit was a gift from Sylvestre Marillonnet, Addgene kit # 1000000044) (WEBER *et al.* 2011; WERNER *et al.* 2012) as described by Marillonnet and Grützner (2020). For DNA targeting, the dead version of the Cas9 gene with double nuclease mutations (D10A and H840A) from *S. pyogenes* optimized for *Arabidopsis* codons was employed (DREISSIG *et al.* 2017). First, all individual components, including *Sp-dCas9*, *z.dCas9i*, 6xALFA-tags, 3x *eGFP*, *mRuby*, *NbALFA*, *RPS5A* promoter, *Ubi4* promoter, *Pea3A* terminator, *rbcSE9* terminator, and *U6 (At-26)* promoter, were amplified using specific primer sets (Appendix Table 1). The primers utilized featured overhangs containing *Bpi*I restriction sites (5'-gaagac) along with 4-nt fusion sites, corresponding to the level-0 vector employed (Table 4). The *Sp-dCas9*, 3x *eGFP*, *mRuby*, *Ubi4* promoter, *U6 (At-26)* promoter and *Pea3A* terminator were amplified separately from previously described vectors Sp-dCas9-eGFP and Sp-dCas9-mRuby (Dreissig et al. 2017). *NbALFA* fragment was amplified from the vector pET51b(+)_eGFP_NbALFA . This vector was a gift from Kai Johnsson (Addgene plasmid # 136626; http://n2t.net/addgene:136626; RRID: Addgene_136626) (FARRANTS *et al.* 2020). *RPS5A* promoter and *rbcSE9* terminator was amplified from dCas9:2xMS2:GFP. The 6x ALFA-tags with GGGGS linker were amplified from a synthesized DNA fragment obtained from Eurofins Genomics (Table 2). Similarly, to generate the CRISPR imaging constructs comprising four copies of the nuclear localization sequence (NLS), *Sp.dCas9*, and 6x ALFA-tags (GS), was amplified separately as described above. Primers were specifically designed to integrate two NLS sequences on both the N and C termini of Sp.dCas9 and 6x ALFA-tags.

In the case of *z.dCas9i*, primers were designed to introduce the point mutations (D10A and H841A) in the RuvC1 and HNH nuclease domains of zCas9i using the GoldenMutagenesis web tool (https://msbi.ipb-halle.de/GoldenMutagenesisWeb/) as described in (PÜLLMANN *et al.* 2019). These primers were used to amplify the *zCas9i* sequences, which included 2x NLS sequences as two separate fragments containing *Bpi*I restriction sites (5'-gaagac) along with 4-nt fusion sites from the Addgene vector pAGM47523. This vector was a gift from Sylvestre Marillonnet (Addgene plasmid #153221; http://n2t.net/addgene:153221; RRID: Addgene_153221) (GRÜTZNER *et al.* 2021). All the primers used in this study was summarized in Appendix Table 1.

Next, these amplified components were individually cloned into various Level-0 vectors (Table 4) through Golden Gate cloning reactions using the *Bpi*I restriction enzyme, following the protocol described by Weber et al. (2011). The resulting cloning products were transformed into *E. coli* strain DH10B through electroporation and were then plated on LB plates supplemented with spectinomycin, IPTG, and X-gal. Efficient cloning of the insert into the level-0 vector yielded white colonies, which were then selected. Then, insert sequences were confirmed using Sanger and nanopore sequencing platforms provided by Eurofins GmbH, Germany. After verification, the transcript units were assembled into the Level-1 vector pICH47761. These units consisted of the UBi4 promoter followed by Sp.dCas9 or z.dCas9i, 3x eGFP, 6x ALFA GS, and the Pea3A terminator. For constructs involving Sp.dCas9, they included either 1 or 4 NLS sequences, while for those with z.dCas9i, they specifically contained 4 NLS sequences. Similarly, transcript units containing RPS5A promoter - mRuby-NbALFA - rbcSE9 terminator, were assembled into Level-1 vector pICH47751. Additionally, a transcript unit comprising the U6 (At-26) promoter and telomere sgRNA for Sp.dCas9 was cloned into a level-1 vector pICH47742. This was achieved by combining a level-0 vector containing the U6 (At-26) promoter and telomere sgRNA with a scaffold sequence, which was amplified from the previously mentioned vector (Sp-dCas9-eGFP) using primers.

These transcripts were assembled into level-1 vectors using the Golden Gate cloning reaction using the *Bsa*I restriction enzyme, following the protocol described by Weber et al. (2011). The cloned products were transformed into *E. coli* and plated on LB plates supplemented with ampicillin, IPTG, and X-gal. White colonies were selected, and confirmation was carried out through restriction digestion. Finally, constructs containing Sp. dCas9-3x eGFP-ALFA-tag with *A. thaliana* telomere sgRNA under the U6 promoter, and z.dCas9i-3x eGFP-ALFA-tag with *A. thaliana* telomere sgRNA under the U6 promoter, as well as mRuby-NbALFA expressing constructs, were each cloned into Level-2 vectors pAGM4723, using Golden Gate cloning with the *Bpi*I restriction enzyme, following the procedure described previously. The cloned products were then transformed into *E. coli* and plated on LB plates supplemented with kanamycin. Subsequently, white colonies were selected and confirmed through restriction digestion.

Table 4: Level 0 modules used in this study

Level-0 modules	Relevant characteristics
pICH41258	Sp.dCas9-NLS
pICH41258	Sp.dCas9-2xNLS
pICH41258	z.dCas9i-2xNLS
pICH41295	Ubi4 promoter
pICH41295	RPS5A promoter
pICH41276	Pea3A terminator
pICH9121	rbcSE9 terminator
pAGM1299	3x eGFP
pICH41295	U6 (At-26) promoter
pAGM1301	6x ALFA-tag (GS)
pAGM1301	6x ALFA-tag (GS)-2xNLS
pAGM1299	NbALFA
pICH41258	mRuby

3.15 Transient transformation of *N. benthamiana* with CRISPR live imaging construct

All the level-2 plant expression vectors were individually introduced into the *Agrobacterium tumefaciens* strain GV3101 via electroporation. They were then plated on YEB (beef extract 5 g/l, tryptone 5 g/l, sucrose 5 g/l, yeast extract 1 g/l, MgSO4 300 mg/l, agar 20 g/l, pH 7.2), plates supplemented with 50 mg/ml rifampicin and 100 mg/ml kanamycin and incubated at 28 °C for 48 hours. Subsequently, Agrobacteria carrying the expression vectors were cultured overnight at 28 °C in YEB medium supplemented with antibiotics. The Agrobacteria culture was then centrifuged, and the pellet was resuspended in an infiltration buffer (10 mM MgCl2, 10 mM MES, pH 5.6). The optical density at 600 nm (OD600) was determined and adjusted to OD600 0.8, followed by incubation in the dark at RT for 90 min. The bacteria were then injected into *N. benthamiana* leaves using the syringe method as described by (PHAN AND CONRAD 2016). The infiltrated plants were subsequently grown in a greenhouse under 16/8 hours light/dark conditions at a temperature of 22 °C for 48 hours. For co-transformation experiments, bacterial cultures with an equivalent OD600 of 0.8 were mixed in a 1:1 ratio prior

to the transformation process. Plant samples were analyzed by microscopy after 48 hours of infiltration. *In vivo* fluorescence signals were visualized by cutting a portion of the infiltrated leaf and utilizing a 60x NA 1.2 water objective.

3.16   Immunostaining and fluorescence *in situ* hybridization (FISH)

For immunostaining, after 48 hours of transient expression, leaf tissue expressing dCas9-3x eGFP-ALFA-tag along with telomere sgRNA was fixed in 4% formaldehyde, as described previously. Then, leaf nuclei were extracted using LB01 buffer, filtered, and spun onto a glass slide with a CytoSpin3 (Shandon) at 500 rpm for 5 min using 200 µl of nuclei suspension. The slides were washed twice in 1x PBS for 5 min each. Then, the slides were blocked with 100 µl of 4% bovine serum albumin (BSA) in 1x PBS and carefully covered with parafilm tape. They were then incubated at RT for 60 min in a humid chamber. The slides were washed twice in 1x PBS for 5 min each. Subsequently, 50 µl of GFP antibody (directly labeled GFP mouse antibody Dylight 488; Rockland, cat. 200-341-215) in 2% BSA (diluted at a 1:2500 dilution) in 1x PBS was applied. The slides were carefully covered with parafilm tape and incubated at RT for 1 hour in a humid chamber.

To combine immunostaining with FISH, the immunostained slides were washed twice in 1x PBS for 5 min each at RT in the dark. Subsequently, the slides were dehydrated in an ethanol series (70%, 90%, and 96%) for 2 min each at RT and air-dried in the dark. Then, the slides were fixed in a 3:1 fixative (3-parts ethanol and 1-part acetic acid) for 24 hours in dark. Later, the slides were sequentially dehydrated in an ethanol series (70%, 90%, and 96%) for 2 min each at RT and air-dried in the dark. Afterwards, an overnight pre-hybridization was performed at 37 °C by adding 15 µl of hybridization buffer (containing 50% (vol/vol) formamide, 10% (vol/vol) dextran sulfate in 2x SSC). The slides were carefully covered with parafilm tape and incubated overnight in a humid chamber at 37 °C. Following this, the slides were washed twice in 2x SSC for 5 min each at RT in the dark and then sequentially dehydrated in an ethanol series (70%, 90%, and 96%) for 2 min each at RT before being air-dried in the dark. Then the chromosomal DNA was denatured by incubating the slides in the denaturing solution (0.2 M NaOH in 70% ethanol) for 10 min at RT in the dark and subsequently incubated in ice-cold 1x PBS for 1 minute at RT in the dark. Next, the slides were sequentially dehydrated in an ethanol series (70%, 90%, and 96%) for 2 min each at RT before being air-dried in the dark. Then, 14 µl of FISH hybridization solution along with 1 µl of 5' Cy5-labeled telomere

oligonucleotide probe (10 µM) (Supp. Table 1) was added per slide and covered with coverslips, followed by hybridization at 37 °C overnight in a humid chamber. The slides were then washed twice in 2x SSC for 5 min each at RT in the dark and then sequentially dehydrated in an ethanol series (70%, 90%, and 96%) for 2 min each at RT before being air-dried in the dark. Finally, 8 µl of VECTASHIELD solution containing DAPI (1:1000) was applied to each slide and stored at 4 °C until further microscopy.

3.17 Detection of live telomere signals with minibody

For the subsequent minibody-based detection of CRISPR-ALFA-tag live telomere signals, nuclei slides were prepared from the *N. benthamiana* leaf expressing dCas9-3x eGFP-ALFA-tag along with telomere sgRNA as described previously. Slides were then washed twice in 1x PBS for 5 min each and blocked, followed by detection with minibody, and subsequently detected with a secondary goat anti-rabbit Alexa 555 antibody as described above.

3.18 Tyramide-based signal amplification of CRISPR-FISH signals

For tyramide-based amplification, CRISPR-FISH was initially performed as previously described using 3' biotinylated tracrRNA until post-fixation, followed by washing for 5 min in 1x PBS at RT. Tyramide signal amplification was conducted using the Biotin XX Tyramide SuperBoost™ Kit, Streptavidin (Cat no: B40931, ThermoFisher), following the manufacturer's instructions. Subsequently, slides were blocked with 2 - 3 drops of blocking buffer for 30 min at RT in a humid chamber, followed by washing in 1x PBS for 5 min. Then, 2 - 3 drops of HRP-conjugated streptavidin per slide were applied and carefully covered with parafilm, followed by incubation for 1 hour at RT in a humid chamber. A working solution of tyramide was prepared by mixing 5 µl of 100x Tyramide stock solution, 5 µl of 100x H_2O_2 solution, and 500 µl of 1x reaction buffer, which was then mixed by vortexing and stored on ice until used. This prepared tyramide working solution would be sufficient for 5 slides. Post-incubation with HRP-conjugated streptavidin, slides were washed thrice in 1x PBS for 5 min each at RT. Then, 100 µl of tyramide working solution was added per slide and incubated in a humid chamber for 10 min at RT in the dark. The reaction was terminated by adding 100 µl of reaction stop reagent for 1 minute at RT. The slides were washed thrice in 1x PBS for 5 min each at RT. Later, slides were incubated with 50 µl of streptavidin-conjugated FITC (S3762, Sigma-Aldrich) diluted 1:50 in 1% BSA in 1x PBS per slide at 37 °C for 1 hour in a humid chamber. Subsequently, the slides

were washed thrice in 1x PBS for 5 min each in the dark, dehydrated, and counterstained as described for standard CRISPR-FISH.

3.19   CRISPR-FISH with pepper sgRNA

Telomere sgRNA fused with 4 and 8 copies of pepper aptamers were commercially produced and supplied by Daicel Arbor Biosciences, USA. RNP complexes were assembled by mixing 1 µl (10 µM) of pepper sgRNA, 1 µl of dCas9 protein fused with ALFA-tags (1 µM), 10 µl of 10x Cas9 buffer, 10 µl of (10 mM) DTT, and 80 µl of ddH2O. The mixture was then incubated at 26 °C for 10 min and kept on ice until used. Prepared 100 µl of RNP complex was sufficient for 4 slides. CRISPR-labeling was performed as described above using ALFA-tagged dCas9 and detection with minibody and secondary goat anti-rabbit Alexa 555 antibody as described above.

3.20   Indirect CRISPR-FISH with quantum dots (QD)

This was performed as described for indirect CRISPR-FISH until blocking and washing in 1x PBS. Then specimens were incubated with 50 µl Streptavidin conjugated QD CPN^{TM} 510 (510BS04, Stream Bio, UK) (1:100 diluted) in 1% BSA in 1xPBS for 60 min at 37 °C under parafilm in a humid chamber followed by washing thrice for 5 min each in 1x PBS at RT in the dark. The subsequent steps of dehydration and counterstaining were performed as described for standard CRISPR-FISH.

3.21   Fluorescence microscopy

Microscopic images were captured using an epifluorescence microscope (Olympus BX61) equipped with a cooled charge-coupled device (CCD) camera (Orca ER; Hamamatsu). All fluorescence images were initially captured in grayscale and later pseudo-colored using ImageJ software for analysis and visualization. Chromogenic in situ imaging was performed using the Axiophot light microscope (Carl Zeiss) equipped with an Axiocam 506 color camera.

Live imaging of probes were examined in a Zeiss LSM980 confocal laser scanning microscope (Carl Zeiss, Jena, Germany) with a C-apochromat 40x /1.2 water objective. Nuclear GFP and mRuby signals were analyzed using appropriate filters. Image size was 518 x 206 pixels, pixel dwell time 1,56 µs and pinhole set at 40 µm. For time series Z-stacks with 0,6 µm intervals were recorded every 30 seconds.

3.22 CRISPR-FISH signal quantification

For the quantification of CRISPR-FISH ALFA-tag signals, a standardized protein concentration of 1 mg/ml of all dCas9-ALFA variants fused with various copies of the ALFA-tag was applied for labeling *A. thaliana* centromere repeats as described above. Subsequently, all fluorescence images were captured with a CCD camera using an exposure time of either 100 ms or 50 ms, and ImageJ software was employed to measure the signal intensities. In brief, each nuclear area was defined using the threshold function in ImageJ (Fig. 7). Measurements, including area, mean, minimum and maximum grey values, and integrated density, were then recorded for both green (anti-rabbit antibody Alexa488 - minibody) and red (tracrRNA labeled with Atto550) channels within the identified nuclear regions. Additionally, equivalent measurements were taken inside the nuclear areas, excluding centromere signals in both red and green channels, to calculate the nuclear background. Subsequently, the nuclear background was subtracted from the actual target signals to determine the green and red signal intensities. To compensate for potential slide-to-slide and experiment-to-experiment variations as well as different exposure times the red tracrRNA signal was considered as a reference to calculate the relative green fluorescence intensities as green/red signal ratios. Box plots were prepared using an online tool BoxPlotR, (http://shiny.chemgrid.org/boxplotr/).
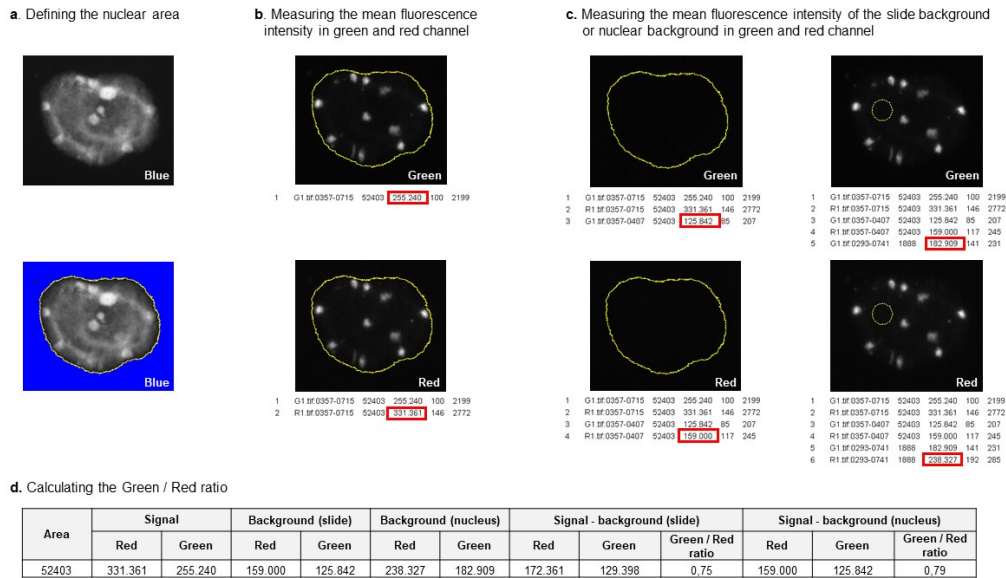
Fig 7: Workflow of the CRISPR ALFA-tag signal quantification using ImageJ: (A) First, the nuclear area was delineated using the threshold function. (B) Various measurements were then collected from the designated area in both the green and red channels. (C) Similarly, equivalent measurements were taken within the nuclear regions, with centromere signals excluded, in both the red and green channels. (D) The nuclear background was subtracted from the actual target signals to calculate relative fluorescence intensities.

3.23 Statistical analysis

To evaluate if the observed differences in relative signal intensities are significant, we initially performed the parametric one-way analysis of variance (ANOVA). Since the normality test failed, we finally used the non-parametric Kruskal-Wallis test. Subsequently, a pairwise multiple comparison was done (Dunn's method) (DUNN 1961).

3.24 Indirect CRISPR-FISH method with FluoroNanogold

Indirect CRISPR-FISH with FluoroNanogold was performed as described for indirect CRISPR-FISH until blocking and washing in 1x PBS. Then specimens were incubated with 50 µl Fluorescein FluoroNanogold-Streptavidin conjugate (7016, Nanoprobes, USA) (1:100 diluted) in 1% BSA/1xPBS for 90 min at RT under parafilm in a humid chamber followed by washing thrice for 5 min each in 1x PBS and then proceeded as described for silver enhancement.

3.25 Silver enhancement of FluoroNanogold

After the incubation with Fluorescein-FluoroNanogold-Streptavidin (7016, Nanoprobes, USA, diluted 1:100) conjugate or Alexa Fluor 488 FluoroNanogold-Fab anti-rabbit IgG (7204,

Nanoprobes, USA, diluted 1:100), followed by three washes with 1x PBS in the dark, the slides were treated with 50 mM glycine in 1x PBS for 5 min at RT in the dark. Subsequently, the slides were washed three times for 5 min each in 1x PBS followed by two washes in ddH20 for 5 min each at RT in the dark.

The 1.4 nm gold particles were enhanced using the HQ SILVER™ ENHANCEMENT KIT (2012, Nanoprobes, USA). The HQ SILVER working reagent was prepared by first adding equal volumes of Dispensing Initiator (A) and Moderator (B) to a 1.5 ml Eppendorf tube and vortexing to mix. An equal volume of Activator (C) was then added to the same 1.5 ml Eppendorf tube and mixed by vortexing (Note: components A, B, and C should be allowed to thaw to RT before preparing the HQ Silver working reagent). The slides were incubated with 100 µl of prepared HQ SILVER reagent in the dark for various times ranging from 3 to 25 min and then washed five times in ddH20 for 1 minute each at RT in the dark. Finally, they were air-dried in the dark, and non-fluorescent signals were analyzed using light microscopy.

3.26   Indirect CRISPR-FISH employing an anti-FITC antibody

To employ the rabbit anti-FITC antibody, the target DNA was first labeled with biotinylated RNP complex and subsequently detected using streptavidin-FITC for 1 hour at 37 °C. Then slides were washed three times in 1x PBS for 5 min each at RT in the dark, and further incubated with 50 µl of anti-FITC rabbit antibody (80003–1-RR, Proteintech, diluted 1:100) diluted in 1% BSA in 1x PBS for 1 h at 37 °C under parafilm in a humidity chamber. These slides were washed three times in 1x PBS for 5 min each at RT and further incubated with anti-rabbit antibody conjugated to Alexa 555 (1:100 diluted) diluted in 1% BSA in 1x PBS for 1 h at 37 °C under parafilm in a humidity chamber, followed by three washes in 1x PBS for 5 min each in the dark. Subsequently, slides were dehydrated, and counterstained as described for standard CRISPR-FISH. For silver enhancement, after incubation with rabbit anti-FITC antibody and further washing with 1x PBS, slides were incubated with 50 µl of Alexa Fluor® 594 FluoroNanogold anti-rabbit Fab (7304, Nanoprobes, USA, diluted 1:100) in 1% BSA in 1x PBS for 90 min at 26 °C under parafilm in a humidity chamber and then proceeded as described for silver enhancement.

3.27   Immunostaining of *B. napus* using anti-CENH3

4% formaldehyde-fixed *B. napus* nuclei slides were prepared as described previously (Isнɪɪ *et al.* 2019). After washing twice in 1x PBS at RT, slides were blocked with 100 µl of 4% BSA in 1x PBS under parafilm for 30 min at RT in a humid chamber, and then washed for 5 min in 1x PBS. Then, 50 µl of primary antibody (rabbit anti-CENH3 antibody, specific for *B. napus*, diluted 1:100, kindly provided by N. Ohmido, Kobe, Japan) in 1% BSA in 1x PBS was applied per slide and incubated at 4 °C overnight under parafilm in a humid chamber. The slides were washed three times in 1x PBS for 5 min each at RT and further incubated with secondary goat anti-rabbit Alexa 555 (diluted 1:100) in 1% BSA in 1x PBS for 1 hour at 37 °C under parafilm in a humid chamber, followed by three washes in 1x PBS for 5 min each in the dark. Subsequently, slides were dehydrated, and counterstained as described for standard CRISPR-FISH. For silver enhancement, following the incubation with rabbit anti-CENH3 antibody and subsequent washing with 1x PBS, slides were incubated with 50 µl of Alexa Fluor® 488 FluoroNanogold™-Fab' anti-rabbit IgG in 1% BSA in 1x PBS for 90 min at 26 °C under parafilm in a humidity chamber. After this incubation, the slides proceeded as described for silver enhancement.

3.28   Resin embedding and sectioning

Resin embedding of specimens was carried out using the TAAB 812 Resin kit (T024, Taab Laboratory Equipment Ltd). To prepare 10 ml of resin, 2.65 g MNA, 5.40 g Epson 812, 1.95 g DDSA and 0.15 g DMP-30 were added in sequence to the glass bottle placed on a magnetic stirrer and mixed with a stirring rod until a homogeneous orange solution was observed. (Note: The prepared resin can be kept at RT if used on the same day, otherwise it should be stored at 4 °C for use the following day. Each slide requires 1.5 ml of resin to prepare the block). To improve the transfer of the fixed samples from the coverslip to the resin block and to improve the imaging of the samples with TEM, the coverslips were coated with the 15 nm carbon film using the Jeol JEE-420D vacuum evaporator. Later, the carbon-coated coverslips were attached to the glass slide using a fixogum, and then the formaldehyde-fixed nuclei were spun onto the carbon-coated coverslip using a Cytospin at 700 rpm for 5 min. The coverslips were then dehydrated using freshly prepared ethanol series (70%, 80%, 90% and 100%) for 10 min each and air dried at RT.

The use of ACLAR film as a surface substrate for the preparation of chromosome spreads improved the transfer of metaphase chromosomes from film to resin (Gнаzɪzаdeн *et al.* 2008).

To improve the transfer of 3:1 (ethanol: acetic acid) fixed metaphase chromosomes from the slide to the resin, we used ACLAR® Embedding Film (0.2 mm thickness) (10501, Ted Pella, USA) as a substrate for dropping the chromosome spreads. The ACLAR film was cut to the size of a coverslip (24 x 32 mm) and glued to the glass slide using MGK-S mounting solution (Matsunami Glass Ind., Ltd, Japan) and dried overnight in an oven at 40 °C. Then, the 3:1 fixed *V. faba* chromosomes were dropped onto the ACLAR film on the glass slide placed on the heating plate at 55 °C, and later the slide was dried and the regions of the chromosomes were marked by observation under a light microscope.

To prepare the resin block, nuclei and chromosomes with a carbon-coated coverslip / ACLAR film glued to the slide were placed in a 1.5 ml Eppendorf tube so that the sample area touched the tube filled with the prepared resin, and then both the tube and the slide were inverted to ensure that the sample on the slide was covered with the resin. The Eppendorf tube containing the resin was then incubated together with the slide at 40 °C for 24 hours, followed by 60 °C for 3 days in an incubator. The coverslip was then carefully removed from the hardened resin in the Eppendorf tube with the tweezers, and the tube was cut open with the blade to release the block of resin.

3.29   Sectioning of resin blocks and electron microscopy

Using a Leica EM UC7 ultramicrotome (Leica Microsystems, USA), 10 μm ultrathin sections were cut from the resin block mounted on the stage using the carbon layer as a guide. The microtome sections were then collected on Formvar/Carbon 200 mesh TH, gold grids (01803G, Ted Pella, USA) and examined using a Hitachi H7500 transmission electron microscope (TEM) equipped with a Morada G2 CCD camera and images taken at an accelerating voltage of 80 kV.

To observe the surface structure of the fixed nuclei or chromosomes, isolated nuclei and chromosomes were directly spun on the round shape carbon seal (7300, NISSHIN EM CO. LTD, Japan) glued on the glass slide. Then nuclei containing carbon seal was mounted on the aluminum specimen mounts and surface structures were examined using Hitachi S-4800 high-resolution scanning electron microscope (SEM).

4. Results

4.1 CRISPR-CID - an *in situ* chromogenic DNA repeat detection system for research and life science education

4.1.1 Application of anti-Cas9 for the detection of dCas9-binding sites

High-copy repeats in fixed chromosomes and nuclei can be fluorescently labeled using CRISPR-FISH (Ishii *et al.* 2019; Potlapalli *et al.* 2020). To explore the possibility of using the CRISPR/dCas9 approach to detect repeats non-fluorescently, a new CRISPR-FISH strategy should be developed to indirectly label the DNA repeat. This is necessary as non-fluorescent labeling of DNA repeats will only be possible in an indirect manner. Therefore, it will be necessary to test first if indirect detection systems work at all. Therefore we amimed to establish an indirect CRISPR-FISH variant by combining immunofluorescence with standard CRISPR-FISH. In this approach, ATTO550-tagged bipartite gRNA-guided CRISPR-FISH will be combined with a Cas9-specific antibody and an anti-mouse conjugated FITC. In principle, once the CRISPR-dCas9 RNP complex binds to the target DNA, an anti-Cas9 mouse antibody is employed to detect the DNA sites bound by the RNP (Fig. 8A). Subsequently, these sites are indirectly detected using the anti-mouse FITC conjugate (Fig. 8A). To test this strategy we tried labeling centromere and knob repeats on formaldehyde fixed *A. thaliana* and *Z. mays* nuclei respectively using previously reported crRNAs. This resulted in green labeling of centromere and knob repeats, accompanied by background noise in their respective nuclei (Fig. 8B). Further colocalization of indirect anti-Cas9 (green) and tracrRNA-Atto (red) signals proves the functionality of the indirect CRISPR-FISH method (Fig. 8B). Overall, these results demonstrate the efficient indirect labeling of DNA repeats by combining CRISPR-FISH with a Cas9 antibody.
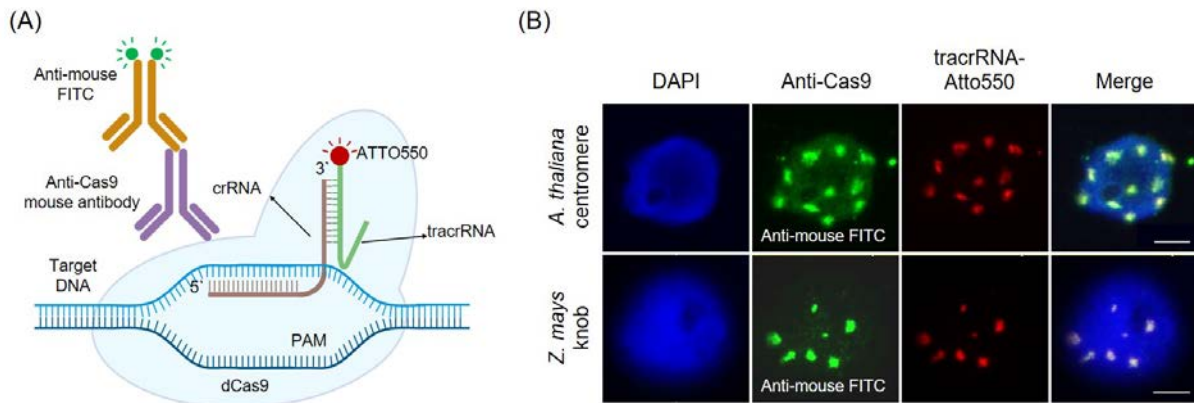
Fig 8: (A) Schematic of indirect CRISPR-FISH to label repeat sequences with Cas9 antibody and later detection with anti-mouse FITC. (B) Visualization of centromere repeats in *A. thaliana* (top) and knob repeats in *Z. mays* (bottom) using CRISPR-FISH and immunofluorescence. Cas9 antibody was detected with anti-mouse FITC (green) and tracrRNA was labelled with Atto550 (red). Scale bars, 5 µm.

4.1.2 Non-fluorescent labeling of DNA repeats by combining CRISPR-FISH with immunoassay

To replace the fluorescence-based detection of anti-Cas9 binding sites with a non-fluorescence method, we employed alkaline phosphatase (AP) for the detection of the target DNA sequences. In this approach, anti-mouse conjugated alkaline phosphatase will be used to detect anti-Cas9 binding sites. Later application of a red chromogenic substrate will enable the reaction with alkaline phosphatase, resulting in red-colored target-specific non-fluorescent signals at the RNP binding sites (Fig. 9A). Testing this strategy on formaldehyde-fixed nuclei of *A. thaliana* and *Z. mays* resulted in red labeling of centromeres (Fig. 9B) and knob (Fig. 9C) repeats, with background noise observed in their respective nuclei. To confirm that the observed signals were indeed present within the nuclei, hematoxylin was tested as a counter-stain (Fig. 9B & C). However, hematoxylin, even in the absence of CRISPR-dCas9 labeling, strongly stained the chromocenters where actual *A. thaliana* centromeres are positioned during interphase (SIMON *et al.* 2015), obscuring the true location of the centromeres (Fig. 9B, right). Therefore, hematoxylin is not a suitable counter-stain for *A. thaliana* nuclei when combined with a non-fluorescent CRISPR-ISH method. In contrast, *Z. mays* nuclei showed red-colored knob-specific signals after hematoxylin counter-staining (Fig. 9C, middle). The same chromogenic approach without subsequent counter-staining was used to detect *Fok*I and sub-telomeric repeats in *V. faba* and *A. fistulosum* nuclei, respectively (Fig. 9D, E). This resulted in red colored labeling of target DNA repeats along with increased

background noise in both species. However, only a few nuclei exhibited target-specific signals in all the species tested, indicating a low efficiency of this indirect detection method using the Cas9 antibody in combination with anti-mouse conjugated alkaline phosphatase. These results also suggest the need to investigate appropriate nuclear stains across different species to complement non-fluorescent CRISPR-ISH labeling.
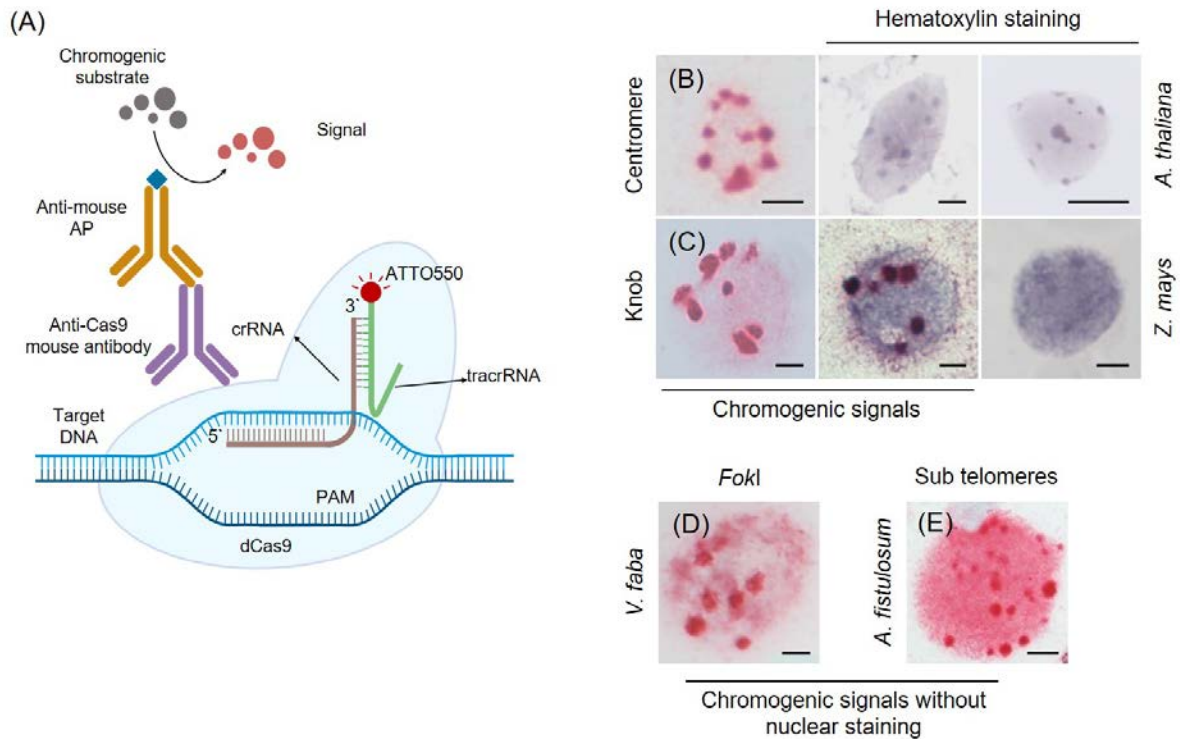
Fig 9: Non-fluorescent labeling of DNA repeats by combining CRISPR-FISH with immunoassay. (A) Schematic of CRISPR-FISH for non-fluorescent labeling of repeat sequences using Cas9 antibody and anti-mouse alkaline phosphatase (AP) and application of red chromogenic substrate develops red colored precipitate at RNP bound sites. (B) Non-fluorescent labeling of centromere repeats in *A. thaliana* nuclei (left) without staining, (middle) with hematoxylin counterstaining and (right) with counterstaining only as control without labelling. In *A. thaliana* nuclei, hematoxylin also stained the chromocenters where the actual centromeres were located, so the red chromogenic centromeric dots were masked by hematoxylin. (C) Non-fluorescent labeling of knob repeats in *Z. mays* nuclei (left) without staining, (middle) with hematoxylin counterstaining and (right) with counterstaining only as control without labelling. Red-colored spots indicate centromere and knob-specific signals. Non-fluorescent labeling of (D) *Fok*I and (E) sub telomeric repeats on formaldehyde fixed *V. faba* and *A. fistulosum* nuclei, respectively, without counterstaining. Scale bars, 5 μm.

4.1.3   Identification of suitable nuclear counter-stains

Selecting the best counter-stain is crucial to ensure that non-fluorescent, target-specific signals are specifically localized to nuclei or chromosomes. For this purpose, several nuclear dyes were tested with formaldehyde-fixed *A. thaliana* and *V. faba* nuclei. Among 7 tested dyes, 2 % methyl green (w/v), 4 % methylene green (w/v), 4% neutral red (w/v), hematoxylin (100% stock solution) and methylene blue (100% stock solution) dyes successfully labled *V. faba* nuclei at room temperature within 2 min (Fig. 10A). Only a weak staining of nuclei was observed with naphthol green, even with increased concentration (data not shown). In contrast, no staining of *A. thaliana* nuclei was observed using methylene green, methyl green, or neutral red. However, hematoxylin and methylene blue stained *A. thaliana* nuclei within 10 min, with stronger staining observed with hematoxylin. Both dyes stained chromocenters with high intensity, rendering them unsuitable as they obscure the actual centromere regions (Fig. 10B). Moreover, microscopic observations revealed a likely correlation between the counter-staining ability of chromatin and the genome size of the species. For instance, the small-genome species *A. thaliana* (157 Mb) exhibited weaker staining compared to the large-genome species *V. faba* (13 Gb, (JAYAKODI *et al.* 2023)). Overall, neutral red and hematoxylin were chosen from the tested dyes due to their specific staining of the nuclei with clear staining of the nuclear periphery, unlike the other dyes. Subsequent testing of these selected dyes on *Z. mays* and *A. fistulosum* resulted in successful staining of the nuclei in both species (Fig. 10C). However, to attain a clear contrast between the chromogenic signals of the target sequence and the nuclei, it is crucial to select the appropriate counter-stain according to the chromogenic substrate utilized.
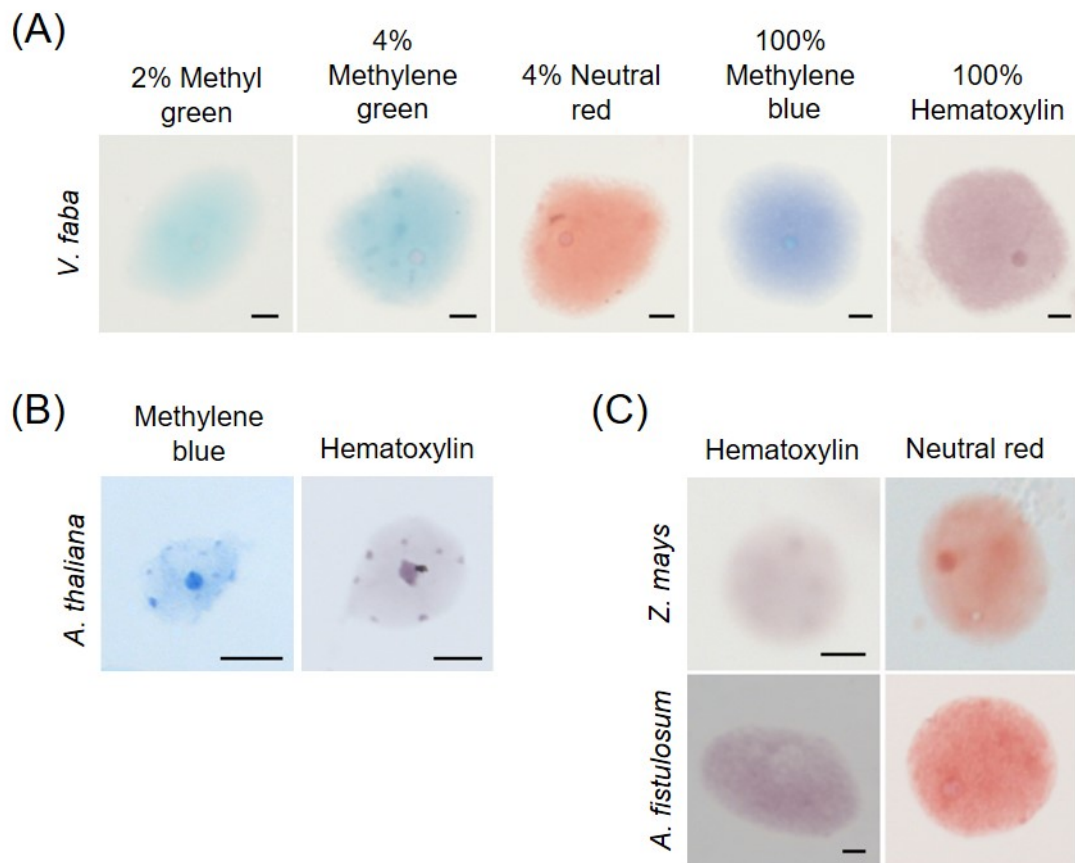
Fig 10: Comparison of different nuclear stains on fixed nuclei. (A) Staining of formaldehyde fixed *V. faba* nuclei with methyl green, methylene green, neutral red, methylene blue and hematoxylin dyes for 2 min application. (B) Staining of *A. thaliana* nuclei with 100% methylene blue (right) and 100% hematoxylin (left) dyes. Hematoxylin and methylene blue also stained the chromocenters. (C) Staining of *Z. mays* and *A. fistulosum* nuclei dyes with hematoxylin and neutral red dyes for 2 min. Scale bars, 5 µm

4.1.4 Application of biotinylated tracrRNA improved indirect CRISPR-ISH

To improve and simplify the indirect CRIPSR labeling approach, we thought to employ 3' biotin-labeled tracrRNA in combination with CRISPR-FISH. In principle, biotin-labeled tracrRNA and target-specific crRNA are combined to form mature gRNA and activate the dCas9 for binding target sequences (Fig. 11A). Later, the RNP binding sites were detected by a streptavidin-conjugated FITC (Fig. 11A). To assess the functionality of this approach, we labeled centromere and telomere repeats on formaldehyde-fixed *A. thaliana* and *N. benthamiana* nuclei using indirect CRISPR-FISH and detected them indirectly with streptavidin FITC (Fig. 11B). As a positive control, standard FISH with biotin-labelled oligo-probes specific for Arabidopsis-type telomeres and centromeres were used (Fig. 11C). This resulted in labeling

centromeres and telomeres in both species using indirect CRISPR, with a similar labeling pattern observed with DNA FISH, demonstrating the capability of biotinylated tracrRNA to activate the RNP complex and recruit streptavidin FITC for indirect DNA repeat labeling. To further confirm the specificity of the indirect CRISPR-FISH signals, we simultaneously labeled *A. thaliana* centromeres and *Z. mays* knob repeats with both indirect CRISPR-FISH and standard CRISPR-FISH (Fig. 11D). The colocalization of both green and red signals proves the specificity of the method.

Next, to compare the labeling efficiency of indirect CRISPR-FISH, signals from *A. thaliana* centromeres and *Z. mays* knob repeats in 2C sorted nuclei were quantified independently using both standard and indirect CRISPR-FISH. In the counting assay, approximately 8 and 7 centromere-specific signals were detected in *A. thaliana* (Fig. 11E), and about 6 knob-specific signals were detected in *Z. mays* (Fig. 11F) by standard and indirect CRISPR-FISH, respectively. Additionally, 47 out of 50 *A. thaliana* nuclei (Fig. 11G) and 45 out of 50 *Z. mays* nuclei (Fig. 11H) showed centromere-specific and knob-specific signals, respectively, generated by both standard and indirect CRISPR-FISH. Overall, the quantification results demonstrated satisfactory labeling efficiency of indirect CRISPR-FISH using a 3' biotin-labeled tracrRNA compared to standard CRISPR-FISH.
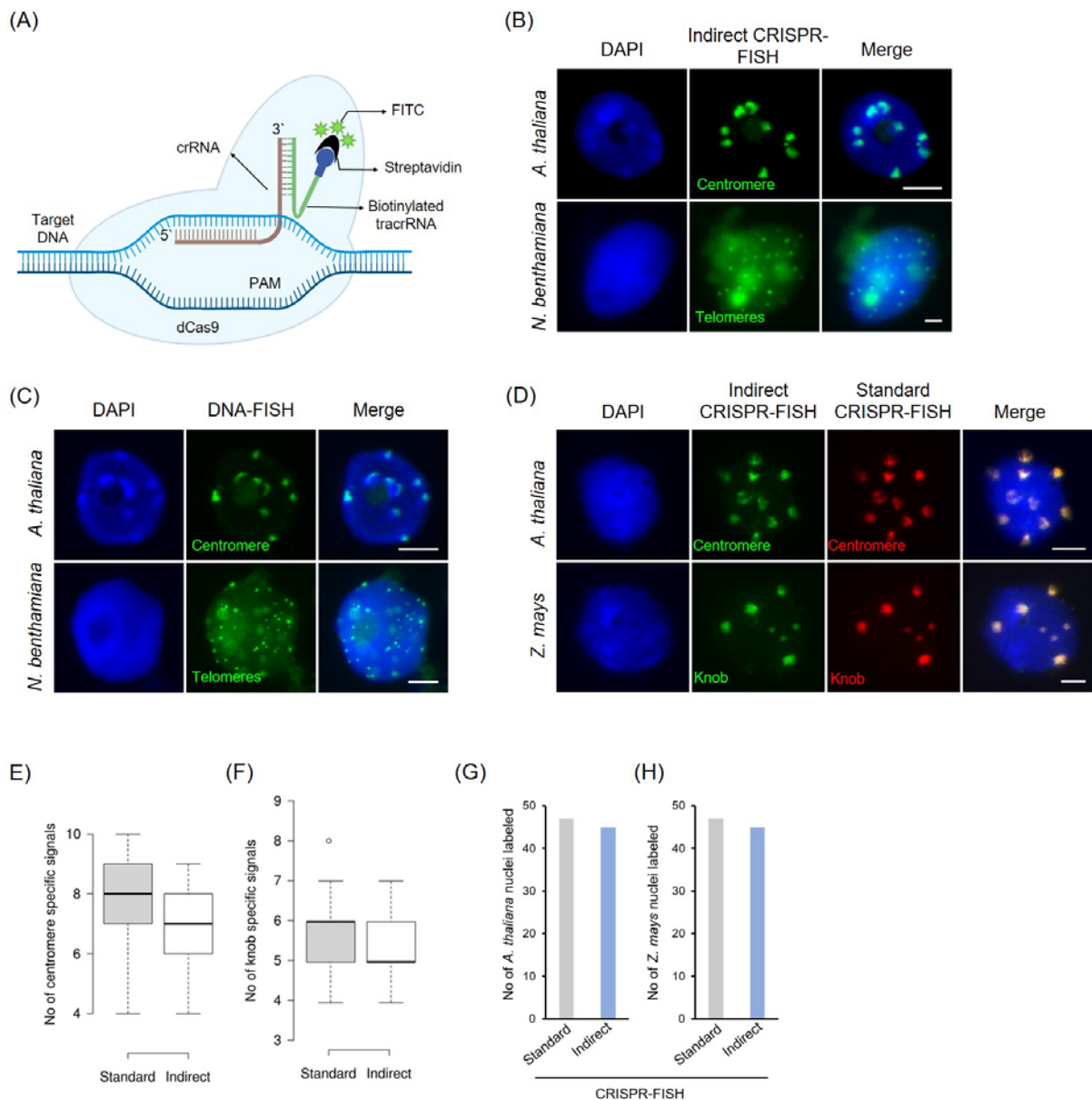
Fig 11: Indirect CRISPR-FISH labeling of DNA repeats using biotinylated tracrRNA. (A) Schematic of indirect CRISPR-FISH for the labeling of repeat sequences using biotinylated tracrRNA and detection with streptavidin FITC. (B) Visualization of centromere repeats in A. thaliana (top) and telomere repeats in N. benthamiana (bottom) with indirect CRISPR-FISH using biotinylated tracrRNA and detected with streptavidin FITC. (C) Visualization of centromere on fixed *A. thaliana* and telomere repeats in *N. benthamiana* with DNA FISH using biotin-labelled oligo probes and detected with streptavidin FITC. (D) Images showing colocalization of indirect CRISPR-FISH (green) and standard CRISPR-FISH (red) spots labeling centromeres and knob repeats in *A. thaliana* and *Z. mays* nuclei, respectively. Biotinylated tracrRNA was detected using streptavidin FITC (green). Comparison of labeling efficiency between two methods, number of (E) centromere and (F) knob signals generated per nucleus by standard CRISPR-FISH and indirect CRISPR-FISH methods, n =50 nuclei. Upper and lower whiskers indicate the maximum and minimum number of signals observed. The black line in the middle of each box plot indicates the median. Bar graph comparing the efficiency of the two methods, number of nuclei with (G) centromere and (H knob repeats on fixed 2C nuclei of *A. thaliana* and *Z. mays* using standard CRISPR-FISH and indirect CRISPR-FISH, respectively, n =50 nuclei. DNA stained with DAPI (blue). Scale bars, 5 μm.

4.1.5 Application of biotinylated tracrRNA enabled CRISPR-CID

To assess the potential of 3' biotin-labeled tracrRNA for non-fluorescent labeling of DNA, we utilized it in combination with either streptavidin-conjugated alkaline phosphatase (AP) (Fig. 12A) or streptavidin-conjugated horseradish peroxidase (HRP) (Fig. 12C) along with their corresponding chromogenic substrates. We termed this strategy "CRISPR-CID", a **CRISPR**-Cas9 mediated **c**hromogenic *in situ* **d**etection method. The application of the streptavidin-conjugated alkaline phosphatase enzyme and the red substrate for signal detection in formaldehyde-fixed *A. thaliana* and *Z. mays* nuclei using centromere and knob-specific gRNA, respectively, resulted in a specific labeling of the repeats (Fig. 12B). However, CRISPR-CID in combination with the alkaline phosphatase generated specific, but fuzzy signals. In contrast, the application of the peroxidase enzyme along with green chromogenic substrate resulted in clear green-colored centromere and knob repeat signals (Fig. 12D). To counter-stain *Z. mays* nuclei after the chromogenic reaction, the specimens were stained in 4% neutral red for 2 mins. The application of a standard light microscope revealed strong green knob-specific signals with light orange-stained nuclei (Fig. 12E). To assess the efficiency of CRISPR-CID, we compared the number of knob repeat-specific signals generated by indirect CRISPR-FISH and CRISPR-CID. About 6 and 5 knob-specific signals were counted after indirect CRISPR-FISH and CRISPR-CID, respectively (Fig. 12F). This demonstrates the efficient non-fluorescent labeling of CRISPR-CID in combination with streptavidin-HRP on formaldehyde-fixed nuclei.
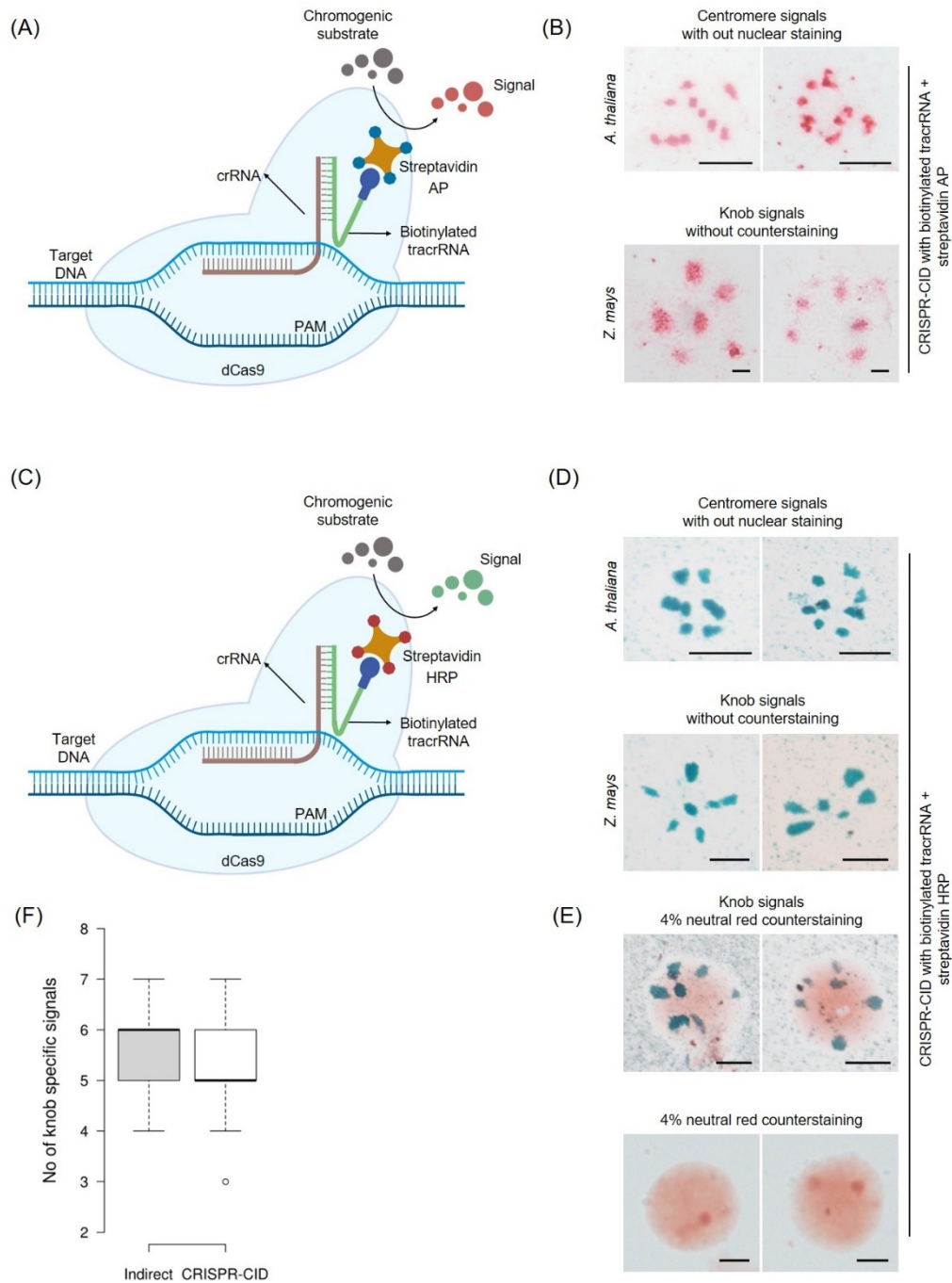
Fig 12: CRISPR-Cas9-mediated chromogenic in situ detection of repeat sequences in fixed samples. (A) Schematic of CRISPR-CID for labeling repeat sequences using biotinylated tracrRNA and streptavidin alkaline phosphatase (AP) and application of red chromogenic substrate develops red colored precipitate at RNP bound sites. (B) CRISPR-CID-based non-fluorescent labeling of centromeres (top) and knob repeats (bottom) in *A. thaliana* and *Z. mays* nuclei without counterstaining using streptavidin AP and red chromogenic substrate. Red-colored spots indicate centromere and knob-specific signals. (C) Schematic of CRISPR-CID for labeling repeat sequences using biotinylated tracrRNA and streptavidin-horseradish peroxidase (HRP) and application of green chromogenic substrate develops green colored precipitate at RNP bound sites. (D) CRISPR-CID-based non-fluorescent labeling of centromeres (top) and knob repeats (bottom) in *A. thaliana* and *Z. mays* nuclei without counterstaining using streptavidin HRP and green chromogenic substrate. Green-colored spots indicate centromere and knob-specific signals, respectively. (E, top) CRISPR-CID labeling of knob repeats *in Z. mays* nuclei counterstained with 4% neutral red and (E, bottom) counterstained only as a control with no labelling. (F) Comparison of labeling efficiency between two methods, number of knob signals generated per nucleus by indirect CRISPR-FISH and CRISPR-CID methods, n =50 nuclei. Upper and lower whiskers indicate the maximum and minimum number of signals observed. The black line in the middle of each box plot indicates the median. Scale bars, 5 μm

4.1.6 CRISPR-Cas9-mediated chromogenic in situ detection of repetitive sequences in ethanol: acetic acid fixed chromosomes and nuclei

Finally, to test whether also CRISPR-CID labels repeats in conventionally 3:1 (ethanol: acetic acid) fixed chromosomes and nuclei, we employed *Z. mays* and *V. faba* chromosomes for labeling the knob and *Fok*I repeats, respectively. After CRISPR-CID application, either 4% neutral red or with 100% hematoxylin was used to stain the chromosomes for 2 min. CRISPR-CID successfully labelled knob repeats in *Z. mays* chromosomes, and specific signals were observed at the terminal regions of the chromosome arms (Fig. 13A, top). Also, CRISPR-CID labelled *Fok*I repeats in the mid-arm position of the long arms of all *V. faba* chromosomes. *Fok*I represents one of the most abundant satellites identified in a plant species thus far (Kato *et al.* 1984) (Fig. 13B, top). The application of 4% neutral red after CRISPR-CID resulted in both species in light red counter-stained chromosomes. The application of hematoxylin in combination with CRISPR-CID exhibited green counter-stained chromosomes in both species (Fig.13A, B, bottom). Using CRISPR-CID in combination hematoxylin also successfully labeled the centromere repeats of *A. thaliana*, sub-telomeric repeats of *A. fistulosum* and the major satellite repeats of mouse chromosomes (Fig. 13C). As a positive control, streptavidin conjugated FITC was used to detect indirect CRISPR-FISH specific signals in 3:1 fixed A. thaliana, *Z. mays, V. faba*, *A. fistulosum*, and mouse chromosomes (Fig. 14).
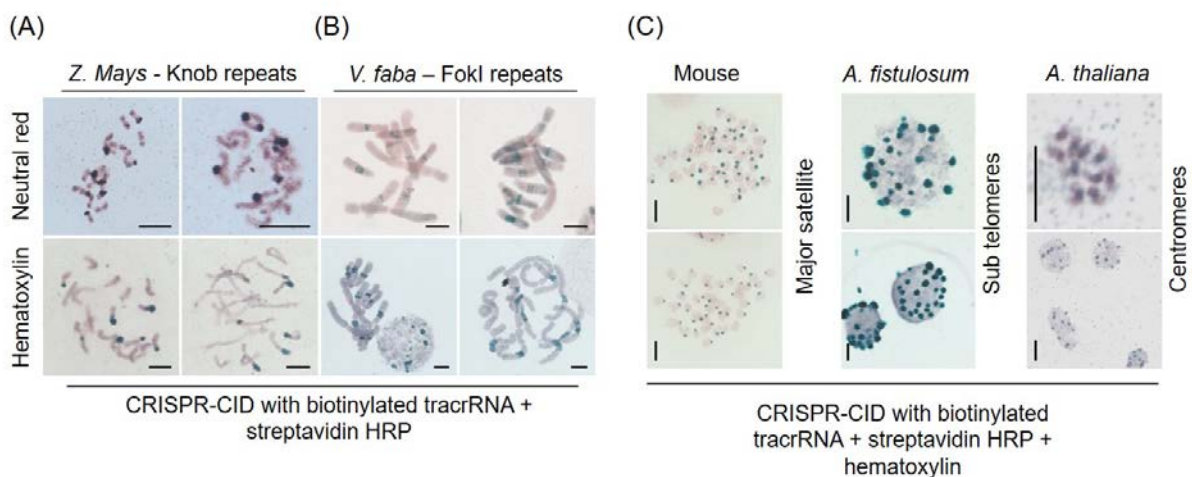
Fig 13: CRISPR-Cas9-mediated chromogenic in situ detection of repetitive sequences in ethanol: acetic acid fixed chromosomes and nuclei. Non-fluorescent visualization of (A) knob and (b) FokI repeats on *Z. mays* and *V. faba* chromosomes using the CRISPR-CID method in combination with (a, b, top) neutral red and (A, B, bottom) hematoxylin staining. (C) Visualization of centromere, sub telomere and major satellite repeats in *A. thaliana*, *A. fistulosum* and mouse ethanol: acetic acid fixed chromosomes using CRISPR-CID. Nuclei and chromosomes were stained with hematoxylin. Scale bars, 5 μm.
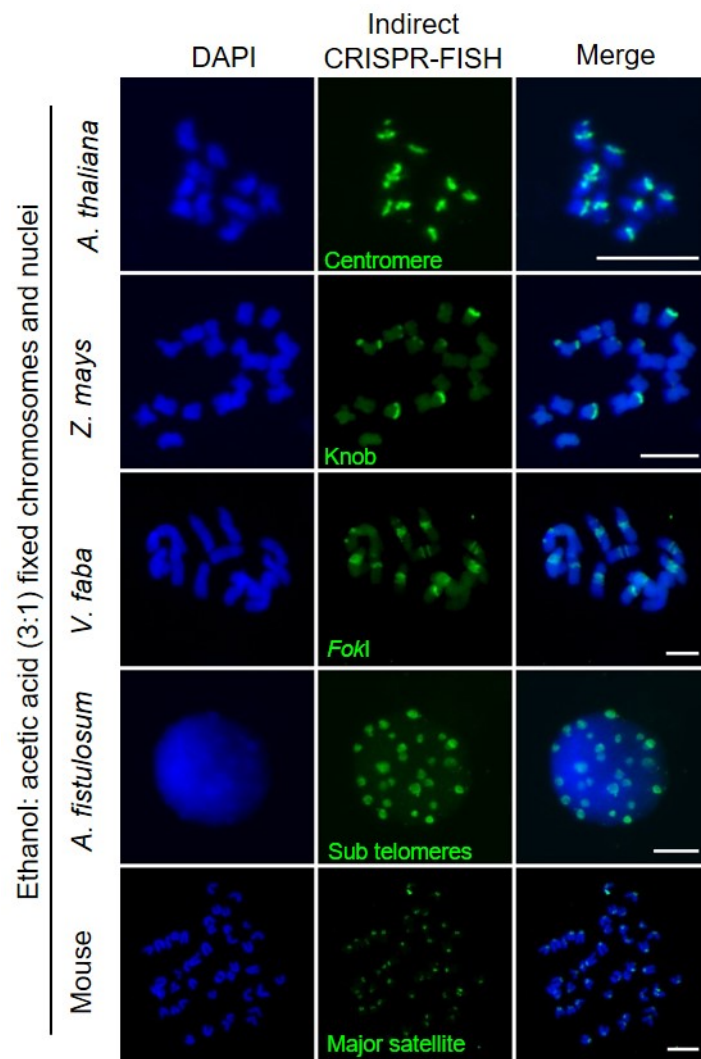
Fig 14: Indirect CRISPR-FISH labeling on conventionally fixed nuclei and chromosomes. Visualization of centromere, knob, FokI, sub telomere and major satellite repeats in *A. thaliana, Z. mays, V. faba, A. fistulosum* and mouse ethanol: acetic acid fixed chromosomes using indirect CRISPR-FISH with biotinylated tracrRNA and detection with streptavidin FITC. DNA stained with DAPI (blue). Scale bars, 5 µm.

4.1.7   Investigating dCas9-HRP fusion for non-fluorescent labeling

To simplify CRISPR-CID-based non-fluorescent labeling, the dCas9 protein was engineered by fusing HRP to its C-terminus and purifying it recombinantly. However, labeling centromere repeats on formaldehyde-fixed *A. thaliana* nuclei was not observed (Fig. 15A), revealing that the purified dCas9-HRP protein lacked activity in binding to target DNA, unlike the dCas9 protein alone, which successfully labeled the repeats (Fig. 15B). Furthermore, testing HRP activity with 3,3′,5,5′-Tetramethylbenzidine (TMB) failed to produce the green color in the

presence of dCas9-HRP, confirming inactive HRP functionality. In contrast, the control application of streptavidin HRP with TMB exhibited a green color change (Fig. 15C). Additionally, the quantity of purified dCas9-HRP protein was significantly lower compared to dCas9 alone (data not shown). Overall, the results indicate that the fusion of HRP with dCas9 rendered the protein inactive, thereby hindering its activity and resulting in the failure to label target DNA.
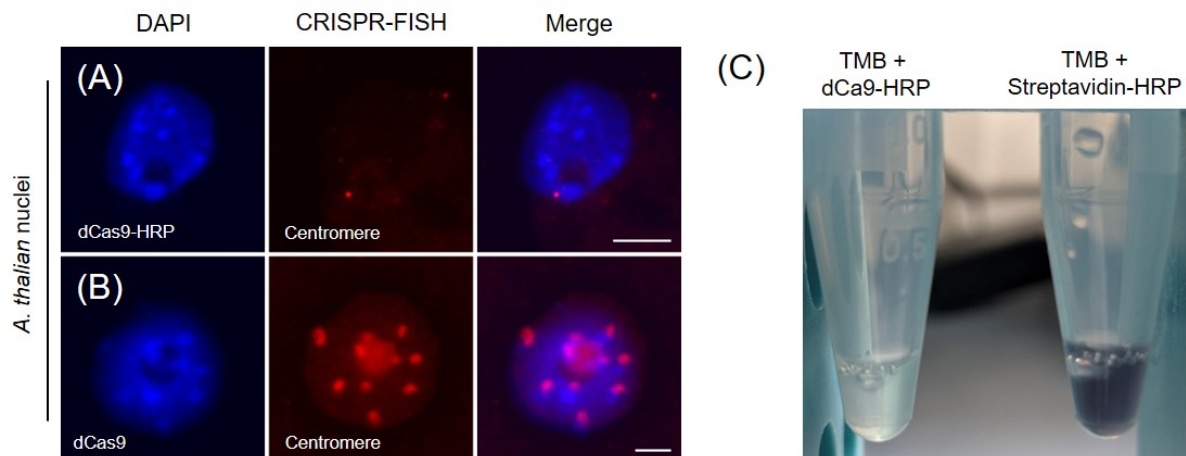
Fig 15: Fusion of HRP with dCas9: (A) Labeling of *A. thaliana* centromeres using dCas9-HRP protein resulted in failed labeling, compared to (B) centromere labeling with dCas9 protein as the control. (C, left) dCas9-HRP failed to change TMB into a green color, whereas (C, right) streptavidin HRP successfully changed the color of TMB to green, serving as the control. Bar, 5 μm

In conclusion, CRISPR-CID demonstrates successful labeling of repetitive sequences in both formaldehyde- and 3:1 (ethanol:acetic acid)-fixed nuclei and chromosomes. Standard light microscopy proves adequate for specimen analysis. The application of horseradish peroxidase-based detection outperforms alkaline phosphatase, yielding clear chromogenic signals with minimal background noise. The attempt to simplify labeling by fusing HRP with dCas9 resulted in the inactivation of both enzymes, leading to the failure of DNA labeling.

4.2 Application of ALFA-tag for enhanced signal intensity in CRISPR-FISH applications

4.2.1 Establishing an ALFA-tag-assisted CRISPR-FISH system for labeling DNA repeats on fixed samples with an ALFA-specific nanobody

CRISPR-FISH is a novel technique that uses a dCas9 protein and ATTO550-tagged bipartite guide RNA to precisely label repetitive sequences on fixed nuclei and chromosomes (Ishii *et al.* 2019; Němečková *et al.* 2019; Potlapalli *et al.* 2020), as well as fixed tissue sections (Nagaki and Yamaji 2020) across diverse species. To improve the CRISPR-FISH toolset for possible low-copy DNA sequences labeling, a novel strategy was adopted, leveraging the ALFA-tag approach. This involved engineering the dCas9 protein with multiple copies of the ALFA-tag. To demonstrate this methodology, a dCas9-ALFA-tagged protein, accompanied by a bipartite guide RNA and a nanobody NbALFA fused with ATTO488, was employed (Fig. 16).
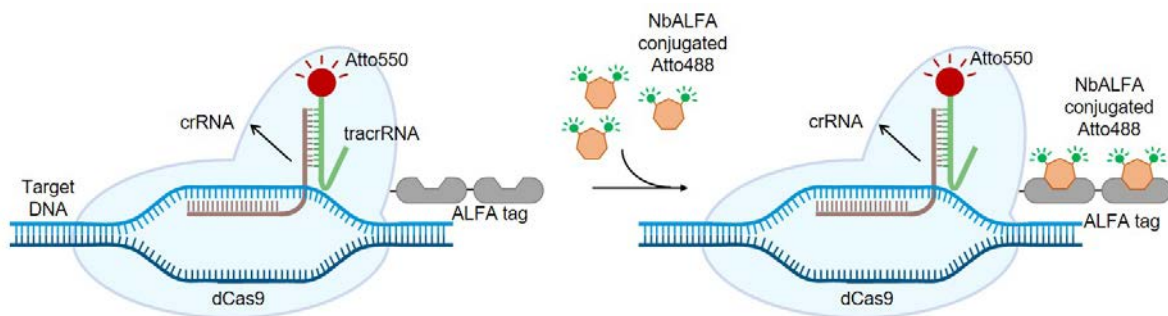
Fig 16: Schematic of CRISPR-FISH in the combination of ALFA-tag and NbALFA. A dCas9 protein from *S. pyogenes* fused with ALFA-tags, ATTO550-tagged bipartite gRNA, is used to label DNA repeats. Covalent detection of ALFA-tagged dCas9 with NbALFA conjugated to ATTO488.

Initially, it was unclear if the dCas9 protein's capability to bind to DNA would be impacted by the addition of the ALFA-tag. In order to address this, we recombinantly purified the modified dCas9 protein after adding one copy of the ALFA-tag to either the N-terminus (Fig. 17A) or the C-terminus (Fig. 17B). For testing this approach, guide RNAs targeting centromeres and knobs were employed for CRISPR-FISH labeling on formaldehyde fixed nuclei of *A. thaliana* and *Z. mays*, respectively. The dCas9-ALFA-tagged protein effectively labeled the centromeres and knob repeats in both nuclei (Fig. 17 A & B). Moreover, the colocalization of red and green signals, generated from Atto550-labeled tracrRNA and NbALFA conjugated to ATTO488, respectively, was observed irrespective of the ALFA-tag's placement at the N- or C-

terminus of dCas9. This suggests that the ALFA-tag can be smoothly combined with the functionality of dCas9. Overall this result indicates that the dCas9 protein's ability to bind DNA is not hindered by the ALFA-tag, regardless of where it is located in the protein sequence.
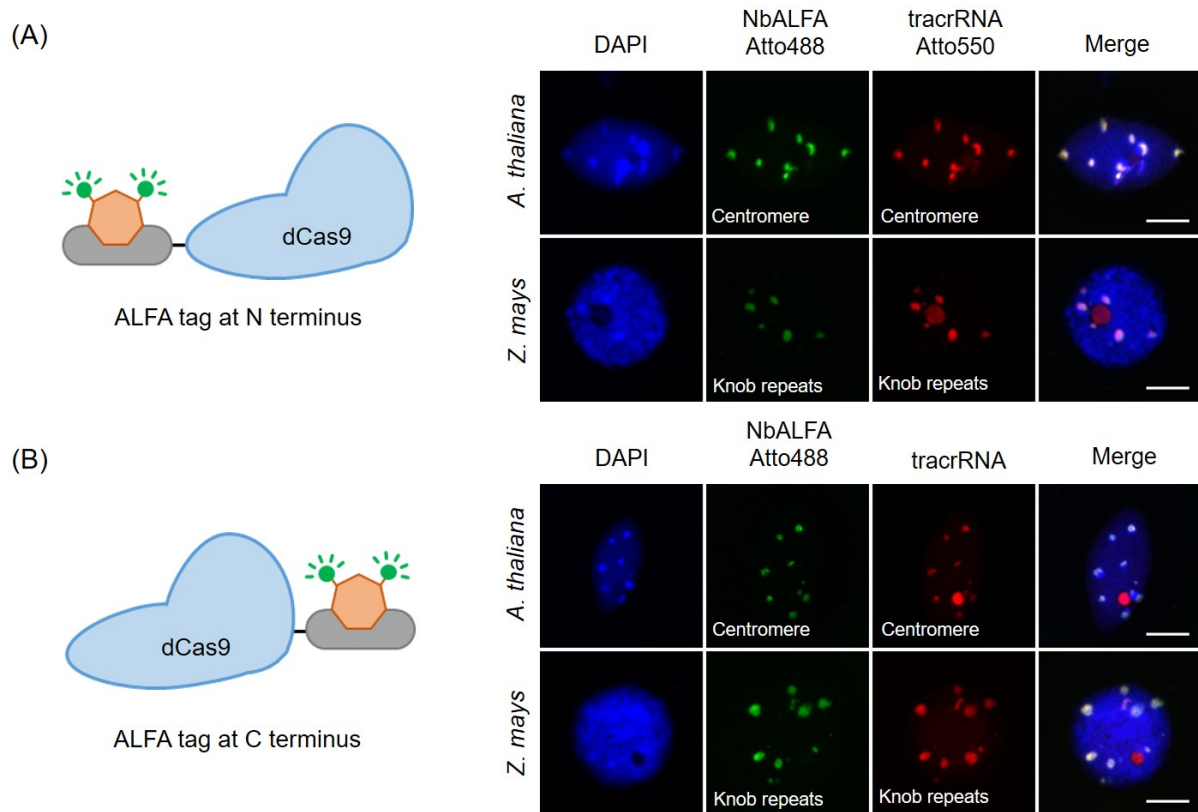
Fig 17: Sketch illustrating the dCas9 protein fused with the ALFA-tag at either the (A) N-terminus or the (B) C-terminus. On the right side, visualization of *A. thaliana* centromere and *Z. mays* knob repeats in fixed nuclei using a modified dCas9 proteins with a single ALFA-tag at either the (A) N-terminus or the (B) C-terminus. On the right side, there is a green signal represent NbALFA Atto488, and red signals correspond to ATTO550-tagged tracrRNA. Scale bars: 10 µm.

Next, the applicability of the dCas9-ALFA-tag approach was then assessed on conventionally fixed chromosomes for the labeling of repetitive DNA sequences. The experiments were successful in labeling knob, *Fok*I, and major satellite repeats on 3:1 (ethanol: acetic acid) fixed chromosomes of (Fig. 18A) *Z. mays*, (Fig. 18B) *V. faba*, and (Fig. 18C) mouse, respectively. Furthermore, the co-localization of both red and green signals provides strong evidence of specificity.
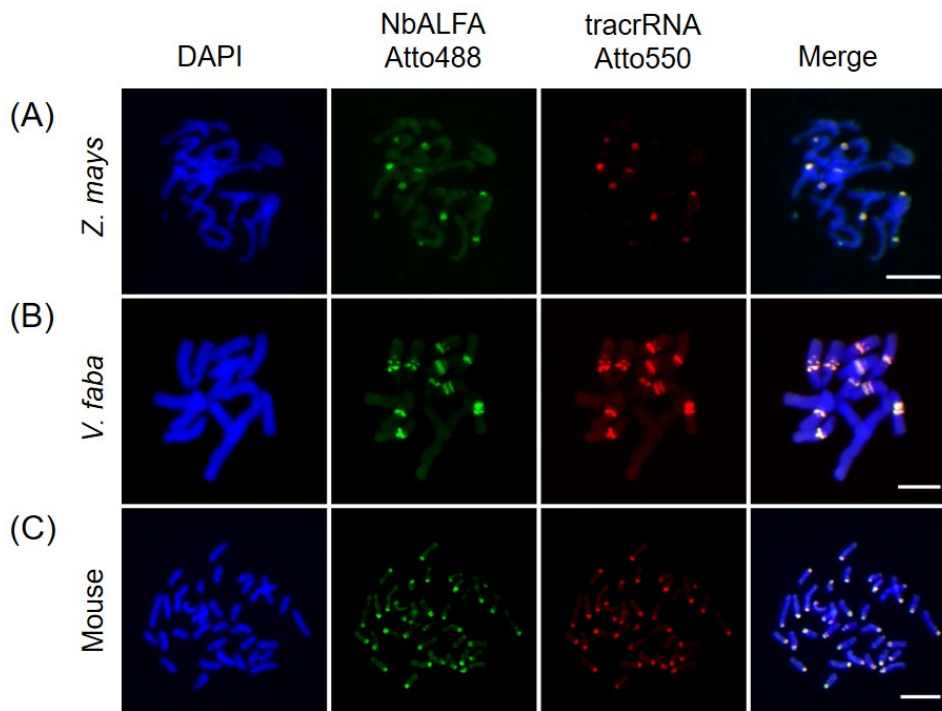
Fig 18: CRISPR-ALFA-tag-based labeling of knob repeats, FokI repeats and major satellite repeats on conventionally 3:1 (ethanol: acetic acid) fixed chromosomes of (A) *Z. mays*, (B) *V. faba* and (C) mouse, respectively. Green signals represent NbALFA Atto488, and red signals correspond to ATTO550-tagged tracrRNA. Scale bars: 10 μm.

Next, to investigate whether the dCas9-ALFA system could enhance DNA labeling signal intensities, dCas9-ALFA-tag proteins were engineered. These proteins were fused with either three copies of the ALFA-tag at the N-terminus or three ALFA copies each on both the N- and C-termini of the dCas9 protein (Fig. 19A). Using centromere-specific gRNA, these proteins were used to visualize the centromeres on formaldehyde-fixed *A. thaliana* nuclei, successfully labeling the centromeres (Fig. 19A). However, increasing the number of ALFA-tags did not result in an obvious signal increase of NbALFA conjugated ATTO488. Additionally, to evaluate whether the recombinantly purified NbALFA-eGFP could produce stronger signal intensities than NbALFA-Atto488, we labeled the *A. thaliana* centromere repeats with dCas9 fused with 6x copies (3+3x) of the ALFA-tags in combination with NbALFA-eGFP. But also, in this case no obvious enhancement in signal intensities was observed (Fig. 19B). These results suggest that increasing the number of ALFA-tags in combination with NbALFA-Atto488 or NbALFA-eGFP does not necessarily enhance the signal intensities. Further optimization of the system might be required to achieve the desired increase in signal intensity.
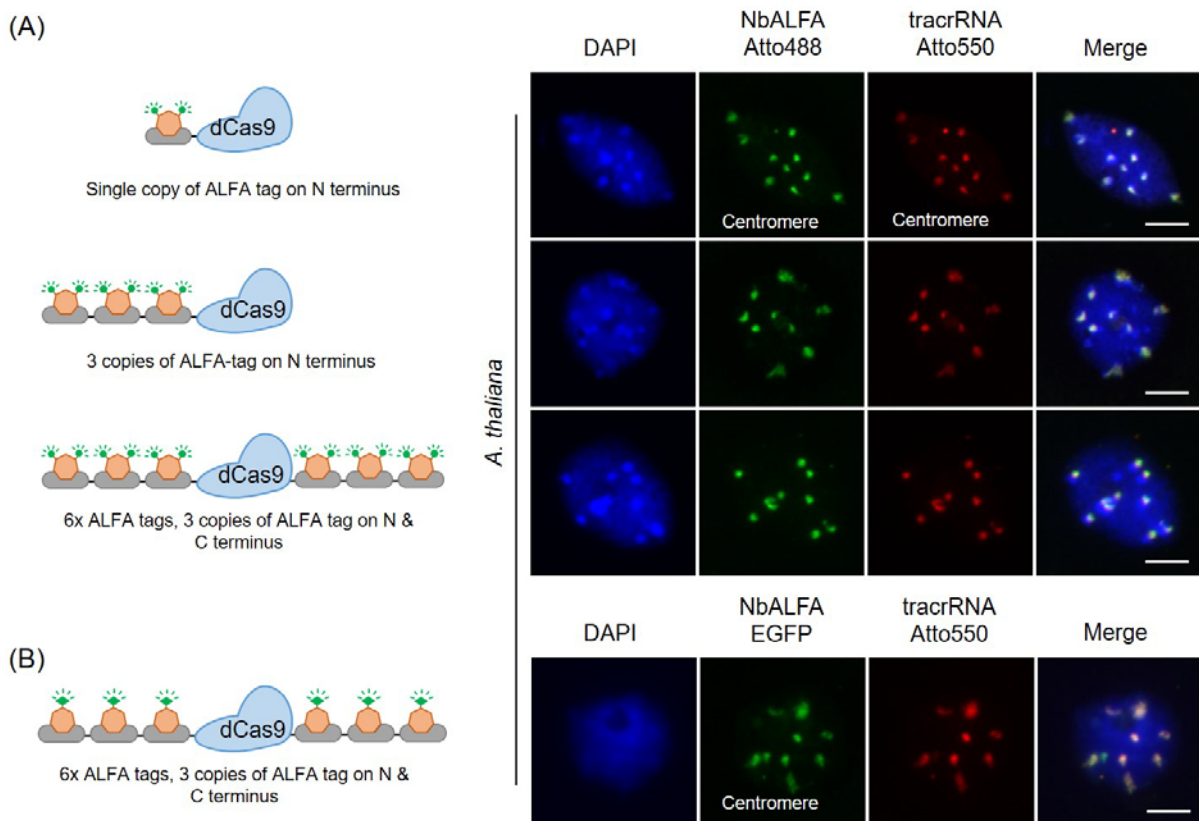
Fig 19: Visualization of centromere repeats using dCas9 protein fused with multiples copies of ALFA-tag and NbALFA combination. (A) Sketch illustrating the dCas9 protein fused with either (upper)1x or (middle) 3x ALFA copies at the N-terminus and (lower) 6x copies (3x on each end) of dCas9 protein. On the right side, visualization of centromere repeats using dCas9 proteins and detected with NbALFA conjugated to ATTO488. (B) Sketch illustrating the dCas9 protein fused with 6x copies (3x on each end) of ALFA-tags. On the right side, labeling of *A. thaliana* centromeres with dCas9-ALFA-tag along with EGFP-NbALFA. Green signals represent (A) NbALFA Atto488 or (B) EGFP NbALFA, and red signals correspond to ATTO550-tagged tracrRNA. Nuclei were counterstained with DAPI (in blue). Scale bars: 10 µm.

4.2.2 Enhanced centromere signal intensity with the dCas9-ALFA system in combination with a minibody

To address the lack of signal intensity increase resulting from the combination of NbALFA with increasing ALFA copies, we introduced a minibody into our experimental approach. This minibody is a single-domain antibody (sdAb) consisting of an anti-ALFA single-domain antibody genetically fused to the IgG FC domain of the commonly used host species (FRODYMA *et al.* 2022; NOZAWA *et al.* 2022). The minibody provides a high affinity for the ALFA-tag and exhibits attributes similar to a conventional IgG-type antibody. In our approach, we employed

a minibody genetically fused to a rabbit FC domain (Fig. 20A). In practice, following the binding of dCas9-ALFA to the target DNA, the minibody detects the ALFA-tagged RNP complex and is subsequently visualized by an Alexa 488 conjugated anti-rabbit antibody (Fig. 20B). To assay functionality, centromere repeat DNA in fixed nuclei of *A. thaliana* was visualized using dCas9 protein fused with a single copy of ALFA-tag on N- terminus and minibody. Detection with anti-rabbit Alexa 488 revealed clear green centromere labeling, with signals precisely colocalized with tracrRNA signals (Atto550), indicating centromere specificity (Fig. 20C).
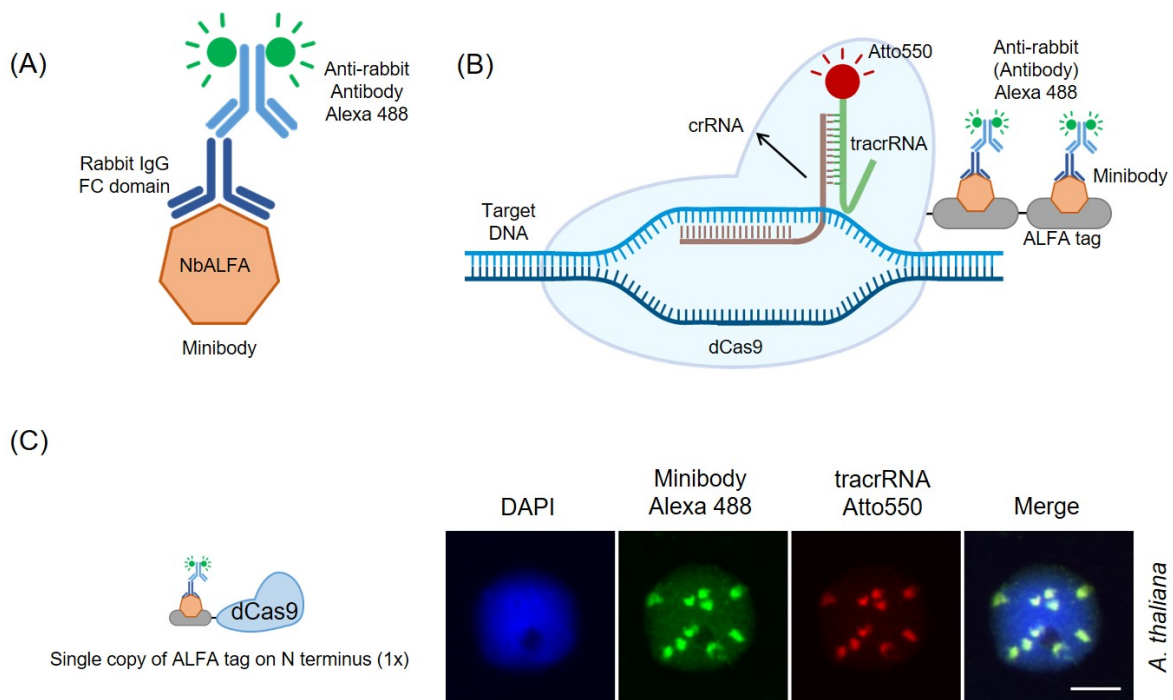
Fig 20: Sketch of the (A) minibody having anti-ALFA single-domain antibody genetically fused to rabbit FC domain. (B) Schematic of CRISPR-FISH in the combination of ALFA-tag and minibody, later detected with anti-rabbit Alexa 488. (C) On the left side, there is a sketch illustrating the dCas9 protein fused with single copy of ALFA-tag. Visualization of centromere repeats using dCas9 protein fused with ALFA-tag and detected with minibody and anti-rabbit Alexa 488. Green signals represent anti rabbit Alexa 488, and red signals correspond to ATTO550-tagged tracrRNA. Scale bars: 10 µm.

Next, to assess the potential to enhance the signal intensity, we applied dCas9-ALFA fusion proteins with 1, 3 or 6 ALFA-tag copies to label the centromere on fixed *A. thaliana* nuclei (Fig. 21A, right). Remarkably, notable variations in minibody signal intensities were observed among different ALFA copy numbers, prompting a quantitative analysis (Fig.21A, left). To confirm that these differences indeed resulted from the increase of ALFA copies, red signal

intensities from the Atto550-conjugated tracrRNA were used as references to calculate the relative green (Alexa 488) fluorescence intensities (see Materials & Methods). While we found for the dCas9-ALFA constructs with 1 and 3 ALFA-tag copies at the N-terminus only a low and not significant increase (means: 3.22 and 3.47, respectively), 6 copies (3 at both ends) resulted in a significant increase (mean: 8.49) (Fig. 21C) corresponding to a roughly 2.5-fold change. In summary, these results confirm the consistent ability of the minibody to enhance CRISPR-FISH signal intensity with increased ALFA copies.
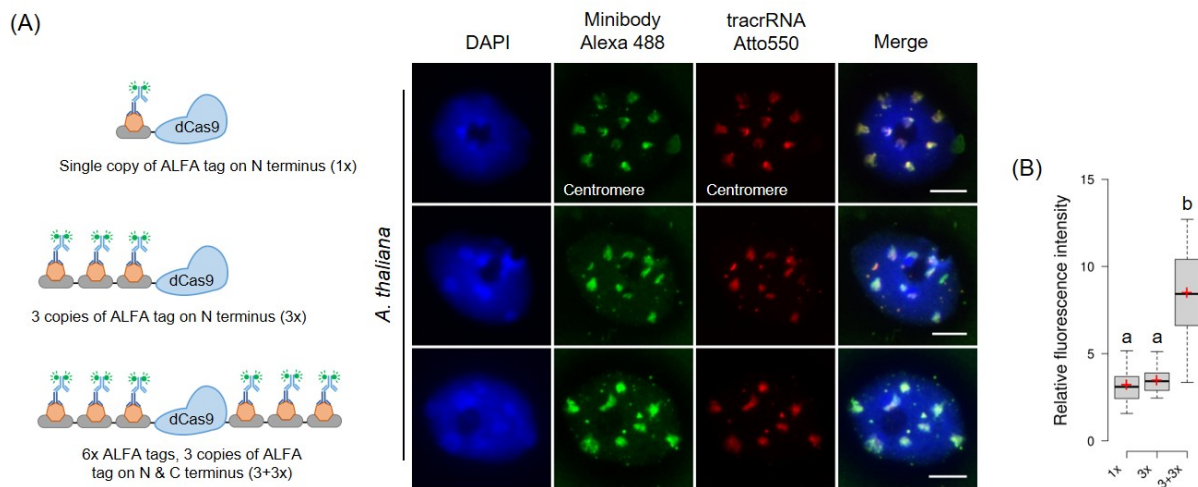
Fig 21: (A) Sketch illustrating the dCas9 protein fused with either (upper) 1x or (middle) 3x ALFA copies at the N-terminus and (lower) 6x copies (3x on each end) of dCas9 protein. On the right side, visualization of centromere repeats using dCas9 proteins and detected with minibody and anti-rabbit Alexa 488. Green signals represent anti-rabbit Alexa 488, and red signals correspond to ATTO550-tagged tracrRNA. Nuclei are counterstained with DAPI (in blue). Scale bars: 10 μm. (B) Boxplots showing the relative fluorescence intensity from centromere foci generated by different dCas9 ALFA copy variants in conjunction with the minibody. The numbers 1x, 3x, and 3+3x represent varying configurations of ALFA-tags fused to the dCas9 protein at both the N- and C-termini. Each analysis comprises 50 nuclei. The boundaries of the box indicate the 25th and 75th percentile, the error bars the 10th and 90th percentile, the black line the median and the orange-colored plus symbol the mean. Different letters indicate significant differences between groups (P<0.05).

To explore if increasing the ALFA copy number further enhances signal intensities, we also tested dCas9 N-terminally fused with 6x and 12x ALFA copies as well as 24x ALFA copies (12x on each terminus) (Fig. 22A). In all cases, the centromere clusters of *Arabidopsis* were successfully labeled, but labeling with the 24x ALFA copies was weaker and showed an increased level of background signals (Fig. 22B). Quantitative analysis revealed for the dCas9 protein fused with 12x ALFA copies a further increase in signal intensity (mean: 14.31), while

6x copies resulted in slightly weaker signals (mean: 7.37) than 3+3x (6 copies; mean: 8.49), but still stronger compared to constructs with one or three copies (Fig. 22C).

(A)

6 copies of ALFA tags on N terminus (6x)

12 copies of ALFA tags on N terminus (12x)

24x ALFA tags, 12 copies of ALFA tags on N & C terminus (12+12x)
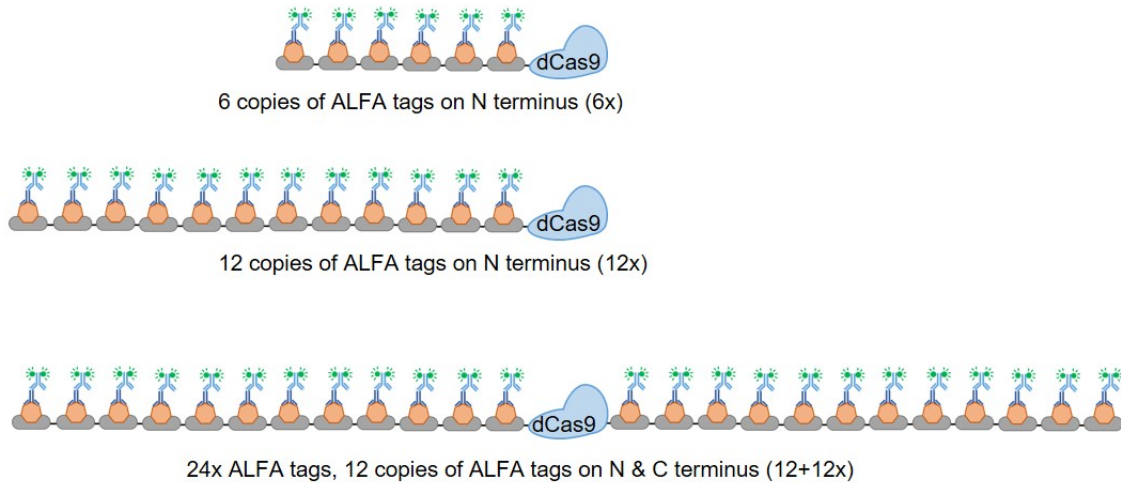
(B)
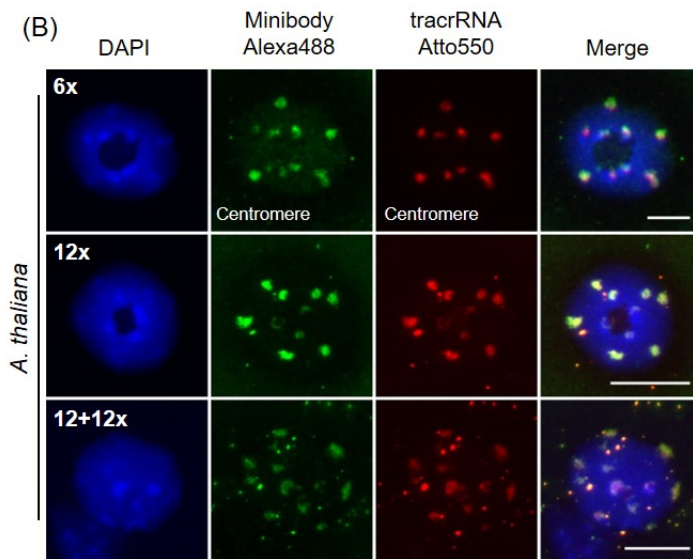
(C)
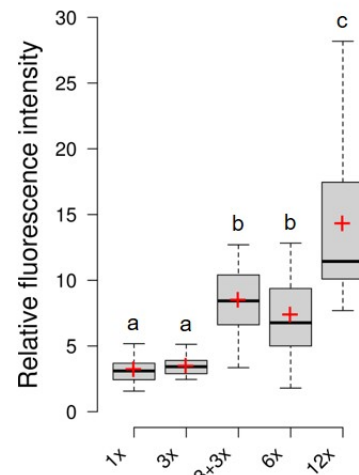
Fig 22: Enhanced centromere labeling intensities with dCas9 fused with 12x ALFA-tags: (A) Sketch illustrating the dCas9 protein fused with (upper) 6x, (middle) 12x ALFA copies at the N-terminus and (lower) 24x copies (12x on each end) of dCas9 protein. (B) Visualization of centromere repeats using dCas9 protein fused with ALFA copies: (upper) 6x ALFA copies, (middle) 12x ALFA copies, and (lower) 24x ALFA copies fused to dCas9 protein. Detection was performed using minibody and anti-rabbit Alexa 488. dCas9 fused with 24x ALFA exhibited minimal labeling. Green signals represent anti-rabbit Alexa 488, and red signals correspond to ATTO550-tagged tracrRNA. Nuclei were counterstained with DAPI (in blue). Scale bars: 10 μm. (C) Boxplots showing the relative fluorescence intensity from centromere foci generated by different dCas9 ALFA copy variants in conjunction with the minibody. The numbers 1x, 3x, 3+3x, 6x, 12x, represent varying configurations of ALFA-tags fused to the dCas9 protein at both the N- and C-termini. Each analysis comprises 50 nuclei. The boundaries of the box indicate the 25th and 75th percentile, the error bars the 10th and 90th percentile, the black line the median and the orange-colored plus symbol the mean. Different letters indicate significant differences between groups (P<0.05).

4.2.3 Enhanced CRISPR-FISH signal intensity through the incorporation of linkers between ALFA-tag copies

Using linker sequences between independent fusion proteins enhances their stability, activity, and independent functionality (CHEN *et al.* 2013b; GUO *et al.* 2021). Glycine-rich linkers, which are naturally occurring and non-interfering with protein function, have proven to be particularly useful in this regard (REDDY CHICHILI *et al.* 2013). To assess the impact of incorporating linkers between individual ALFA-tags on the minibody signal intensity, we generated dCas9 proteins fused with glycine linker (GGGGS), allowing for a distinct separation of individual ALFA-tag copies (Fig. 23A). These modified proteins were successfully utilized to label the *A. thaliana* centromere repeats, facilitating subsequent quantitative analysis (Fig. 23B). Further quantification of *A. thaliana* centromere repeat signals revealed that dCas9 proteins fused with 12x (6+6x) ALFA-tag copies separated by linkers displayed the highest relative signal intensity (mean: 16.29) in comparison to all other constructs (Fig. 23C) probably due to sterical advantages during the ALFA-tagged RNP complex detection by the minibody. However, this holds only true for high copy numbers since we observed no increase in signal intensity when we compared the linker-separated 6x ALFA-tag construct (mean: 7.00) with the same construct without linkers (mean: 7.37). Therefore, another possible explanation might be that not the GS linkers but more the arrangement of the ALFA-tag copies (all at the N terminus or distributed on both termini) has an impact on the results. When the ALFA-tags are located on both sides, the dCas9 protein itself might work as a big linker, allowing for better detection of the ALFA-tag copies. This is supported by the fact that the 3+3x construct outperformed the 6x and 6xGS constructs (mean: 8.49 versus 7.37 and 7.00, respectively), similar as dCas9 proteins with 6+6xGS ALFA-tag copies do with the 12x construct with copies only at the N terminus (means: 16.29 versus 14.31).
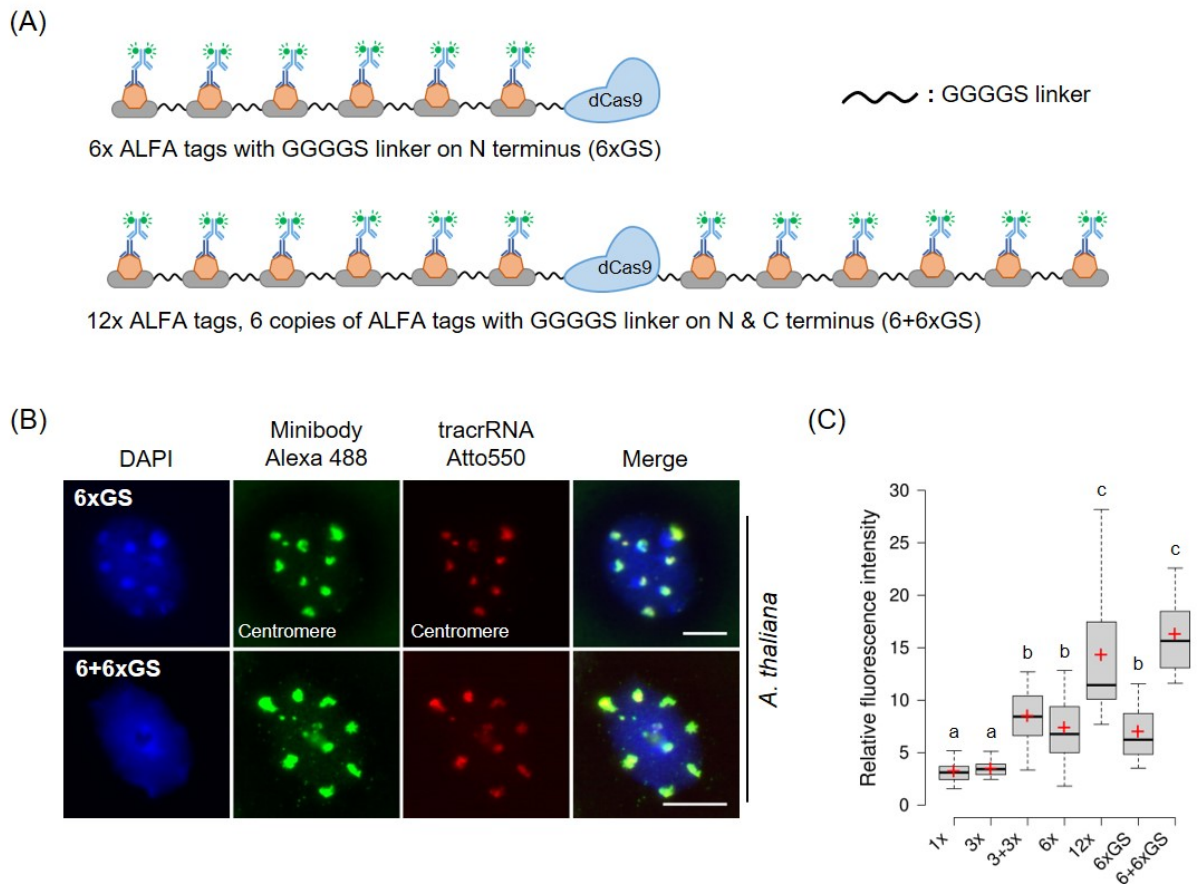
Fig 23: Increased labeling intensities by using linkers between ALFA-tag copies. (A) Sketch illustrating the dCas9 proteins fused with either (upper) 6x ALFA copies on N-terminus or (lower) 12x ALFA copies, 6x on each N- and C- terminus end of dCas9 protein separated by glycine linkers (GGGGGS). (B) Visualization of centromere repeats showing enhanced signal intensities with dCas9 protein fused with either (upper) 6x or (lower) 12 ALFA copies, separated by glycine linkers (GGGGGS) and detected with minibody and anti-rabbit Alexa 488. Green signals represent anti-rabbit Alexa 488, and red signals correspond to ATTO550-tagged tracrRNA. Nucleus is counterstained with DAPI (in blue). Scale bars: 10 µm. (C) Boxplots showing the relative fluorescence intensity from centromere foci generated by different dCas9 ALFA copy variants in conjunction with the minibody. The numbers 1x, 3x, 3+3x, 6x, 12x, 6xGS and 6+6x GS represent varying configurations of ALFA-tags fused to the dCas9 protein at both the N- and C-termini. GS represents the (GGGGS) glycine serine liners. Each analysis comprises 50 nuclei, except for 6xGS and 6+6x GS where 25 nuclei were analyzed. The boundaries of the box indicate the 25th and 75th percentile, the error bars the 10th and 90th percentile, the black line the median and the orange-colored plus symbol the mean. Different letters indicate significant differences between groups (P<0.05).

4.2.4 Live imaging of telomere repeats in *N. benthamiana* with dCas9-ALFA-tag

Fusing fluorescent proteins directly to dCas9 successfully labeled telomeres in live leaf cells of *N. benthamiana* (Dreissig *et al.* 2017; Khosravi *et al.* 2020b). To evaluate the *in vivo* labeling potential of the dCas9-ALFA-tag for DNA repeats, we fused ALFA-tags, to the *Streptococcus pyogenes* dCas9 protein. To maintain construct compactness and alleviate the load on dCas9, we incorporated six ALFA-tag copies separated by glycine linkers (GGGGS) at the C-terminal end of the dCas9 protein fused with 3x copies of *eGFP* and utilized a previously reported telomere-targeting sgRNA under the *A. thaliana U6-26* promoter. The dCas9-3x eGFP-ALFA-tag, along with telomere sgRNA was incorporated into the plant expression vector (Fig. 24A) and then transiently infiltrated into *N. benthamiana* leaves. After 48 h, telomere-like fluorescence puncta were observed, along with non-specific background labeling of the nucleolus (Fig. 24C). As expected, no telomere-specific labeling was observed when infiltrated with a similar construct lacking the telomere sgRNA, resulting in only non-specific labeling of the nucleolus (Fig. 24D). The specificity of the in vivo dCas9-ALFA-tag telomere labeling was confirmed by clear co-localization of red telomere FISH signals with green signals caused by dCas9-3x eGFP-ALFA-tag with telomere-specific sgRNA (Fig. 24E). As addional control, dCas9-ALFA-tag telomere labeling was detected using the minibody, subsequently labeled with anti-rabbit Atto488 (Fig. 24F). Notably, we did not detect telomere signals with minibody in nuclei expressing the dCas9-3x eGFP-ALFA-tag without telomere gRNA (Fig. 24G).

To assess *in vivo* recruitment of NbALFA by dCas9-ALFA-tags for telomere labeling, we employed recombinant NbALFA fused with *mRuby*, regulated by the *RPS5A* promoter. Both vectors were separately introduced into *N. benthamiana* leaves: dCas9-3x eGFP-ALFA-tag with telomere gRNA (Fig. 24A) and mRuby-NbALFA (Fig. 24B). After 48 h, both dCas9-3x eGFP-ALFA-tag and mRuby-NbALFA led to dual labeling of telomeres in green and red (Fig. 24H). Omitting gRNA resulted in only faint green and red labeling of the nucleus without telomere labeling (Fig. 24I). Collectively, these findings showcase the targeted in vivo recruitment of mRuby-NbALFA by dCas9-3x eGFP-ALFA-tags, accomplishing dual labeling of telomeres and confirming specificity through signal colocalization.
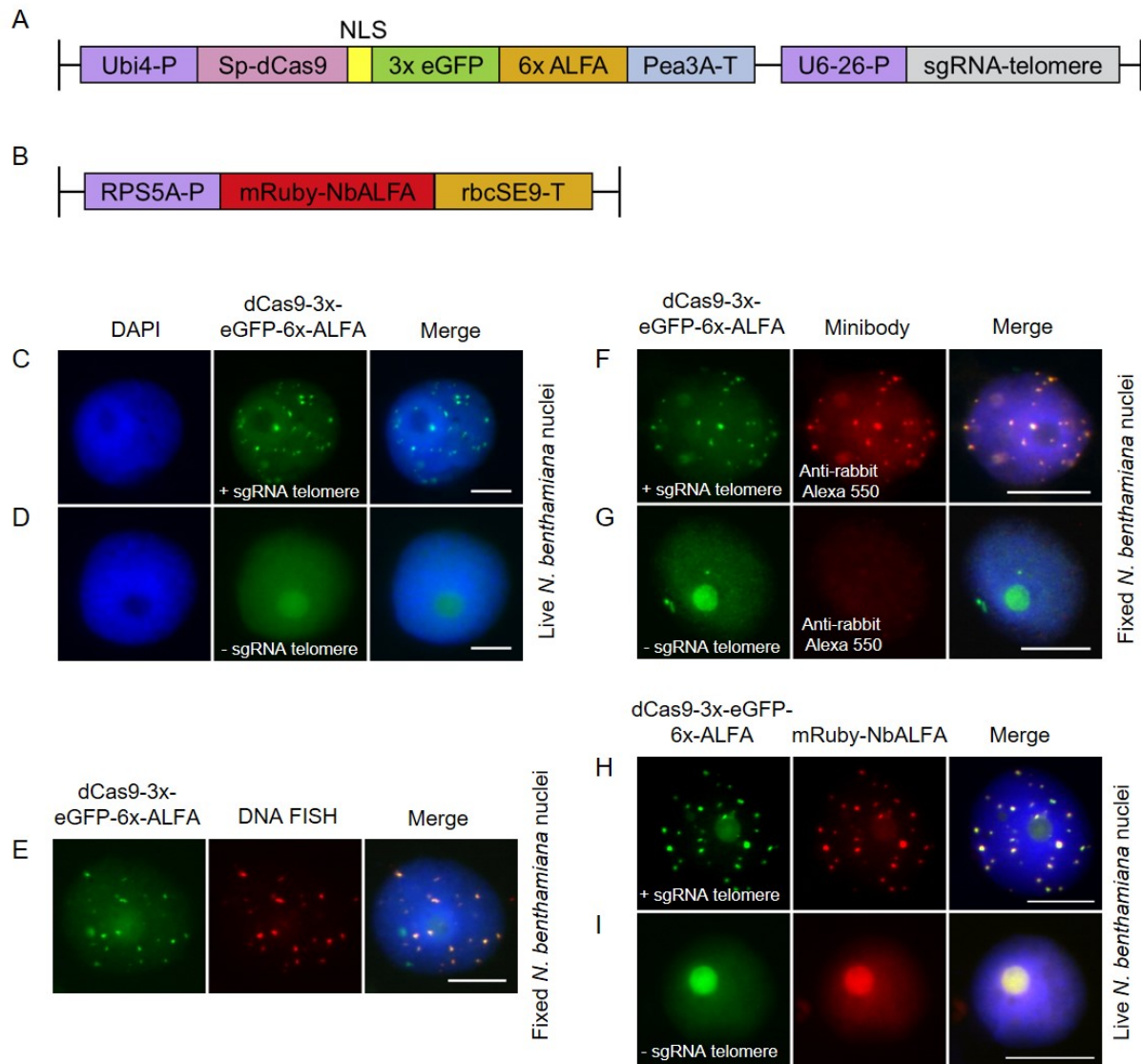
Fig 24: (A) Illustration of the Sp. dCas9-3x eGFP-ALFA-tag construct. Transcription of sp-dCas9-3x eGFP-ALFA-tag was initiated by the parsley ubiquitin 4 promoter and terminated by the pea 3A terminator, respectively. The nuclear localization of dCas9 was achieved using an SV40 NLS DNA sequence Transcription of the sgRNA scaffold was initiated by the Arabidopsis ubiquitin 6 promoter. (B) Illustration of mRuby-NbALFA, where transcription was initiated by RPS5A promoter and terminated by the rbcSE9 terminator. (C) Sp.dCas9-3x eGFP-ALFA-tag and sgRNA -telomere were used for live imaging of telomeres in *N. benthamiana* leaf cells during interphase. (D) As a negative control, the telomere sgRNA was omitted. (E) The specificity of live telomere labeling using the dCas9-eGFP-ALFA-tag was confirmed by co-localization with DNA FISH. (F) Detection of telomere labeling of Sp.dCas9-3x eGFP-ALFA-tag with minibody and staining with anti-rabbit Alexa 488 resulted in telomere like signals. (G) As a negative control, minibody applied to the leaf nuclei without expressing telomere sgRNA. (H) Dual labeling of telomeres in *N. benthamiana* using Sp.dCas9-3x eGFP-ALFA-tag and mRuby-NbALFA yielded green and red signals, with evident co-localization. This confirms the specificity of NbALFA towards ALFA-tagged dCas9. (I) Similar experiment without expressing telomere sgRNA as a negative control. Nuclei were counterstained with DAPI (in blue). Scale bars: 10 µm.

4.2.5 dCas9-ALFA-tag labeling with increasing NLS copy number to improve the nuclear import

Cas9 nuclease requires efficient nuclear import for efficient DNA cleavage in eukaryotic cells (GRÜTZNER *et al.* 2021). Cas9 variants containing up to four nuclear localization signals (NLSs) consistently showed significantly enhanced nuclear localization and activity in animal systems (KOBLAN *et al.* 2018; MAGGIO *et al.* 2020). To evaluate the potential enhancement in nuclear import and labeling efficiency, we engineered a dCas9 construct with four copies of the NLS sequence within the framework of the dCas9-ALFA-tag sequence (Fig. 25A). After 48 h of transiently infiltrated *N. benthamiana* leaves, strong telomere-like fluorescence puncta were observed, along with a non-specific background labeling of the nucleolus (Fig. 25B). As expected, without telomere sgRNA, only a non-specific nucleolar labeling was observed (Fig. 25C). *In vivo* telomere labeling was confirmed by co-localization of red telomere FISH signals with green signals from dCas9-3x eGFP-ALFA-tag (4x NLS) with telomere-specific sgRNA (Fig. 25D). Additionally, co-transformation of dCas9-3x eGFP-ALFA-tag (4x NLS) and mRuby-NbALFA resulted in dual labeling of telomeres in green and red (Fig. 25E). Omitting gRNA resulted in only faint green and red labeling of the nucleus without telomere labeling (Fig. 25F). When compared with normal dCas9-ALFA-tag vectors, brighter telomere signals were observed. This may be attributed to enhanced nuclear import of the protein, resulting in increased protein dosage within the nuclei and, consequently stronger labeling. However, further confirmation through quantification is warranted.
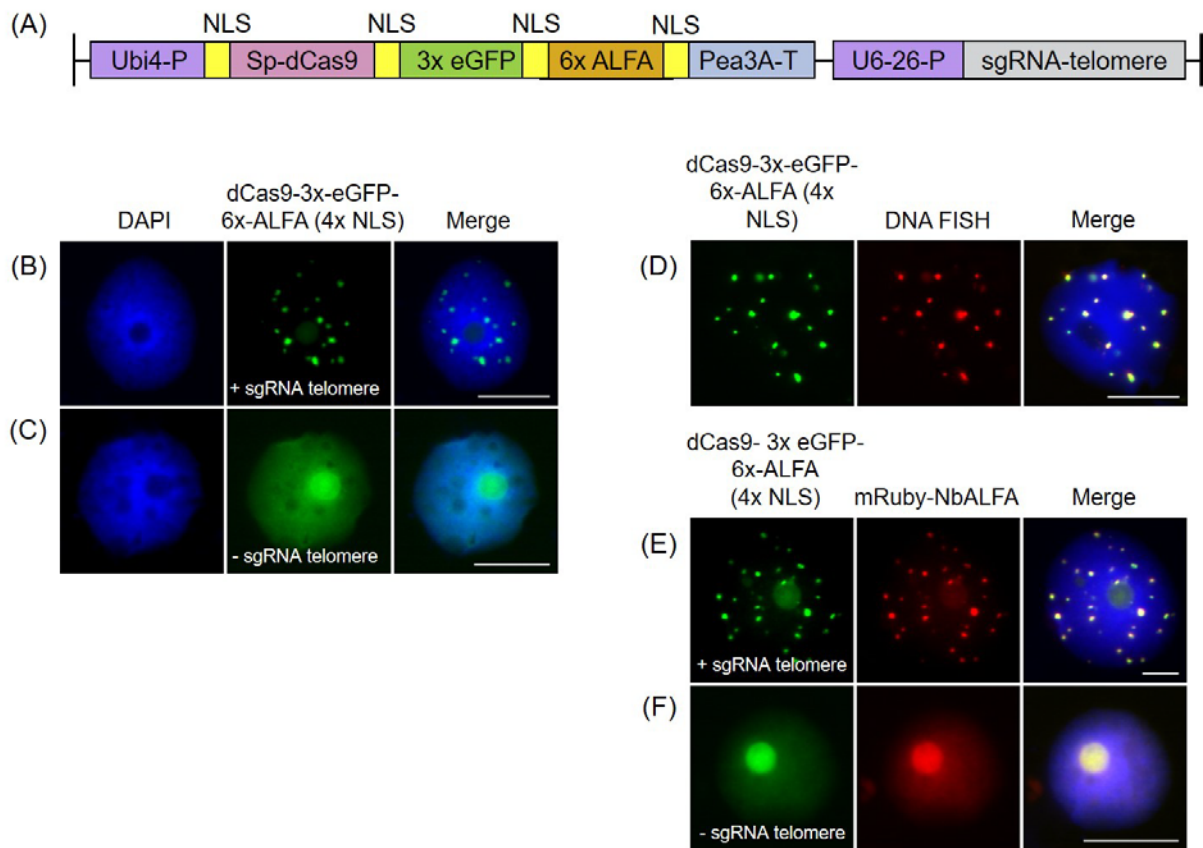
Fig 25: dCas9-ALFA-tag labeling with increasing NLS copies: (A) Illustration of the Sp. dCas9-3x eGFP-ALFA-tag construct. Transcription of sp-dCas9-3x eGFP-ALFA-tag was initiated by the parsley ubiquitin 4 promoter and terminated by the pea 3A terminator, respectively. The nuclear localization of dCas9 was achieved using four copies of SV40 NLS DNA sequence. Transcription of the sgRNA scaffold was initiated by the Arabidopsis ubiquitin 6 promoter. (B) Sp-dCas9-3x eGFP-ALFA-tag containing 4x NLS and sgRNA -telomere were used for live imaging of telomeres in *N. benthamiana* leaf cells during interphase. (C) As a negative control, the telomere sgRNA was omitted. (D) The specificity of live telomere labeling using the dCas9-eGFP-ALFA-tag was confirmed through clear co-localization with DNA FISH, thus validating the labeling specificity. (E) Dual labeling of telomeres in *N. benthamiana* using Sp-dCas9-3x eGFP-6x ALFA-tag and mRuby-NbALFA yielded red and green signals, with evident co-localization. This confirms the specificity of NbALFA towards ALFA-tagged dCas9. (F) Similar experiment without expressing telomere sgRNA as a negative control. Nucleus is counterstained with DAPI (in blue). Scale bars: 10 μm.

4.2.6 Application of an intronized Cas9 gene for dCas9 expression in combination with ALFA-tag in *N. benthamiana*

Recently, the utilization of an intronized *Cas9* was reported, where Arabidopsis introns were incorporated within the *Cas9* sequence (GRÜTZNER *et al.* 2021). This approach demonstrated highly efficient genome editing in *A. thaliana*, with a concurrent increase in the expression of the intronized Cas9. To investigate whether this approach could also improve labeling efficiency of dCas9 in *N. benthamiana*, we introduced point mutations (D10A and H841A) in the RuvC1 and HNH nuclease domains of zCas9i, a Cas9 variant previously utilized for genome editing (GRÜTZNER *et al.* 2021). The catalytically inactive z.dCas9i was utilized to create the z.dCas9i-ALFA-tag expression vector containing four NLS copies. This construct was transiently infiltrated into *N. benthamiana* leaves along with telomere-targeting sgRNA (Fig.26A). After 48 hours, strong telomere-like fluorescence puncta were observed. No nucleolar labeling occured (Fig. 26B). In the absence of telomere sgRNA, an only non-specific nucleolar labeling was seen (Fig. 26C). Telomere labeling was confirmed by co-localization of red telomere FISH signals with green signals from dCas9-3x eGFP-ALFA-tag (4x NLS) with telomere-specific sgRNA (Fig. 26D). Co-transformation of dCas9-3x eGFP-ALFA-tag (4x NLS) and mRuby-NbALFA resulted in dual telomere labeling in green and red (Fig. 26E). Omitting the sgRNA did not yield telomere-specific signals but resulted in uniform labeling of nuclei in both green and red (Fig. 26F). When compared with the normal dCas9-ALFA-tag vectors, this resulted in clear telomere signals with less nucleoplasm background labeling. However, this should be further confirmed by quantification.
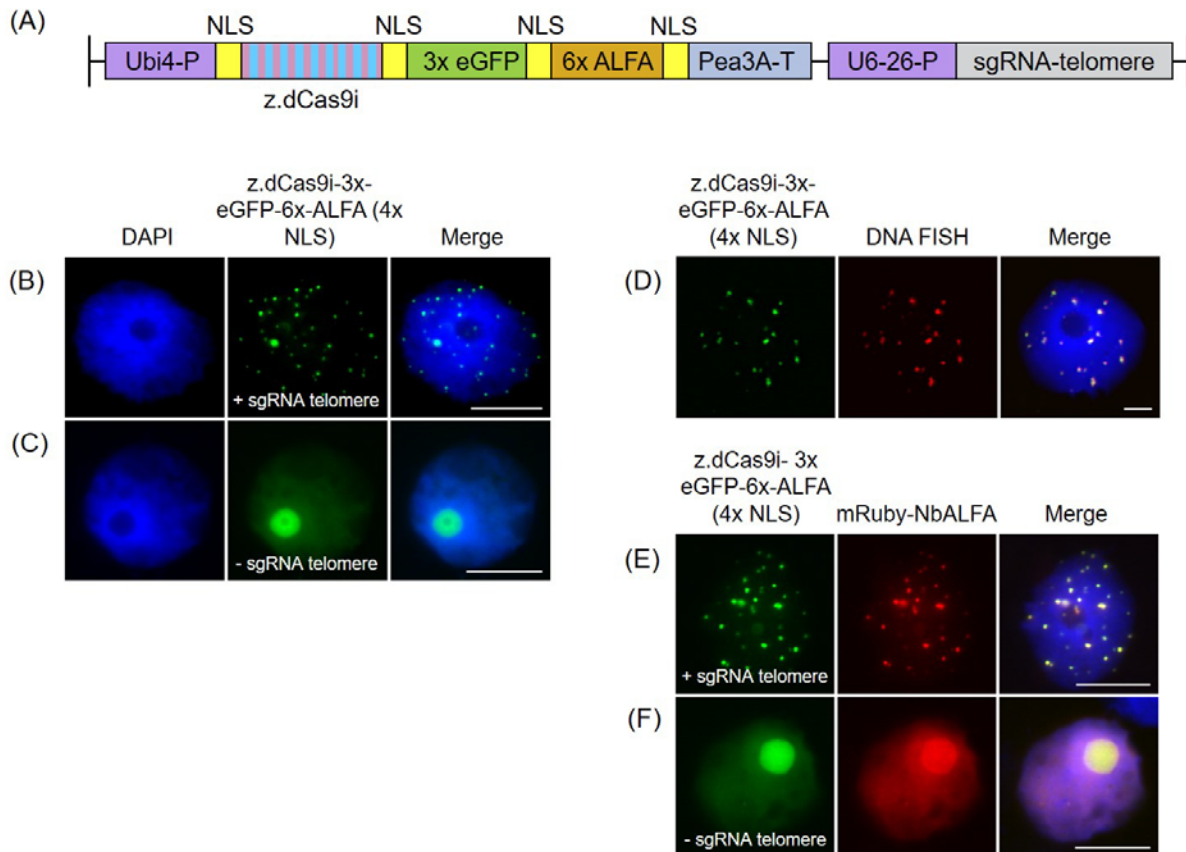
Fig 26: dCas9-ALFA-tag expression using an intronized Cas9 gene (A) Illustration of the Z.dCas9i-3x eGFP-ALFA-tag construct with intronized Z. dCas9 gene. Transcription of sp-dCas9-3x eGFP-ALFA-tag was initiated by the parsley ubiquitin 4 promoter and terminated by the pea 3A terminator, respectively. The nuclear localization of dCas9 was achieved using four copies of SV40 NLS DNA sequence Transcription of the sgRNA scaffold was initiated by the Arabidopsis ubiquitin 6 promoter. (B) Z.dCas9i -3x eGFP-ALFA-tag containing 4x NLS and sgRNA -telomere were used for live imaging of telomeres in *N. benth*amiana leaf cells during interphase. (C) As a negative control, the telomere sgRNA was omitted. (D) The specificity of live telomere labeling using the dCas9-eGFP-ALFA-tag was confirmed through clear co-localization with DNA FISH, thus validating the labeling specificity. (E) Dual labeling of telomeres in *N. benthamiana* using Z.dCas9i -3x eGFP-6x ALFA-tag and mRuby-NbALFA yielded red and green signals, with evident co-localization. This confirms the specificity of NbALFA towards ALFA-tagged dCas9. (F) Similar experiment without expressing telomere sgRNA as a negative control. Nucleus is counterstained with DAPI (in blue). Scale bars: 10 μm.

4.3 Tyramide signal amplification in combination with CRISPR-FISH

Tyramide Signal Amplification (TSA) is a sensitive *in situ* method utilizing horseradish peroxidase (HRP)-catalyzed tyramide deposition near the target nucleic acid sequence or protein (Raap *et al.* 1995). Typically, it involves the use of HRP-conjugated antibodies or streptavidin. To combine TSA with CRISPR-FISH, we utilized a biotinylated tracrRNA for the indirect labeling of DNA repeats with a streptavidin conjugate. Biotin-conjugated tracrRNA enabled the combination of TSA with indirect CRISPR-FISH. In this approach, the RNP complex labels the target DNA first, followed by the application of streptavidin HRP to interact with the biotinylated tracrRNA. Subsequent incubation with the biotin tyramide working solution results in the deposition of biotin-tagged tyramide in the proximity of target DNA sequences. Finally, the application of streptavidin-FITC allows the generation of strong fluorescence signals (Fig. 27A). Using this strategy; we successfully increased the signal size of the *A. thaliana* centromere repeats on fixed nuclei (Fig. 27B). Compared to signals obtained by using streptavidin FITC without TSA application the signal size increased roughly two-fold. However, the centromere signals looked fuzzier due to more dispersed tyramide deposition near the target sequence (Fig. 27B). In summary, we successfully combined TSA with CRISPR-FISH by utilizing biotinylated tracrRNA. This implementation has the potential to enhance the sensitivity of CRISPR-FISH.
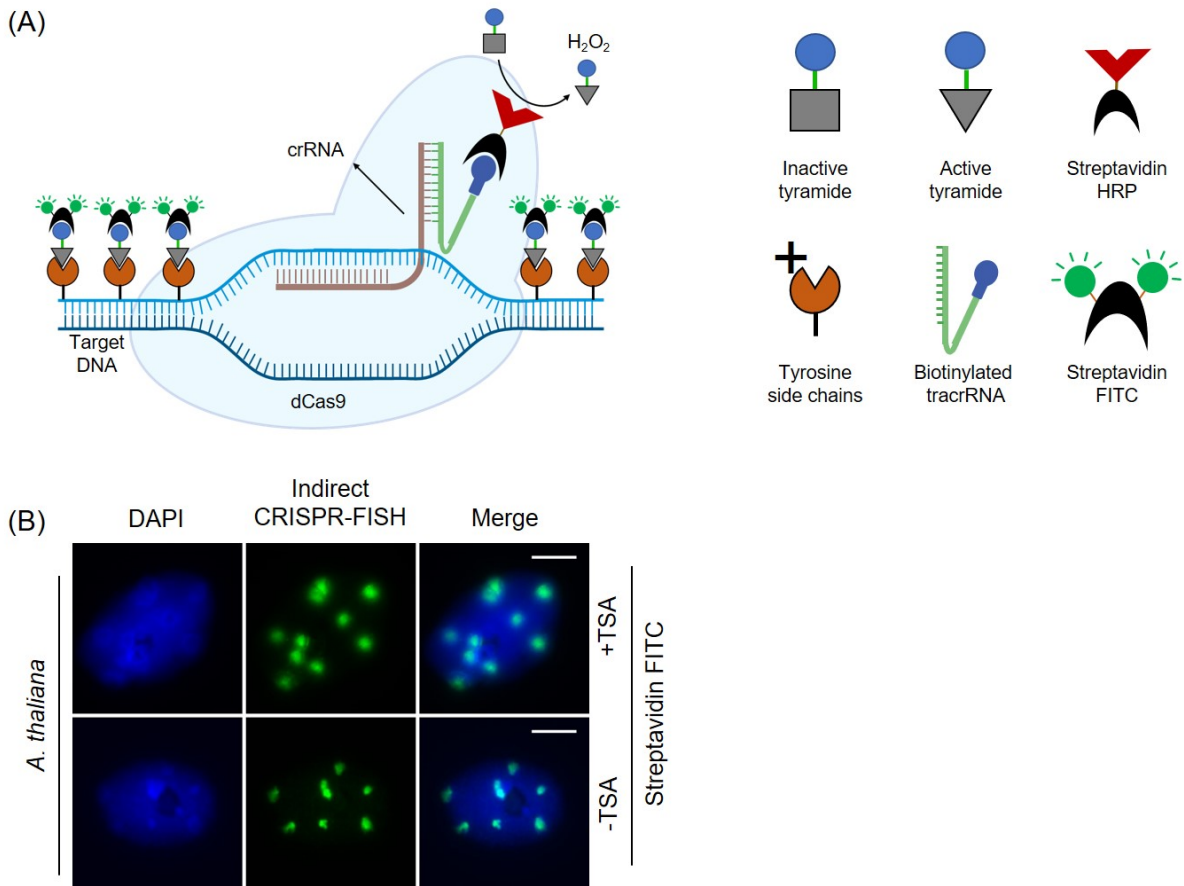
Fig 27: Tyramide signal amplification system in combination with indirect CRISPR-FISH. (A) Schematic of method. A dCas9 protein in combination with biotin-tagged bipartite gRNA, is used to label DNA repeats. The horseradish peroxidase, conjugated to the streptavidin, in the presence of H2O2 catalyzes the conversion of labeled biotin tyramide into a reactive radical. The biotin tyramide radical then covalently binds to nearby tyrosine residues and later application of streptavidin FITC, provides high-density labeling. (B) Labeling of *A. thaliana* centromeres using indirect CRISPR-FISH after TSA application (upper). As a negative control (lower), centromere visualized with streptavidin FITC without TSA application. Nuclei were counterstained with DAPI (in blue). Scale bars: 10 µm.

4.4   Application of RNA aptamers in the combination of CRISPR-FISH

To enhance CRISPR-based live-cell imaging efficiency, Khosravi et al. (2020) employed an RNA aptamer-based CRISPR/dCas9 system to visualize telomere repeats in *N. benthamiana* plants. However, this approach is incompatible with CRISPR-FISH on fixed samples. Thus, we aimed to utilize an advanced fluorescent RNA technology pioneered by Chen et al. (2019). Their approach employs fluorescent RNA aptamers known as 'Peppers', which bind and activate fluorescent ligands called "HBC" ((4-((2-hydroxyethyl)(methyl)amino)-benzylidene)-cyanophenyl-acetonitrile) (CHEN *et al.* 2019) (Fig. 28A), facilitating dynamic visualization of RNA and genomic loci in live mammalian cells (CHEN *et al.* 2019). Peppers exhibit bright, stable fluorescence across a range of emission wavelengths, and their fluorescence increases linearly with copy number when arranged in tandem arrays.

We aimed to utilize the advantages of 'Peppers' to enhance the intensity of the CRISPR-FISH signals. To test the Pepper system in plants, *A. thaliana*-specific telomere sgRNA was designed with 4x and 8x Pepper-type aptamers inserted into the sgRNA tetraloop and loop2. To test whether the Pepper telomere-specific sgRNA can direct dCas9 to telomere sequences on fixed *N. benthamiana* nuclei, we used dCas9-ALFA (3+3x) tag recombinant protein detected by minibody along with Pepper sgRNA. However, dCas9-ALFA (3+3x) with (Fig. 28B) 4x and (Fig. 28C) 8x Pepper telomere sgRNA failed to label telomeres on formaldehyde fixed *N. benthamiana* nuclei. In contrast, dCas9-ALFA (3+3x) with standard telomere gRNA (crRNA and Atto550 labeled tracrRNA) successfully labeled telomere repeats (Fig. 28D), confirming its active binding to the target DNA. This result confirms the active binding of dCas9-ALFA (3+3x) to the target DNA. The lack of labeling activity with Pepper sgRNA alongside dCas9-ALFA (3+3x) could be attributed to inactive sgRNA.
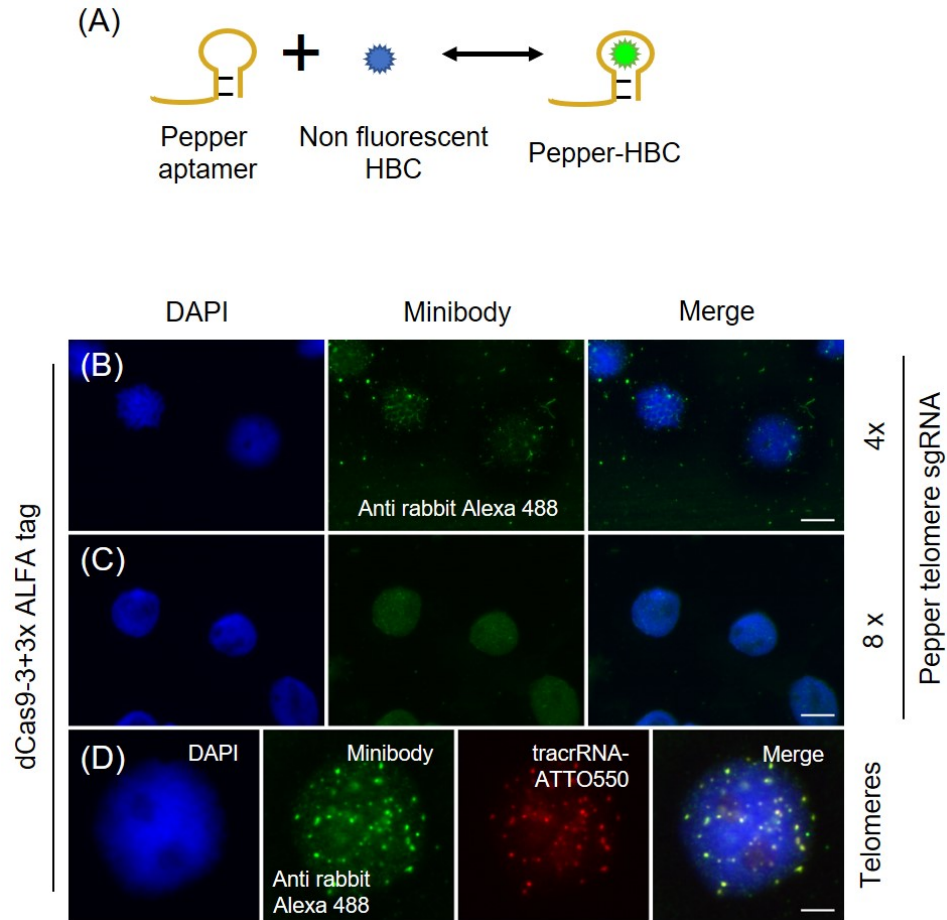
Fig 28: CRISPR-FISH in combination with fluorescent RNA technology (A) Schematic representation of the Pepper-HBC complex (based on Chen et al. 2019). Absence of telomere labeling with CRISPR-FISH in the combination of dCas9-ALFA-tag (3+3x) with (B) 4x and (C) 8x pepper telomere specific gRNA in *N. benthamiana* nuclei and detection with anti-rabbit Alexa 488. (D) Telomere labeling by dCas9-ALFA-tag (3+3x) in the combination of telomere-specific gRNA and minibody in *N. benthamiana* nuclei and detection with anti-rabbit Alexa 488. Scale bars: 10 μm.

4.5 Application of quantum dots for CRISPR-FISH labeling

Compared with fluorescence dyes, compact quantum dots (QDs) probes offer exceptional photostability and highly fluorescent owing to their enhanced brightness (RESCH-GENGER *et al.* 2008; LIU *et al.* 2018). To assess whether combining quantum dots with CRISPR-FISH would improve labeling efficiency, we attempted to label telomeres on fixed *N. benthamiana* nuclei using biotinylated tracrRNA in indirect CRISPR-FISH, detected with streptavidin-coated QD 510. However, no telomere signals were observed following the application of QD 510 (Fig. 29A, left). Conversely, control application of streptavidin FITC resulted in telomere labeling in fixed nuclei (Fig. 29A, right). Similarly, no labeling was observed after standard DNA FISH when using biotin-labeled telomere oligos in combination with streptavidin QD 510 (Fig. 29B, left). In contrast,streptavidin FITC-based detection resulted in telomere labeling after standard FISH (Fig. 29B, right). The failed telomere labeling with QD 510 could be attributed to the large QD diamter of around 70 - 80 nm, making it difficult to penetrate the nucleus and resulting in failed labeling in both indirect CRISPR-FISH and DNA FISH.
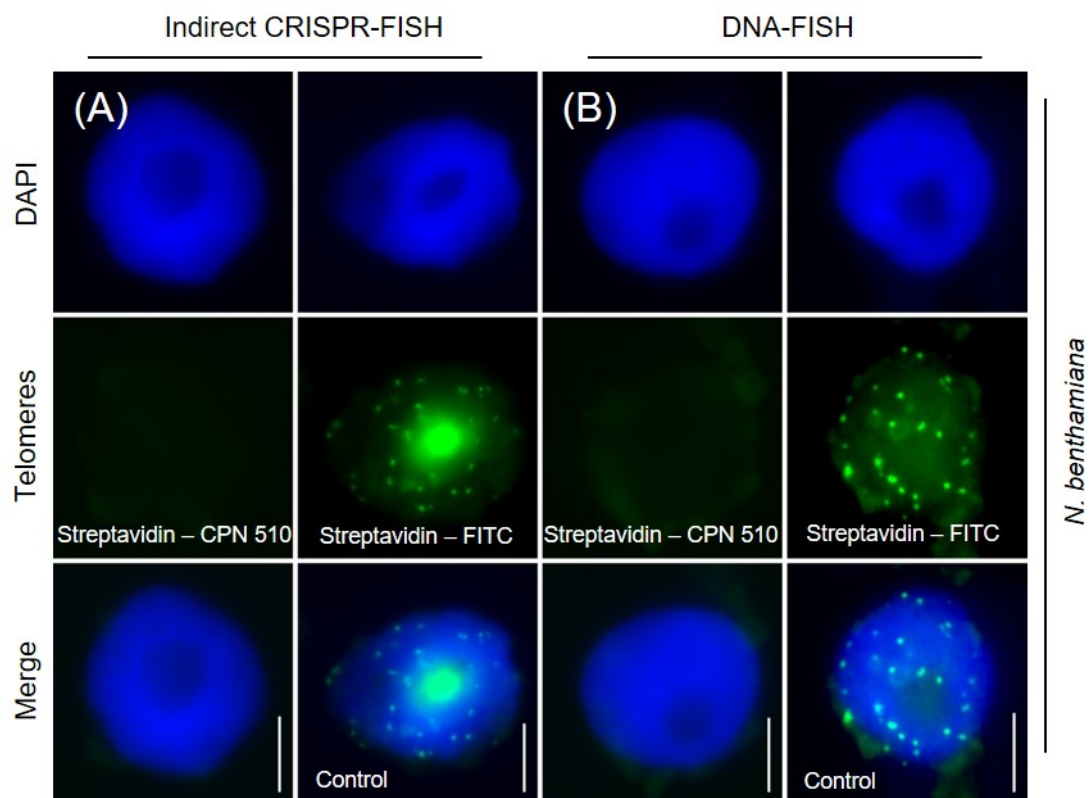
Fig 29: (A) Labeling of telomeres in fixed *N. benthamiana* nuclei with indirect CRISPR-FISH and detection with streptavidin conjugated to QD 510, and as a control with streptavidin conjugated to FITC. (B) Similar labeling with DNA FISH with biotin oligo with detection carried out using streptavidin conjugated to QD 510, and FITC was used as the control. Scale bar 5 um.

4.6 CRISPR-FISH labeling of non-repetitive sequences in *A. thaliana*

CRISPR-FISH has been successful in labeling high-repeat sequences. To expand the utility of CRISPR-FISH, we aimed to test its capability in labeling non-repetitive sequences. To achieve this, a pool of single-copy specificguide RNAs (in total 3200 crRNAs) targeting a 456 kb-long region on *A. thaliana* chromosome 5 was designed and synthesized by Daicel Arbor Biosciences (USA). The labeling of single-copy sequences using the pooled gRNAs was tested on 4% formaldehyde-fixed *A. thaliana* nuclei. As a control, direct CRISPR-FISH with *Arabidopsis* centromere-specific gRNA was utilized. Unfortunately, no labeling was observed using the pooled gRNA targeting the 456 kb region of chromosome 5 (Fig. 30a), while the control exhibited centromere signals (Fig. 30b).

Potlapalli et al. (2020) revealed that CRISPR-FISH displays high labeling efficiency with 3:1 fixed samples. To assess if CRISPR-FISH could label single-copy sequences using pooled gRNAs on 3:1 material, we employed 3:1 fixed nuclei and chromosomes. Despite the positive centromere signals in the control (Fig. 30d), no labeling was observed with pooled guide RNAs (Fig. 30c). We hypothesized that the failed labeling could be attributed to the use of multiple guide RNAs as a pool, potentially leading to competition for binding the RNP complex to the target DNA, thereby hindering RNP complex binding. To test whether using a large number of gRNAs in parallel hinders RNP complex binding to the target DNA, we combined the centromere guide RNA with a pool of guide RNAs ranging from 12 to 3200 crRNAs and applied them to slides containing *A. thaliana* nuclei. However, we did not observe any change in the labeling intensities of centromeres despite the application of pooled gRNAs (data not shown). This demonstrates that using pooled gRNAs does not affect RNP binding to the target DNA. The absence of labeling using pooled gRNAs may be attributed to the presence of only a single fluorophore (ATTO550) per RNP complex. Developing signal amplification strategies in conjunction with CRISPR-FISH could enhance the labeling of chromosomal single-copy DNA regions.
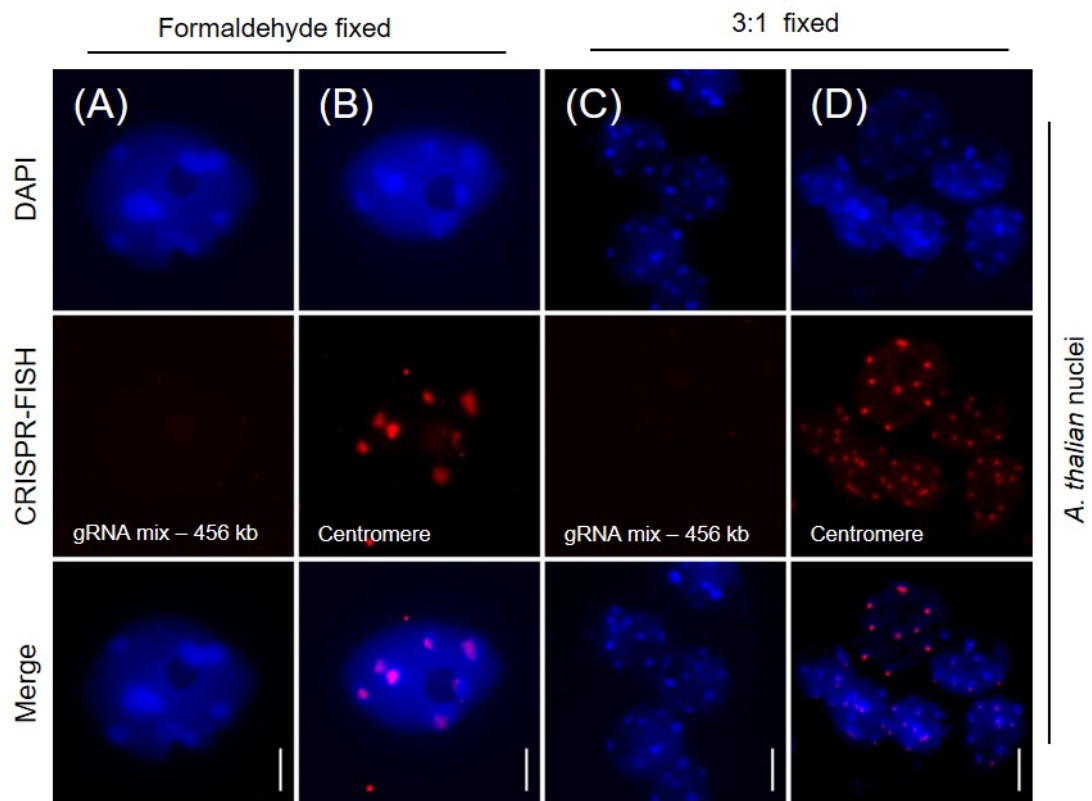
Fig 30: CRISPR-FISH labeling of non-repetitive sequences using pooled gRNAs targeting 456 kb region on chromosome 5 on (A) formaldehyde and (C) 3:1 fixed nuclei of A. thaliana. Additionally, labeling of centromeres was used as positive control (B & C). Scale bar 10 um.

4.7   Development of a CRISPR-ISH method for electron microscopy (CRISPR-EM)

The application of the non-denaturing CRISPR-ISH method, coupled with electron microscope-based signal detection (CRISPR-EM), holds the potential to investigate chromatin structure at the highest resolution, providing additional insights and driving novel developments. To develop CRISPR-ISH for transmission electron microscopy (TEM), we chose to combine the indirect CRISPR-FISH method utilizing biotinylated gRNA with streptavidin FluoroNanogold (Fig. 31A). This unique streptavidin probe contains both a 1.4 nm Nanogold particle and fluorescein fluorophore (Fig. 31B), enabling visualization of the target DNA sequences by both fluorescence and electron microscopy in a single labeling procedure. To test whether streptavidin FluoroNanogold could be used in combination with indirect CRISPR-FISH, we labeled the centromere repeat on formaldehyde-fixed *A. thaliana* nuclei using specific gRNA with indirect CRISPR-FISH and detected with streptavidin FluoroNanogold. As a control, standard CRISPR-FISH using Atto550-labelled tracrRNA and indirect CRISPR-FISH using biotinylated tracrRNA with centromere-specific crRNA were used. Streptavidin FITC was used to detect biotinylated RNP complex binding sites. The result showed labeling of the centromere repeats by indirect CRISPR-FISH using streptavidin FluoroNanogold (Fig. 31C). A similar pattern of centromere-specific labeling was also observed in the positive controls (Fig. 31D & E). Additionally, FluoroNanogold in combination with indirect CRISPR-FISH successfully labeled the centromeres on 3:1 (ethanol: acetic acid) fixed *A. thaliana* metaphase chromosomes (Fig. 31F).

In electron microscopy studies, glutaraldehyde is a commonly used fixative that is well-known for its effectiveness in maintaining the ultrastructure of biological material (Sᴇᴡᴇʟʟ *et al.* 1984). Therefore, imaging centromeres on *A. thaliana* nuclei fixed with 2.5% glutaraldehyde resulted in distinct centromere labeling (Fig. 31G). Overall, these results demonstrate successful labeling of DNA repeats on interphase and metaphase chromosomes using indirect CRISPR-FISH and streptavidin FluoroNanogold under various fixation conditions
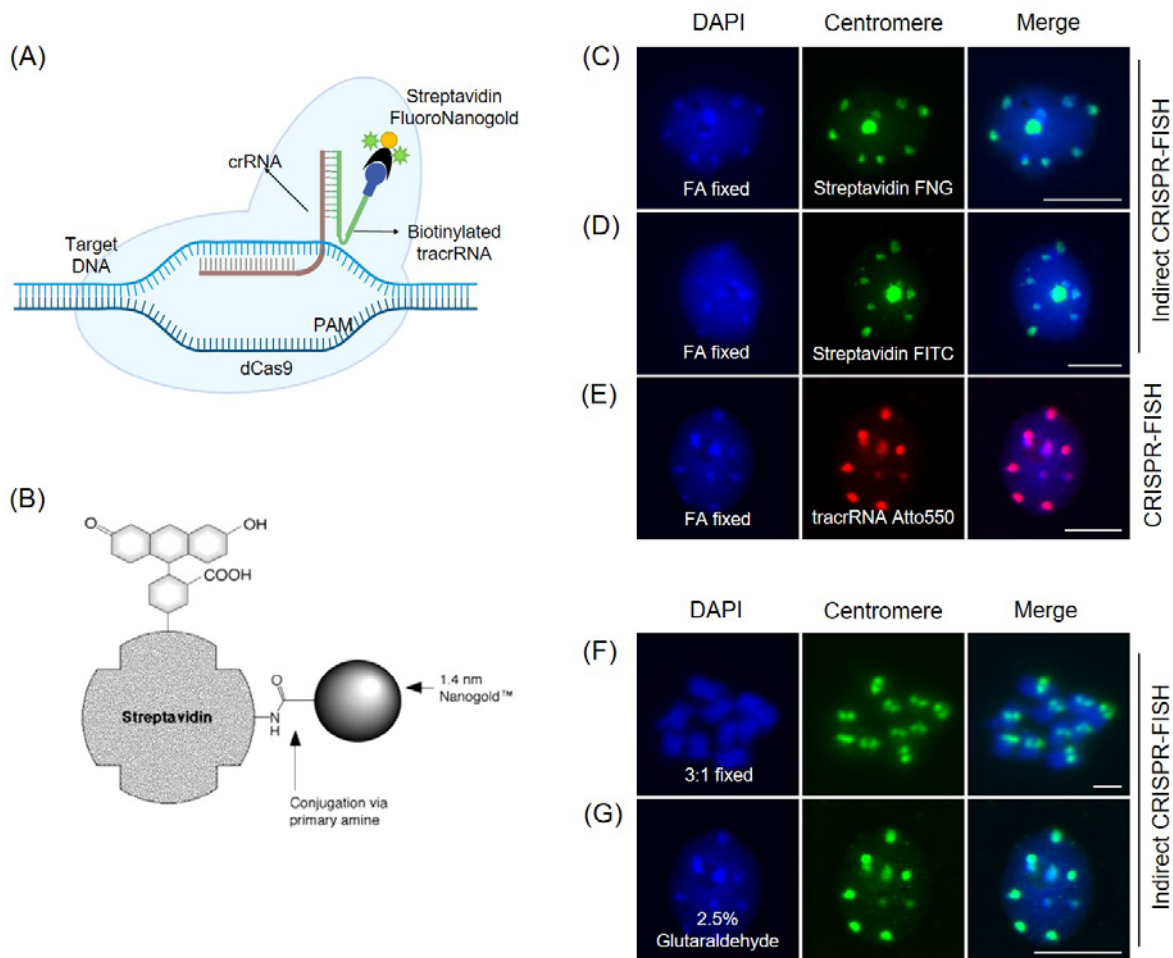
Fig 31: Indirect CRISPR-FISH method for electron microscopy. (A) Schematic overview of the indirect CRISPR-FISH methodology for electron microscopy (EM), utilizing biotinylated tracrRNA in conjunction with streptavidin-conjugated FluoroNanogold. (B) Structure of streptavidin conjugated to fluorescein and Nanogold via primary amines to give FluoroNanogold. Labeling of centromere repeats on formaldehyde-fixed *A. thaliana* nuclei with indirect CRISPR-FISH and streptavidin-conjugated (C) FluoroNanogold or (D) FITC. (E) Standard CRISPR-FISH labeling of centromere repeats using Atto550 tracrRNA. Labeling of centromere repeats on (F) 3:1 fixed chromosomes and (G) glutaraldehyde-fixed *A. thaliana* nuclei with streptavidin FluoroNanogold. Scale bar 10 um.

4.7.1 Optimization of the Nanogold silver enhancement method

Fluorescent labeling of *A. thaliana* centromeres with indirect CRISRP-FISH and streptavidin FluoroNanogold confirms the specificity of the method. However, to visualize the sample under an electron microscope, the size of the 1.4 nm ultra-small gold particles must be increased by silver enhancement. To optimize the conditions for silver enhancement, we opted to label *Fok*I satellite repeats on 3:1 fixed *V. faba* nuclei. It is located in several regions along the long arms of all five acrocentric chromosomes of *V. faba* (Fuchs *et al.* 1994b). This repeat was chosen because of the strong *Fok*I signals generated after *in situ* labeling. Also,

the 3:1 fixation method demonstrated high efficacy in conjunction with CRISPR-FISH (POTLAPALLI *et al.* 2020). Imaging of *Fok*I repeats on 3:1 fixed *V. faba* nuclei showed successful labeling with streptavidin FluoroNanogold in combination with indirect CRISPR-FISH (Fig. 32A). A similar outcome was observed with streptavidin Cy3 (Fig. 32B) and standard CRISPR-FISH (Fig. 32C), employing *Fok*I-specific Atto550 tracrRNA as positive controls. However, despite applying a silver enhancement of 1 -10 min, FluoroNanogold failed to produce non-fluorescent *Fok*I-specific signals (Fig. 32D). In contrast, the positive control streptavidin FluoroNanogold (Fig. 32E) and Cy3 showed fluorescent *Fok*I-specific signals respectively (Fig. 32F). Moreover, extending the silver enhancement time further (15–25 min), did not yield any *Fok*I-specific signals (data not shown). The failure in silver enhancement of *Fok*I-specific non-fluorescent nanogold signals may be attributed to issues with the HQ silver enhancement kit or with streptavidin FluoroNanogold.
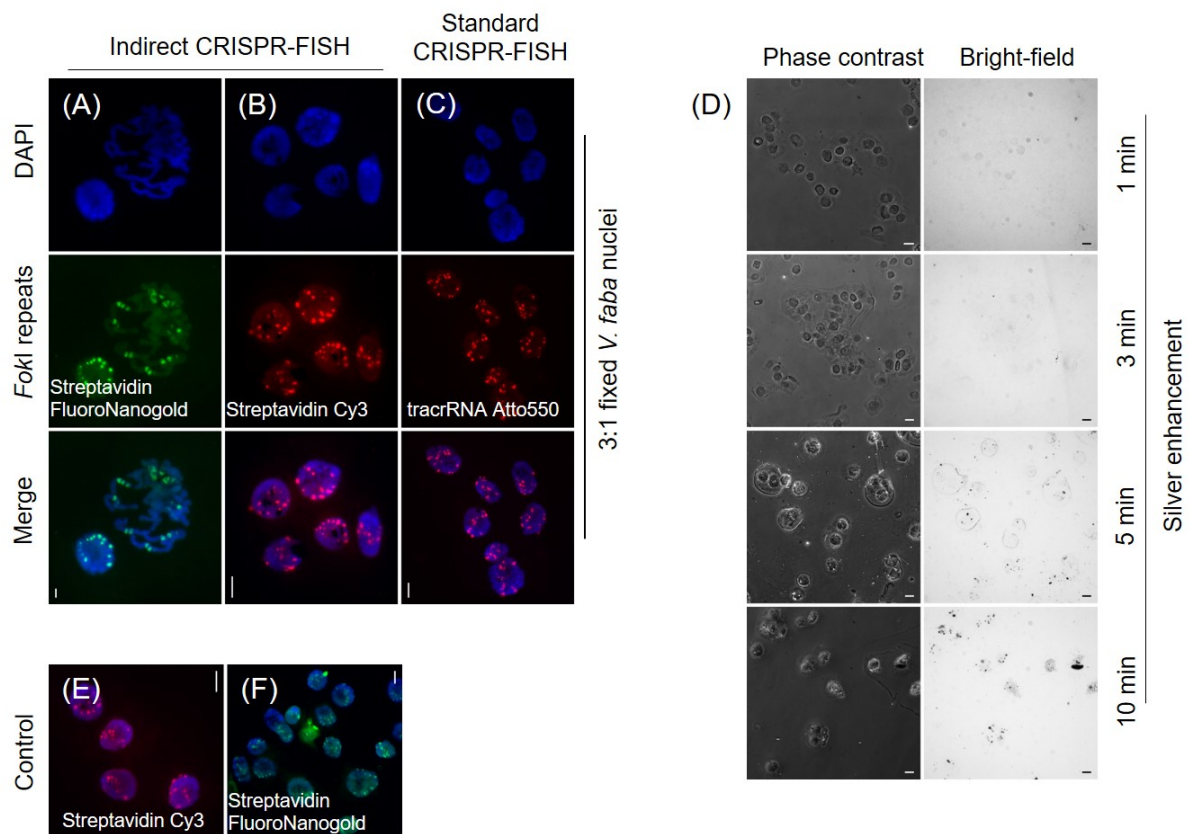
Fig 32: Labeling of *Fok*I repeats with Indirect CRISPR-FISH detection with (A) FluoroNanogold (green) and (B) streptavidin Cy3 (red) and (C) standard CRISPR-FISH labeling of *Fok*I repeats using Atto550 tracrRNA (red). (D) Silver enhancement at varying durations yields no *Fok*I-specific gold signals. As a control *Fok*I repeats detected with (E) streptavidin Cy3 and (F) streptavidin FluoroNanogold. Scale bar 10 um.

To assess the functionality of the HQ Silver Enhancement Kit, we immunolabeled the centromeric CENH3 protein of *Brassica napus* on formaldehyde-fixed *B. napus* interphase nuclei using a combination of rabbit anti-Brassica CENH3 and anti-rabbit FluoroNanogold Alexa Fluor 488 antibodies (Fig. 33A). The anti-BrassicaCENH3 antibody was provided by N. Ohmido (Kobe, Japan). A similar outcome was observed with anti-rabbit Alexa Fluor 555 as a positive control (Fig. 33B). Silver enhancement for a period of time of 8 and 15 min successfully produced clear black-colored CENH3-specific signals (Fig. 33C), confirming the kit's functionality. This suggests that the previous failure in nanogold labeling (Fig. 33B) may be attributed to a defect in the FluoroNanogold streptavidin molecule itself.
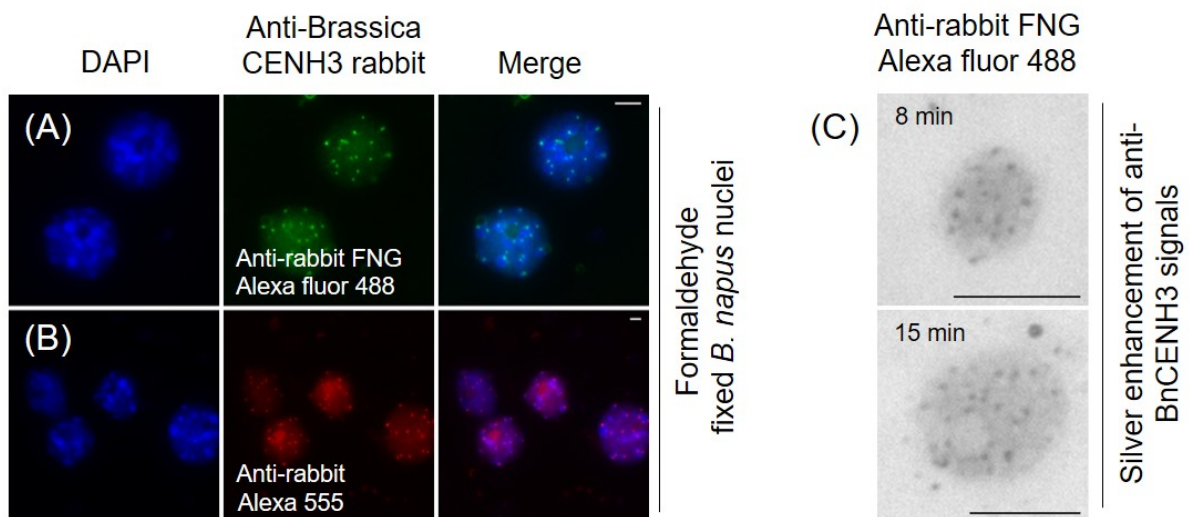
Fig 33: (A) *B. napus* CENH3 immunolabeling with rabbit anti-BrassicaCENH3, detected by anti-rabbit FluoroNanogold Alexa Fluor 488 (green). (B) As a control anti-rabbit Alexa 555 used for detecting the anti-*Brassica* CENH3 antibody. (C) Immunogold labeling of *B. napus* CENH3 with rabbit anti-Brassica CENH3, detected by anti-rabbit FluoroNanogold antibodies, followed by silver enhancement (8 and 15 min). Size bars 10 um.

4.7.2 Nanogold labeling of *Fok*I repeats utilizing indirect CRISPR-FISH with anti-rabbit FluoroNanogold

Due to the non-functionality of the applied streptavidin FluoroNanogold, it cannot be used in combination with indirect CRISPR-FISH. However, we considered combining indirect CRISPR-FISH with biotinylated tracrRNA and anti-rabbit FluoroNanogold antibody, using streptavidin FITC and rabbit anti-FITC as an alternative approach. The imaging strategy involved detecting the RNP complex with streptavidin FITC, followed by rabbit anti-FITC and anti-rabbit FluoroNanogold (Fig. 34A). Testing this on *Fok*I repeat DNA on 3:1 fixed *V. faba* nuclei using

indirect CRISPR-FISH, detected with streptavidin FITC followed by rabbit anti-FITC and anti-rabbit Alexa 555 antibody, successfully labeled the repeats (Fig. 34B). Similarly, applying rabbit anti-FITC followed by anti-rabbit FluoroNanogold and subsequent silver enhancement yielded distinct signals specific to *Fok*I repeats visualized with bright-field microscopy (Fig. 34C). Colocalization of streptavidin-FITC and anti-rabbit FluoroNanogold signals, along with enhanced nanogold signals, confirmed specificity. Overall, the results demonstrate efficient non-fluorescent gold labeling of repeat sequences achieved by combining rabbit anti-FITC with indirect CRISPR-FISH and anti-rabbit FluoroNanogold antibody. Microscopic analysis confirms the effectiveness of the developed method in labeling DNA repeats with nanogold.
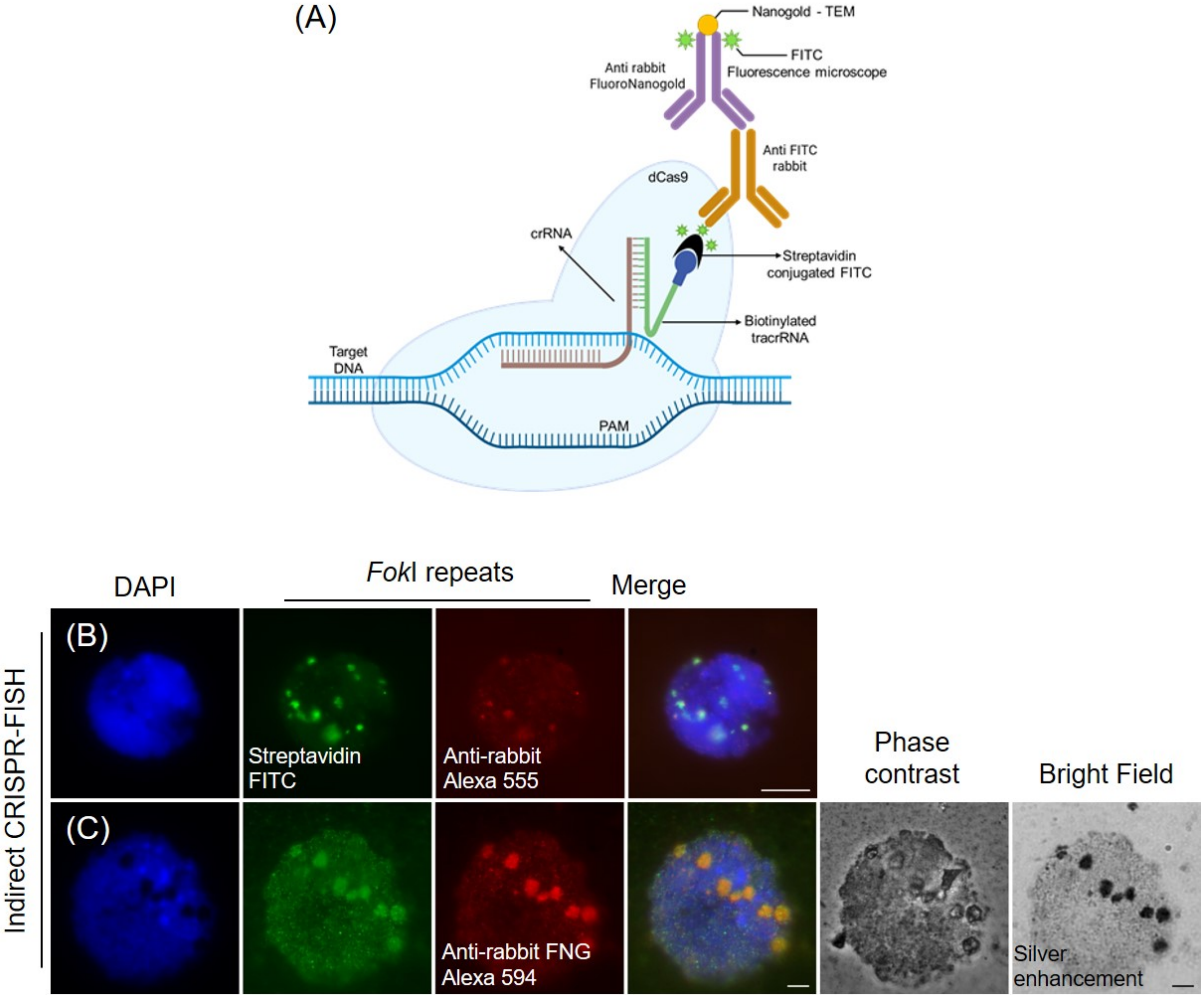
Fig 34: (A) Schematic representation of the gold labeling process for DNA sequences using Indirect CRISPR-FISH with biotinylated tracrRNA. Subsequently, incubation with streptavidin FITC enables the detection of the biotinylated RNP complex. The complex is then detected using a rabbit anti-FITC antibody and further detected with an anti-rabbit FluoroNanogold antibody. (C) Nanogold labeling of *Fok*I repeats of *V. faba* by indirect CRISPR-FISH by combining streptavidin FITC, rabbit anti FITC and anti-rabbit FluoroNanogold antibodies respectively, followed by silver enhancement. (B) As a control, rabbit anti FITC detected with anti-rabbit Alexa 555. Silver enhancement is employed to generate *Fok*I-specific gold signals. Scale bar 10 um.

4.7.3 Nanogold labeling of *Fok*I repeats utilizing dCas9-ALFA-tag and minibody with anti-rabbit FluoroNanogold

dCas9 ALFA-tagged proteins, in combination with a minibody and a fluorescence-labeled anti-rabbit secondary antibody, successfully labeled DNA repeats with increased signal intensities. The minibody, functioning like a conventional anti-rabbit antibody (Frodyma *et al.* 2022; Nozawa *et al.* 2022), can be combined with anti-rabbit FluoroNanogold antibodies for gold labeling. Alternatively, we considered leveraging the dCas9 ALFA-tagged approach for nanogold labeling of repetitive sequences, which could prove valuable for labeling low-copy sequences in the future (Fig. 35A). Testing this on *Fok*I repeat DNA on 3:1 fixed *V. faba* nuclei showed successful detection, confirmed by overlapping green (anti-rabbit FluoroNanogold) and red signals (tracrRNA Atto550) (Fig. 35B). Silver enhancement after incubation with anti-rabbit FluoroNanogold antibody resulted in black *Fok*I repeat-specific signals on *V. faba* nuclei, confirming specificity through colocalization with fluorescent signals (Fig. 35B). dCas9 ALFA-tagged proteins, combined with a minibody and fluorescence-labeled anti-rabbit secondary antibody, efficiently labeled DNA repeats with nanogold. The approach offers versatility, allowing for potential gold labeling of low-copy sequences in the future.
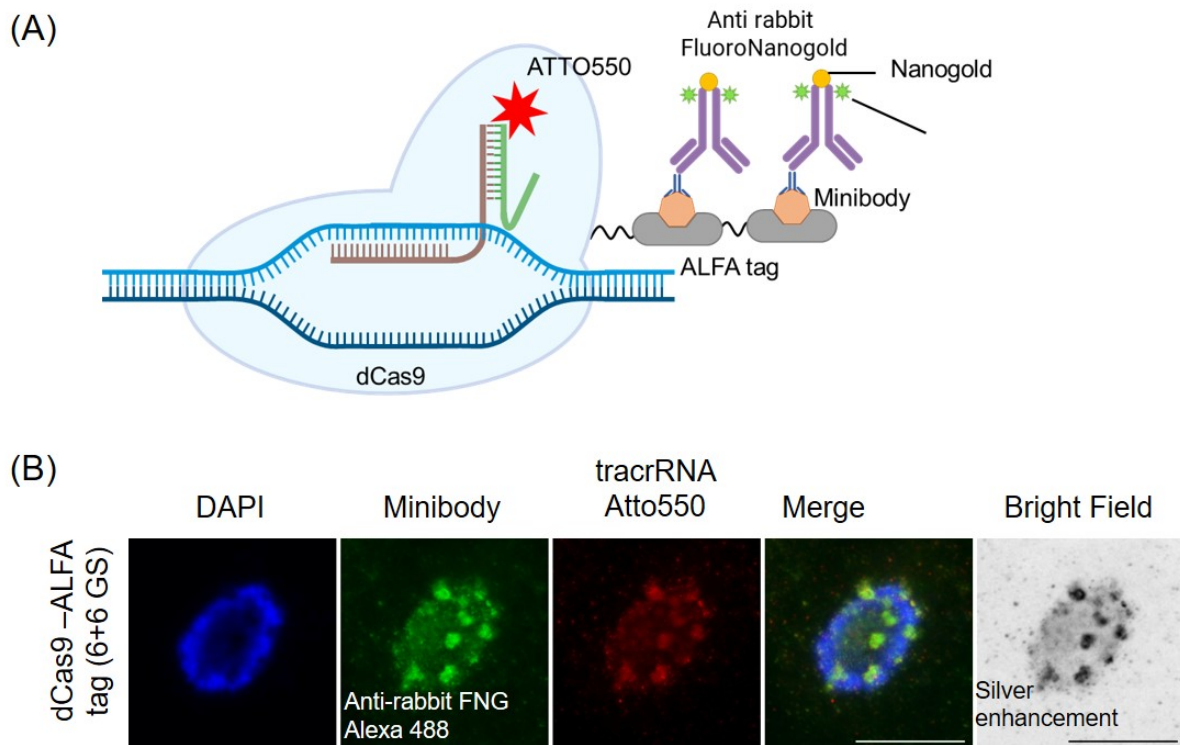
Fig 35: Nanogold labeling of *Fok*I repeats by CRISPR dCas9 ALFA-tag approach. (A) Schematic representation of the gold labeling process for DNA sequences using recombinant dCas9-ALFA protein. Subsequently, incubation with a minibody allows detection of the ALFA-tag RNP complex, which is then detected using an anti-rabbit FluoroNanogold antibody. (B) dCas9-ALFA-tag system based labeling of *Fok*I repeats on 3:1 fixed *V. faba* nuclei using minibody and anti-rabbit FNG Alexa 488. In parallel, signals from tracrRNA Atto550 (red signals) are used as a control. Silver enhancement is employed to generate *FokI*-specific gold signals. Size bar 10 um.

4.7.4 Optimizing sample transfer and fixation conditions for CRISPR-based nanogold detection by electron microscopy

In order to investigate the CRISPR-based nanogold labeling at the high structural resolution, the best fixation conditions that suit electron microscopy should be optimized. At first, 4% formaldehyde fixed *V. faba* nuclei were spun on the gold grids and visualized under TEM. The result showed nuclei-like structure, but the contrast was not enough to detect a good structure (Fig. 36A, upper). The grids were treated with lead citrate to enhance contrast and visualized under TEM. The results showed improved counter-staining of the nuclei (Fig. 36A, lower). Unfortunately, we encountered difficulties in visualizing the 3D structures on the grids using isolated nuclei. One potential improvement could involve visualizing ultra-thin sections prepared from the resin containing isolated nuclei. However, the process of transferring nuclei from the surface of the glass slide to the resin proved to be technically challenging and did not produce satisfactory results (data not shown).

Ghazizadeh et al. (2008) reported using an ACLAR film as a surface substrate for chromosome and nuclei spreads that improved the transfer of chromosomes and nculei to the resin. To test this methodology, a chromosome suspension of *V. faba* was dropped on the ACLAR film, and later transferred to the resin, and the prepared ultrathin sections were visualized under TEM. However, we failed to visualize nuclei (data not shown). This could be may be due to the 3:1 (ethanol: acetic acid) fixation used to prepare the samples.

Parallelly, to investigate the surface structure of *V. faba* nuclei, three different fixation conditions (2.5% glutaraldehyde, 4% formaldehyde and 2% formaldehyde, and 0.5% glutaraldehyde) were used to fix nuclei and visualized them under the scanning electron microscope (SEM). Unfortunately, we could only visualize some structures from two fixation conditions. However, the structures captured with SEM were not ideal for determining the best fixation (Fig. 36Bb). This could be due to the use of a cytospin, which concentrates nuclei on the slide at a higher speed, potentially destroying the nuclei structure.

Overall, our attempts to optimize fixation conditions for electron microscopy visualization of CRISPR-based nanogold labeling did not yield satisfactory results in preserving 3D structures. Both the utilization of ACLAR film for transferring the nuclei to grids and experimentation with different fixation conditions for *V. faba* leaf nuclei failed to yield the desired outcomes. Therefore, further exploration and refinement of fixation protocols are necessary to enhance the visualization of nanogold-labeled structures using electron microscopy.
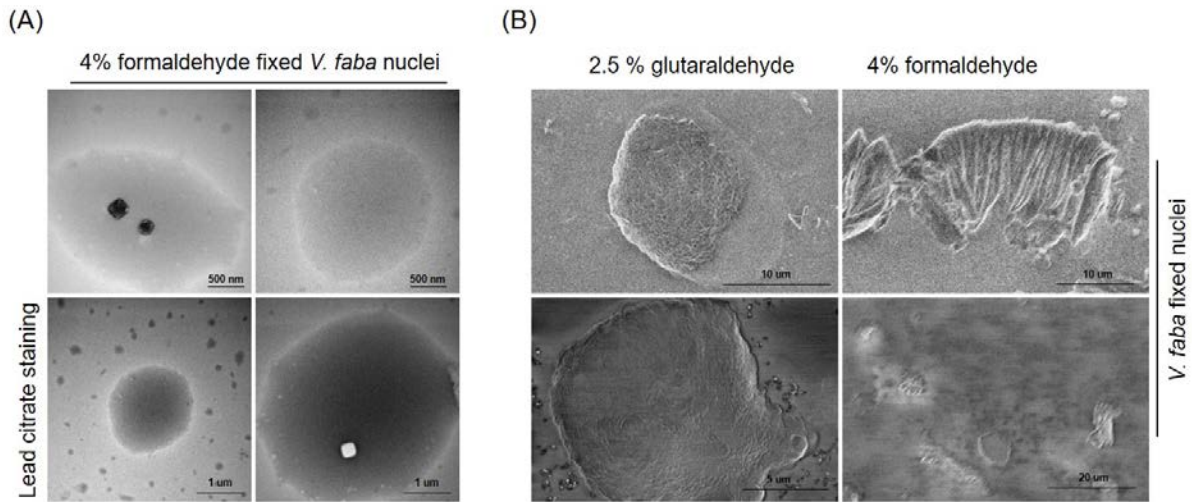
Fig 36: Visualization of isolated *V. faba* nuclei under the electron microscope: (A, upper) Transmission electron microscopy images of 4% formaldehyde fixed *V. faba* nuclei placed on the gold grids with reduced contrast. (A, lower) Improved contrast was achieved by incubating the gold grids with lead citrate. (B) Scanning electron microscopy images of *V. faba* fixed nuclei with (B, left) 2.5% glutaraldehyde and (B, right) 4% formaldehyde, respectively.

5. Discussion

5.1 CRISPR-CID - an in situ chromogenic DNA repeat detection system for research and life science education

Standard CRISPR-FISH uses a fluorescently labelled tracrRNA to visualize repetitive DNA in fixed samples (Ishii *et al.* 2019). In this study, we developed a non-fluorescent CRISPR-ISH method and tested two different strategies for an indirect labeling of DNA. Thereby the use of biotinylated tracrRNA showed a higher efficiency for both fluorescent and non-fluorescent labeling compared to the use of Cas9 antibodies. The lower efficiency using Cas9 antibodies may be due to the effect of formaldehyde post-fixation, which may alter the conformation of the proteins along with their epitopes, thereby reducing the accessibility for the anti-Cas9 antibody (Bogen *et al.* 2009; O'Leary *et al.* 2009). In contrast, the use of biotinylated tracrRNA is more advantageous due to its strong irreversible interaction with streptavidin, which is not affected by the use of stringent washing and fixation conditions (Kolodziej *et al.* 2009). Using biotinylated tracrRNA, CRISPR-CID produced much clearer signals with the streptavidin-horseradish enzyme conjugate than with the alkaline phosphatase conjugate. This may be due to the large size of the alkaline phosphatase (approximately 86 kDa), which may make it difficult to penetrate the chromatin (Bradshaw *et al.* 1981). On the other hand, horseradish peroxidase is only 40 kDa in size, suggesting a better ability to penetrate the chromatin (Rennke and Venkatachalam 1979).

Compared to other tested chromatin counterstains, haematoxylin and neutral red showed optimal staining, providing better contrast between signals and nuclei or chromosomes. However, hematoxylin stained chromocenters in formaldehyde-fixed *A. thaliana* nuclei, but 3:1 (ethanol: acetic acid) fixed sample showed no such pattern, indicating that fixation conditions might affect nuclear counterstaining. Unfortunately, none of the non-fluorescence dyes stained uniformly *A. thaliana* nuclei and this should be investigated further by screening more dyes in future.

Unlike standard FISH, which requires harsh DNA denaturation to hybridize complementary DNA, CRISPR-CID is a fast and convenient method and offers several advantages over conventional DNA detection methods. In particular, the CRISPR-CID application time is much shorter due to the rapid DNA binding of Cas9 (Ishii *et al.* 2019). Unlike standard FISH, which requires expensive fluorescence microscopes and specialists, CRISPR-CID only requires

standard light microscopes to visualize the labeled DNA. In addition, chromogenic signals generated by CRISPR-CID are sufficiently strong to use a 40x lens for visualization and don't fade over time, and specimens can be archived for long periods. Moreover, CRISPR-CID uses mild conditions that make it easy and safe to carry out hands-on investigations in schools or laboratories where expensive fluorescence microscopes and skilled specialists are not available. Therefore, visualization of DNA repeats under a standard microscope in schools would further encourage a deep interest in science and inspire students to examine genomic DNA to better understand the chromatin structure already at an early age. To make the application of CRISPR-CID more accessible to schools, CRISPR-CID could be combined with a paper-based origami microscope called the Foldscope (https://foldscope.com/), which has 140x magnification and is commercially available as a classroom kit (CYBULSKI *et al.* 2014). On top of using pre-assembled dCas9/gRNA RNP complexes to label DNA, it does not require a GMO-related permission and raises no ethical concerns when used in the classroom environment.

However, the application of CRISPR-CID is limited by the requirement of the NGG PAM sequence at the target sequence, which is necessary to design the gRNA. This limitation could be overcome by using engineered Cas9 variants that work with different PAM sequences. The effectiveness of CRISPR-CID in labeling target DNA depends on the copy number of the target sequence, rendering it less efficient when dealing with low or single copy sequences.

Nevertheless, CRISPR-CID has a great deal of potential for future applications. Taking advantage of the biotinylated tracrRNA, it is likely that the sensitivity of the CRISPR-CID method can be increased by combining it with other labeling methods, such as the tyramide amplification system (TSA) for labeling low-copy regions. Besides labeling on fixed nuclei and chromosomes, it could be developed to non-fluorescently label repeats on fixed tissue sections in a similar way as reported by Nagaki and Yamaji (2020).

Furthermore, using recombinant dCas9 proteins fused to horseradish peroxidase enzymes could further simplify the method by allowing the labeling of target sequences in a single step. We aimed to simplify CRISPR-CID labeling by fusing dCas9 with HRP. However, post-protein purification and visualization on a SDS-PAGE gel, the fusion protein showed a significantly lower concentration compared to dCas9 alone (Appendix Fig 1). It's worth noting that dCas9 protein purification was not performed in parallel with the fusion protein, but in our studies,

dCas9 purification consistently yielded higher concentration. The decreased protein concentration observed on the SDS gel can be explained by the glycoprotein nature of HRP. Since *E. coli* lacks the machinery for glycosylation, disulfide bridges crucial for proper protein folding may fail to form, leading to the production of HRP as inclusion bodies, resulting in inactive aggregates (SMITH *et al.* 1990; GUNDINGER AND SPADIUT 2017). In our approach, we utilized a native protein purification strategy, where only soluble fractions were eluted, and inclusion bodies were discarded along with the cell debris pelleted after bacterial cell lysis, potentially resulting in the loss of dCas9-HRP fusion proteins as inclusion bodies. In the future, this issue could potentially be addressed by incorporating an additional PGK-tag to enhance solubility. Moreover, incubating the eluted proteins in hemin, CaCl2, and oxidized glutathione (GSSG) may facilitate the proper folding of the fused HRP protein, as previously described by Chauhan and Kang (2018).

5.2 Application of ALFA-tag for enhanced signal intensity in CRISPR-FISH applications

CRISPR-FISH has demonstrated its ability to label repetitive DNA sequences in fixed samples (Ishii *et al.* 2019; Potlapalli *et al.* 2020). In this study, we have further refined this method to enhance its efficiency. This improvement aimed to boost signal intensities, making it potentially feasible to label low-copy sequences in future. The evaluation of the ALFA-tag, designed to enhance DNA labeling, demonstrated the compatibility with the dCas9-based RNP complex, enabling precise DNA targeting without functional interference. In addition, the dCas9-ALFA-tag system efficiently labels repetitive sequences in both formaldehyde and ethanol-acetic acid fixed samples, highlighting its versatility. However, when examined under a fluorescence microscope, increasing ALFA-tag copies did not boost signal intensity when combined with a fluorescence-labelled NbALFA, possibly due to an allosteric hindrance in NbALFA-ALFA-tag binding, warranting further investigation (Matos 2021).

The minibody, a fusion of an anti-ALFA single-domain antibody and a rabbit FC domain, shows promise for signal amplification in our dCas9-ALFA system. dCas9 with three ALFA-tag copies on both termini demonstrated a higher relative signal intensity compared to variants with lower copy numbers. No significant difference was observed between single and triple ALFA-tagged dCas9 proteins on the N-terminus, possibly due to limited binding space hindering minibody attachment to the three-copy variant. In contrast, dCas9 with two sets of three ALFA-tags, distributed on both termini (resulting in 3+3x sets), provided sufficient space for minibody binding. This was most likely facilitated by the large dCas9 compound situated between them, acting as a substantial spacer. Similarly, the 3+3x ALFA-tagged dCas9 protein resulted in slightly higher fluorescence intensities compared to the 6x ALFA-tagged version despite the same copy number (Fig. 15c). Extending the ALFA-tag to 12 copies further increased the signal intensity. Considering dCas9 with 3x, 6x and 12x ALFA-tag copies, the increase in relative signal intensity is quite linear, starting with a mean of 3.47 over 7.37 to 14.31. However, between 1x and 3x we did not observe any difference. This suggests that in this short construct, not all three ALFA-tag were recognized by minibodies, possibly due to the limited space when ALFA-tags were densely placed. In contrast, fusing 12x ALFA copies to both termini, creating a 24x version, did not further increase the signal. Instead additional background signals appeared, which made quantitative analysis impossible. This may be

attributed to the diminished DNA labeling activity of the dCas9 due to the increased load of ALFA copies (12x) on either side.

Incorporating glycine-rich linkers between ALFA-tag copies did not significantly improve the signal intensity. Detection of *A. thaliana* centromere repeats revealed that the 6x and 6xGS ALFA-tagged dCas9 proteins exhibited similar relative fluorescence intensities (mean: 7.37 versus 7.00), as illustrated in Figure 16c. The 6+6GS ALFA-tagged dCas9 protein revealed with a mean of 16.29, the highest observed intensity of all constructs. However, based on the data obtained for the 6x and 3+3x constructs we assume that also, in this case, the difference between 12x and 6+6x is more caused by the spacing of the two 6x blocks and not by the GS linkers between the individual copies. Although the differences between 3+3x and 6x as well as between 6+6x and 12x are only minor and statistically not significant, they seemed to be real since we found the same tendency in both cases. It needs to be elucidated if incorporating longer linkers like XTEN (Schellenberger *et al.* 2009; Guilinger *et al.* 2014), providing more space for minibody binding to the ALFA-tag might be an option to further increase the efficiency of the method in future.

Furthermore, our study successfully achieved live imaging of telomeres in *N. benthamiana* nuclei by fusing six ALFA-tags to the C-terminal end of dCas9 and mRuby-fused NbALFA. Incorporating four NLS sequences within the construct further enhanced labeling efficiency, likely due to improved protein import into the nucleus. On the other hand, using intronized dCas9 in combination with four NLS sequences improved telomere labeling and reduced cytoplasmic and nucleoplasmic background noise, possibly due to enhanced turnover in the nuclear compartment as reported by (Grützner *et al.* 2021). However, these results should be quantified in future studies to demonstrate the significant improvement in telomere labeling.

The ALFA-tag supported CRISPR-FISH method has the potential for future development in combination with electron microscopy. The ALFA-tag is compatible with glutaraldehyde, a superior fixative, could enable high-resolution DNA labeling within native chromatin structures using CRISPR-FISH. Unlike standard CRISPR-FISH, a limitation of the developed CRISPR-FISH ALFA-tag system is its inability to simultaneously label different target sequences. This limitation could be addressed by using a second tag in parallel, such as the spot-tag (Braun *et al.* 2016; Virant *et al.* 2018), in conjunction with CRISPR-FISH. Live imaging with the dCas9-ALFA-tag method introduces the possibility of targeted pull-down experiments for DNA-

binding proteins using an ALFA-tag-specific affinity resin (KILISCH *et al.* 2021; IGREJA *et al.* 2022), offering valuable applications beyond telomere labeling.

5.3 Tyramide signal amplification in combination with CRISPR-FISH

The combination of Tyramide Signal Amplification (TSA) with indirect CRISPR-FISH resulted in strong labeling of *A. thaliana* centromere sequences. Although the centromere signals were two-fold larger, they appeared to be blurrier after TSA application, possibly due to increased and unspecific fluorescence molecule deposition near the target sequence. We suggest that using TSA's sensitivity alongside the indirect CRISPR-FISH method could be an approach for visualizing small targets, like low-copy sequences, within structurally preserved chromatin in the future. However, for the integration of TSA with CRISPR-FISH, it is necessary to utilize a specialized TSA kit, potentially resulting in an increased overall cost of the assay. On the other hand, TSA might introduce elevated background noise levels.

5.4 Combining RNA aptamers with CRISPR-FISH

Pepper aptamer-based methodologies offer a straightforward and robust approach to visualize various RNA species within live cells. Additionally, the incorporation of pepper aptamers into sgRNA successfully labeled the human centromere in live cells (CHEN *et al.* 2019). In our approach, using the pepper sgRNA specific for telomere labeling led to unsuccessful labeling, potentially due to a change in the sgRNA conformation, resulting in the failure to activate the dCas9 protein. It's worth noting that, to date, pepper aptamers have not been utilized for nucleotide visualization in fixed cell imaging. However, pepper aptamers have demonstrated binding to HBC ((4-((2-hydroxyethyl) (methyl)amino)-benzylidene)-cyanophenyl-acetonitrile) in *in vitro* experiments. On the other hand, this failed labeling could also be attributed to a production error in the sgRNA, resulting in a non-functioning sgRNA. Additionally, in our research, we utilized the dCas9-ALFA-tag protein. It's important to consider that the pepper sgRNA may not be compatible with the dCas9-ALFA-tag protein. This is supported by the fact that the biotinylated tracrRNA + crRNA in combination with dCas9 fused with 12 copies of ALFA-tag failed to label the *Fok*I repeats (Appendix Fig 2), indicating the incompatibility of the dCas9-ALFA-tag system with modified sgRNA. To address this possibility, further testing with pepper sgRNA with either dCas9-biotin or dCas9-eGFP should be conducted.

5.5   Application of quantum dots for CRISPR-FISH labeling

Compact quantum dots (QDs) offer exceptional photostability and robust quantification due to their enhanced and stable brightness (RESCH-GENGER *et al.* 2008; LIU *et al.* 2018). However, in our approach, the use of streptavidin QDs failed to label the repeats in combination with indirect CRISPR-FISH and oligo FISH. This failure in labeling may be attributed to the large diameters of QDs, which range from 70 to 80 nm, hindering their penetration into the nucleus. This can be resolved using the smallest QDs as described by Liu et al. (2018). Further simplification can be achieved by directly fusing the QDs with the tracrRNA using click chemistry. This approach also enables multiplexing by employing different QDs with distinct emission peaks.

5.6   CRISPR-FISH labeling of non-repetitive sequences in *A. thaliana*

CASFISH, employing 73 different sgRNAs, successfully labeled a 5 kb non-repetitive region of the MUC4 gene in HeLa cells (DENG *et al.* 2015). In our approach, using pooled sgRNA (3200) to label a 456 kb-long region on *A. thaliana* chromosome 5, failed to produce any specific signals. Initially, we attributed this failed labeling to potential competition among sgRNAs, which may hinder their binding to the target DNA. Previous reports suggest that not all guide RNAs efficiently cleave the target DNA, rendering them inactive. Additionally, combining active and inactive sgRNAs has been shown to reduce *in vitro* cleavage efficiency due to competition between inactive and active sgRNAs to form the RNP complex (THYME *et al.* 2016). However, in our competition experiments, we did not observe any reduction in efficiency in centromere labeling, ruling out this possibility. One possibility could also be due to errors in synthesis, rendering the sgRNA inactive in activating the dCas9 complex. Additionally, there are other factors reported to reduce genome editing efficiency, such as the GC contents of PAM proximal and distal regions, secondary structure of sgRNA, and chromatin state (JUNG *et al.* 2024). However, it's worth considering that even if a portion of the sgRNA pool binds to the target DNA, the total amount of fluorophore may be below the detection limit of the microscope. In the future, this issue could potentially be addressed by increasing the signal intensities from the target DNA using ALFA-tag or TSA approaches in combination with CRISPR-FISH, without the need for using more sgRNAs.

5.7 CRISPR-ISH for electron microscopy (CRISPR-EM)

In cytogenetic research, investigating the internal ultrastructures of chromatin is essential for understanding the structure and biochemical properties of chromosomes. Combining the electron microscope (EM) with *in situ* hybridization (EMISH) has been utilized to visualize the target DNA in the nuclei at high structural resolution (HUTCHISON *et al.* 1982; CMARKO AND KOBERNA 2007; TRZASKOMA *et al.* 2020; LI *et al.* 2022), aiding in the visualization of 3D chromatin-folding structures (TRZASKOMA *et al.* 2020). However, using the standard ISH protocols combined with EM resulted in several artifacts due to global denaturation (SOLOVEI *et al.* 2002). Developing a DNA labeling method for EM presents two primary technical challenges: first, labeling the DNA without causing damage to the chromatin, and second, effectively transferring the sample from the microscopic slide to the gold grids for visualization with TEM. To address the first challenge, we developed an effective method for labeling DNA repeats using a combination of CRISPR-FISH and FluoroNanogold. We successfully labeled various DNA repeats on nuclei and chromosomes fixed under different fixation conditions using indirect CRISPR-FISH with streptavidin FluoroNanogold, showcasing the method's efficiency. However, attempts to enlarge gold particles for TEM visualization via silver enhancement failed due to probe-related issues. As an alternative approach, combining rabbit anti-FITC with indirect CRISPR-FISH and anti-rabbit FluoroNanogold antibody effectively achieved non-fluorescent gold labeling of *Fok*I repeats. In principle, utilizing the functional streptavidin FluoroNanogold probe in combination with indirect CRISPR-FISH could also facilitate gold labeling of DNA repeats. Furthermore, directly fusing Click Nanogold® to either the dCas9 protein or tracrRNA using click chemistry, as described by (HAINFELD AND POWELL 2000), could streamline the labeling procedure and decrease the overall cost of the components.

In another approach, employing the dCas9-ALFA-tag method in conjunction with minibody and anti-rabbit FluoroNanogold antibody yielded similar gold labeling of *Fok*I repeats. Additionally, labeling *A. thaliana* centromere repeats using the dCas9-ALFA-tag method led to increased signal intensities. Thus, utilizing this approach in combination with anti-rabbit FluoroNanogold antibody holds potential for gold labeling low-copy sequences in the future. An alternative option could involve fusing Click Nanogold® with NbALFA, which could simplify gold labeling in future applications. It is important to note that employing the dCas9-ALFA-tag approach with multiple ALFA-tags may lead to nanogold labeling, but the labeling might not

precisely originate from the exact location of the target site. Additionally, this accuracy might be compromised by the preserved chromatin structure due to the absence of global denaturation. In summary, we have successfully developed two different CRISPR-based methods for gold labeling of repetitive sequences.

In addition to gold labeling, the fixation conditions also play a crucial role in preserving the structure and withstanding the subsequent washing and detection steps involved in DNA labeling. Investigation of *V. faba* nuclei fixed under different fixation conditions using SEM did not reveal natural structures. This could be attributed to the use of cytospin to spin the nuclei onto the slide, which may result in the rupture of the nuclei. This issue could be further rectified by preparing the nuclei on a carbon-coated slide using sucrose buffer, where no pressure will be applied to affix the nuclei to the slide. On the other hand, observing the *V. faba* fixed nuclei on gold grids under TEM did not reveal the expected ultrastructures. This could be due to the thickness of the *V. faba* nuclei, which might be too thick to resolve internal ultrastructure by TEM. To address this issue, we attempted to transfer the nuclei samples from the slide to epoxy resin for further ultrathin sectioning. However, we encountered difficulties in recovering the sample from the slide to the epoxy resin, contradicting previous reports (GHAZIZADEH *et al.* 2008). Using ACLAR film as a surface substrate to prepare the nuclei also failed to reveal the real ultrastructures of the nuclei. This could be attributed to using ethanol and acetic acid to fix the nuclei, which may denature nuclear proteins and alter the chromatin structure. In future studies, testing this approach with glutaraldehyde-fixed nuclei is advisable. Glutaraldehyde is known to be one of the best fixatives for preserving structure and is also compatible with CRISPR labeling techniques.

Looking ahead, our study not only improved current methodologies but also lays the foundation for future investigations. It has the potential to serve as a valuable tool for labeling low or single-copy sequences within preserved chromatin and for examining DNA at the ultrastructural level with electron microscopy. Furthermore, it opens up opportunities for conducting precise *in vivo* pull-down assays targeting DNA-binding proteins. Overall, with enhanced sensitivity, the rapid labeling capability of CRISPR-Cas9 can be integrated with automated microscopy for high-throughput analysis, benefiting both plant biology and diagnostic applications.

6. Outlook

6.1 CRISPR-FISH in suspension

CRISPR-FISH effectively labels DNA repeats in fixed nuclei and tissue sections on glass slides. Expanding this technique to label fixed nuclei and chromosomes in suspension would broaden its utility. Integrating CRISPR-FISH with flow sorting of fluorescence labeled nuclei or chromosomes would be valuable in numerous applications, including molecular cytogenetics, molecular biology, genome sequencing, gene cloning, and proteomics (DOLEŽEL *et al.* 2021; ZWYRTKOVÁ *et al.* 2021). For instance, it could enable the specific flow-sorting of B chromosomes from a pool of chromosomes containing both A and B chromosomes.

6.2 Strategies to enhance CRISPR-FISH-based signal intensities

Combining ALFA-tag and TSA approaches with CRISPR-FISH has shown increased signal intensities. However, for further simplification and cost reduction, testing tracrRNA with a 3' overhang as a bridge sequence is proposed. This sequence could potentially amplify signal intensities using a long single-stranded DNA, synthesized cost-effectively through primer exchange reaction (PER) with short DNA primers, as described by Kishi et al. (2018). Signal amplification could then be achieved using 20 bp oligos fused with fluorophores, which hybridize along the long single-stranded DNA (Fig. 2A), as described by Kishi et al. (2018).

Alternatively, signal amplification can be achieved using DNA origami (reviewed by Dey et al. (2021)) fused with multiple copies of fluorophores. This DNA origami would contain capture oligos capable of hybridizing with the tracrRNA bridge sequences (Fig. 2B). Additionally, modifying the bridge sequence of tracrRNA and the long DNA oligo could enable multiplexing, allowing for the simultaneous labeling of multiple sequences. Furthermore, this method can be easily adapted for non-fluorescent CRISPR labeling by substituting fluorophores with biotin in small oligos.
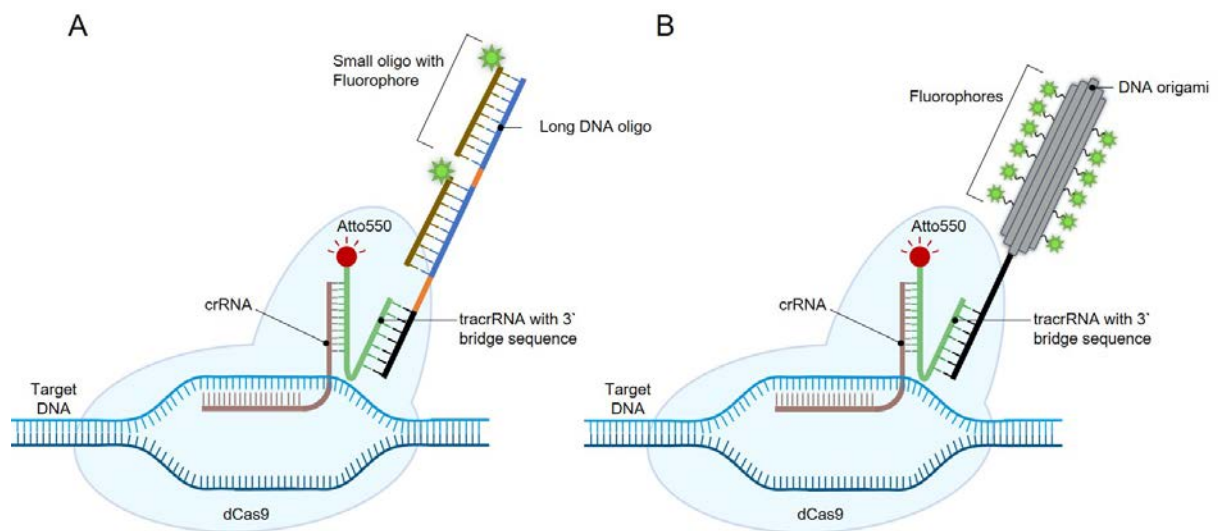
Fig 37: Schematic of CRISPR-FISH strategies for enhancing signal intensities.: A complex consisting of dCas9 with target-specific crRNA and 5' ATTO550-conjugated tracrRNA containing 3' bridge sequences is utilized to bind to the target DNA. The signal is then amplified either by using a (A) long oligo capable of hybridizing to the bridge sequence of tracrRNA, followed by further amplification using multiple small amplifier oligos fused with fluorophores, or by utilizing (B) DNA origami fused with multiple copies of fluorophores.

6.3 Optimizing conditions for nanogold labeling of DNA repeats for CRISPR-ISH applications

In our study, we developed two different methods for nanogold labeling of DNA repeats. Optimizing fixation conditions and techniques for transferring samples to EM-grids will be crucial in the future. Developing a CRISPR-FISH in suspension technique would also simplify this process by allowing CRISPR-ISH to be performed in suspension. Subsequently, mixing the labeled nuclei or chromosomes with epoxy resin and then slicing thin sections would streamline the entire process for analysis under an EM. Additionally, directly fusing nanogold to tracrRNA or dCas9 protein would further simplify the nanogold labeling process and reduce the potential effects of multiple washing steps required in our current methods.

6.4 Strategies to enhance CRISPR imaging in plants

Live CRISPR labeling is currently feasible only in transiently transformed *N. benthamiana*. In the future, this should be further developed using the following strategies.

1. One approach is to utilize an intronized dead Cas9 variant for CRISPR live imaging. The intronized Cas9 variant performed highly efficient genome editing in *A. thaliana*

(GRÜTZNER et al. 2021). Additionally, in our research it showed improved labeling of telomeres in transiently transformed *N. benthamiana*. However, quantification is needed to confirm this.

2. To address the challenge of Sp.Cas9's large size (1368 amino acids) and its potential difficulty in penetrating native chromatin, future research should consider testing smaller CRISPR Cas variants such as Cas12f1 (422 amino acids) or CasΦ (700-800 amino acids) (WU *et al.* 2021), for both live and fixed cell imaging, respectively.

3. Recently, a eukaryotic programmable RNA-guided endonuclease called Fanzor was discovered and demonstrated genome editing in human cells (SAITO *et al.* 2023). Testing such a system in plants is sensible for future CRISPR-based live imaging experiments.

4. To address the hindrance of Cas9 binding to target DNA caused by the chromatin status in CRISPR imaging, Cas9 coupled with chromatin-modulating peptides (CMPs) capable of opening chromatin should be considered. This approach has already demonstrated improved editing efficiency using CMPs (PARK *et al.* 2021).

5. One issue with live CRISPR imaging is the background noise generated from the aggregation of dCas9 or RNP complexes fused with fluorescent reporters that are not bound to target DNA. To address this, the fluorogenic CRISPR (fCRISPR) method was recently developed, where fluorescent reporters are degraded unless they are bound to the sgRNA, increasing the signal-to-noise ratio and sensitivity in human cells (ZHANG *et al.* 2024). Such strategies should be tested in plants for imaging, especially when experimenting with low-copy DNA target sequences.

6. Pre-assembled CRISPR-RNP complexes have been successfully employed for live imaging in mice (GENG AND PERTSINIDIS 2021). In the future, testing such strategies with pre-assembled RNP complexes in plant protoplasts will expand and simplify the CRISPR imaging method.

6.5 Development of CRISPR-dCas-based methods to identify DNA-specific proteins in plants *in vivo*

CRISPR-dCas9 has recently been employed to investigate protein-DNA and protein-chromatin interactions in human and animal cells (Reviewed by Dolgalev and Poverennaya (2021)), but such studies have not yet been reported in any plant species. To establish this system in plants, we're considering TurboID, known for its efficiency as a biotin ligase enzyme (Xu *et al.* 2023). When fused with a protein of interest (POI), TurboID quickly biotinylates nearby proteins in the proximity of 10 nm within min across various temperatures. Additionally, several reports highlight the successful utilization of TurboID in various plant systems to identify neighboring proteins around the tagged bait protein (Mair *et al.* 2019; Zhang *et al.* 2019; Arora *et al.* 2020; Feng *et al.* 2023; Zhang *et al.* 2023; Zhou *et al.* 2023). Therefore, fusing TurboID with dCas9-eYGFP, along with a target-specific sgRNA, has the potential to biotinylate surrounding proteins (Fig. 1). Subsequent total protein isolation, followed by streptavidin pull-down and mass spectrometry analysis, could potentially identify proteins associated with the target DNA or surrounding region. In our preliminary experiments with transiently transformed *N. benthamiana*, where telomere-specific sgRNA was utilized, dCas9-3xEGFP-TurboID effectively biotinylated proteins proximal to the telomeres (data not shown).
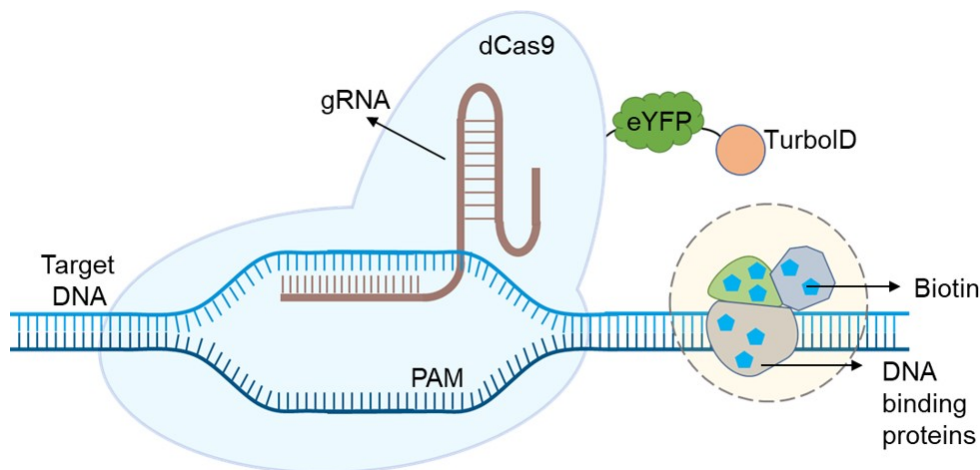
Fig 38: Schematic of the CRISPR-TurboID method: A dCas9 protein fused with eYFP and TurboID, along with target-specific sgRNA, is employed to label DNA *in vivo*. Subsequent application of biotin treatment attaches biotin to proteins proximal to the labeled DNA.

7. Summary

Advancements in CRISPR-based fluorescent and non-fluorescent labeling of repetitive DNA sequences are presented in this study.

i)   Indirect CRISPR-FISH, employing biotin-labeled tracrRNA and streptavidin FITC, demonstrated enhanced labeling efficiency for repetitive sequences compared to the Cas9 antibody-based method.

ii) Non-fluorescent labeling of DNA repeats across diverse species using biotin-labeled tracrRNA and streptavidin HRP under varying fixation conditions was facilitated by CRISPR-CID. This method resulted in sharper signals than those achieved with alkaline phosphatase (AP). Although counterstains like neutral red and hematoxylin uniformly stained nuclei of many species, *A. thaliana* nuclei failed to be uniformly stained. Additionally, repeats were not labeled by applying dCas9-HRP.

iii) Higher signal intensities were demonstrated by combining the CRISPR-ALFA-tag approach with a minibody compared to the NbALFA approach, particularly with 12 copies of the ALFA-tag compared to linker versions. Telomeres in live *N. benthamiana* leaf nuclei were successfully labeled by the dCas9-ALFA-tag, suggesting potential improvements in live imaging through enhanced NLS sequences and intronized dCas9.

iv) *A. thaliana* centromeres were successfully labeled by combining indirect CRISPR-FISH with tyramide signal amplification, leading to an expanded signal radius. However, alternative strategies, such as using quantum dots and employing pooled sgRNAs failed to label target sequences.

v)   Two different approaches for nanogold labeling of repetitive DNA sequences have been developed. In one, indirect CRISPR-FISH with anti-FITC and FluoroNanogold is utilized, while the other approach employs the dCas9-ALFA-tag system with a minibody and FluoroNanogold. However, transferring nuclei from the microscopic slide or ACLAR film to the EM-grids failed and should be optimized in the future.

8. Zusammenfassung

In dieser Studie werden Fortschritte für die nicht-fluoreszierende und fluoreszierende Markierung repetitiver DNA-Sequenzen mit Hilfe der CRISPR Technologie vorgestellt.

i) Indirekte CRISPR-FISH, durch den Einsatz von Biotin-markierter tracrRNA und Streptavidin-FITC konnte im Vergleich zur Cas9 Antikörper-basierten Methode eine verbesserte Markierungseffizienz für repetitive Sequenzen erreicht werden.

ii) Die nicht-fluoreszierende Markierung von DNA-Repeat verschiedener Arten unter Verwendung von Biotin-markierter tracrRNA und Streptavidin-HRP unter unterschiedlichen Fixierungsbedingungen wurde durch CRISPR-CID ermöglicht. Verglichen mit der alkalischen Phosphatase (AP), wurden mit Streptavidin-HRP schärfere Signale erzielt. Obwohl Farbstoffe wie Neutralrot und Hämatoxylin die Zellkerne unterschiedlicher Pflanzenarten gleichmäßig färbten, konnten die Kerne von *A. thaliana* nicht homogen angefärbt werden. Außerdem konnten Sequenzen nicht mit Hilfe von dCas9-HRP markiert werden.

iii) Durch die Kombination des CRISPR-ALFA-tag-Ansatzes mit Minibodies wurden im Vergleich zum NbALFA-Ansatz höhere Signalintensitäten nachgewiesen, insbesondere mit 12 Kopien des ALFA-Tags im Vergleich zu Linker-Versionen. Telomere in lebenden Blattkernen von *N. benthamiana* wurden erfolgreich mit dem dCas9-ALFA-Tag markiert, was auf mögliche Verbesserungen bei der Live-Bildgebung durch NLS-Sequenzen und intronisiertes dCas9 hindeutet.

iv) Die Zentromere von *A. thaliana* konnten durch die Kombination von indirekter CRISPR-FISH mit Tyramid-Verstärkung erfolgreich markiert werden, was zu einem erweiterten Signalradius führte. Bei alternativen Strategien wie der Verwendung von Quantenpunkten und gepoolten sgRNAs konnten jedoch Zielsequenzen nicht erfolgreich markiert werden.

v) Zwei verschiedene Ansätze zur Nanogoldmarkierung von DNA-Repeats wurden entwickelt. Bei der indirekten CRISPR-FISH Methode wird anti-FITC und FluoroNanogold verwendet. Bei dem anderen Ansatz wurde das dCas9-ALFA-Tag System mit einem Minibody und FluoroNanogold kombiniert. Das Übertragen vom Zellkernen von Objektträgern oder ACLAR-Film auf ein EM- Gitter war nicht erfolgreich und sollte in der Zukunft optimiert werden.

9. References

Ageno, M., E. Dore and C. Frontali, 1969 The alkaline denaturation of DNA. Biophys J 9: 1281-1311.

Ananiev, E. V., R. L. Phillips and H. W. Rines, 1998 A knob-associated tandem repeat in maize capable of forming fold-back DNA segments: Are chromosome knobs megatransposons? Proceedings of the National Academy of Sciences 95: 10785-10790.

Arora, D., N. B. Abel, C. Liu, P. Van Damme, K. Yperman *et al.*, 2020 Establishment of proximity-dependent biotinylation approaches in different plant model systems. Plant Cell 32: 3388-3407.

Avramova, Z. V., 2002 Heterochromatin in animals and plants. Similarities and differences. Plant Physiol 129: 40-49.

Barnes, S. R., A. M. James and G. Jamieson, 1985 The organisation, nucleotide sequence, and chromosomal distribution of a satellite DNA from *Allium cepa*. Chromosoma 92: 185-192.

Barrangou, R., C. Fremaux, H. Deveau, M. Richards, P. Boyaval *et al.*, 2007 CRISPR provides acquired resistance against viruses in prokaryotes. Science 315: 1709-1712.

Barroso, M. M., 2011 Quantum dots in cell biology. Journal of Histochemistry & Cytochemistry 59: 237-251.

Bauman, J. G. J., J. Wiegant, P. Borst and P. van Duijn, 1980 A new method for fluorescence microscopical localization of specific DNA sequences by *in situ* hybridization of fluorochrome-labelled RNA. Experimental Cell Research 128: 485-490.

Bedbrook, J. R., J. Jones, M. O'Dell, R. D. Thompson and R. B. Flavell, 1980 A molecular description of telomeric heterochromatin in *Secale* species. Cell 19: 545-560.

Boch, J., H. Scholze, S. Schornack, A. Landgraf, S. Hahn *et al.*, 2009 Breaking the code of DNA binding specificity of TAL-type III effectors. Science 326: 1509-1512.

Bogen, S., K. Vani and S. Sompuram, 2009 Molecular mechanisms of antigen retrieval: antigen retrieval reverses steric interference caused by formalin-induced cross-links. Biotechnic & Histochemistry 84: 207-215.

Bolotin, A., B. Quinquis, A. Sorokin and S. D. Ehrlich, 2005 Clustered regularly interspaced short palindrome repeats (CRISPRs) have spacers of extrachromosomal origin. Microbiology (Reading) 151: 2551-2561.

Bradshaw, R. A., F. Cancedda, L. H. Ericsson, P. A. Neumann, S. P. Piccoli *et al.*, 1981 Amino acid sequence of *Escherichia coli* alkaline phosphatase. Proceedings of the National Academy of Sciences 78: 3473-3477.

Braun, M. B., B. Traenkle, P. A. Koch, F. Emele, F. Weiss *et al.*, 2016 Peptides in headlock – a novel high-affinity and versatile peptide-binding nanobody for proteomics and microscopy. Scientific Reports 6: 19211.

Brown, J. M., S. De Ornellas, E. Parisi, L. Schermelleh and V. J. Buckle, 2022 RASER-FISH: non-denaturing fluorescence in situ hybridization for preservation of three-dimensional interphase chromatin structure. Nature Protocols 17: 1306-1331.

Brown, S. W., 1966 Heterochromatin. Science 151: 417-425.

Chauhan, S., and T. J. Kang, 2018 Soluble expression of horseradish peroxidase in *Escherichia coli* and its facile activation. J Biosci Bioeng 126: 431-435.

Chen, B., L. A. Gilbert, B. A. Cimini, J. Schnitzbauer, W. Zhang *et al.*, 2013a Dynamic imaging of genomic loci in living human cells by an optimized CRISPR/Cas system. Cell 155: 1479-1491.

Chen, B., W. Zou, H. Xu, Y. Liang and B. Huang, 2018 Efficient labeling and imaging of protein-coding genes in living cells using CRISPR-Tag. Nature Communications 9: 5065.

Chen, X., J. Zaro and W.-C. Shen, 2013b Fusion protein linkers: property, design and functionality. Advanced drug delivery reviews 65: 1357-1369.

Chen, X., D. Zhang, N. Su, B. Bao, X. Xie *et al.*, 2019 Visualizing RNA dynamics in live cells with bright and stable fluorescent RNAs. Nature Biotechnology 37: 1287-1293.

Cheng, A. W., N. Jillette, P. Lee, D. Plaskon, Y. Fujiwara *et al.*, 2016 Casilio: a versatile CRISPR-Cas9-Pumilio hybrid for gene regulation and genomic labeling. Cell Research 26: 254-257.

Choulika, A., A. Perrin, B. Dujon and J. F. Nicolas, 1995 Induction of homologous recombination in mammalian chromosomes by using the I-SceI system of *Saccharomyces cerevisiae*. Mol Cell Biol 15: 1968-1973.

Clow, P. A., M. Du, N. Jillette, A. Taghbalout, J. J. Zhu *et al.*, 2022 CRISPR-mediated multiplexed live cell imaging of nonrepetitive genomic loci with one guide RNA per locus. Nature Communications 13: 1871.

Cmarko, D., and K. Koberna, 2007 Electron microscopy in situ hybridization: tracking of DNA and RNA sequences at high resolution. Methods Mol Biol 369: 213-228.

Cuadrado, Á., H. Golczyk and N. Jouve, 2009 A novel, simple and rapid nondenaturing FISH (ND-FISH) technique for the detection of plant telomeres. Potential used and possible target structures detected. Chromosome Research 17: 755-762.

Cui, C., W. Shu and P. Li, 2016 Fluorescence *in situ* hybridization: Cell-based genetic diagnostic and research applications. Frontiers in Cell and Developmental Biology 4.

Cybulski, J. S., J. Clements and M. Prakash, 2014 Foldscope: origami-based paper microscope. PLOS ONE 9: e98781.

de Nooijer, S., J. Wellink, B. Mulder and T. Bisseling, 2009 Non-specific interactions are sufficient to explain the position of heterochromatic chromocenters and nucleoli in interphase nuclei. Nucleic Acids Research 37: 3558-3568.

Dekker, J., M. A. Marti-Renom and L. A. Mirny, 2013 Exploring the three-dimensional organization of genomes: interpreting chromatin interaction data. Nat Rev Genet 14: 390-403.

Deltcheva, E., K. Chylinski, C. M. Sharma, K. Gonzales, Y. Chao *et al.*, 2011 CRISPR RNA maturation by trans-encoded small RNA and host factor RNase III. Nature 471: 602-607.

Deng, W., X. Shi, R. Tjian, T. Lionnet and R. H. Singer, 2015 CASFISH: CRISPR/Cas9-mediated in situ labeling of genomic loci in fixed cells. Proceedings of the National Academy of Sciences 112: 11870-11875.

Dennis, E. S., W. L. Gerlach and W. J. Peacock, 1980 Identical polypyrimidine-polypurine satellite DNAs in wheat and barley. Heredity 44: 349-366.

Dey, S., C. Fan, K. V. Gothelf, J. Li, C. Lin *et al.*, 2021 DNA origami. Nature Reviews Methods Primers 1: 13.

Doležel, J., P. Binarová and S. Lucretti, 1989 Analysis of Nuclear DNA content in plant cells by Flow cytometry. Biologia Plantarum 31: 113-120.

Doležel, J., S. Lucretti, I. Molnár, P. Cápal and D. Giorgi, 2021 Chromosome analysis and sorting. Cytometry A 99: 328-342.

Dolgalev, G., and E. Poverennaya, 2021 Applications of crispr-cas technologies to proteomics. Genes (Basel) 12.

Dominguez, A. A., W. A. Lim and L. S. Qi, 2016 Beyond editing: repurposing CRISPR–Cas9 for precision genome regulation and interrogation. Nature Reviews Molecular Cell Biology 17: 5-15.

Doudna, J. A., and E. Charpentier, 2014 The new frontier of genome engineering with CRISPR-Cas9. Science 346.

Dreissig, S., S. Schiml, P. Schindele, O. Weiss, T. Rutten *et al.*, 2017 Live-cell CRISPR imaging in plants reveals dynamic telomere movements. The Plant Journal: For Cell and Molecular Biology 91: 565-573.

Dunn, O. J., 1961 Multiple comparisons among means. Journal of the American Statistical Association 56: 52-64.

Durm, M., F. M. Haar, M. Hausmann, H. Ludwig and C. Cremer, 1997 Non-enzymatic, low temperature fluorescence in situ hybridization of human chromosomes with a repetitive alpha-satellite probe. Z Naturforsch C J Biosci 52: 82-88.

Esvelt, K. M., P. Mali, J. L. Braff, M. Moosburner, S. J. Yaung *et al.*, 2013 Orthogonal Cas9 proteins for RNA-guided gene regulation and editing. Nature Methods 10: 1116-1121.

Farrants, H., M. Tarnawski, T. G. Müller, S. Otsuka, J. Hiblot *et al.*, 2020 Chemogenetic control of nanobodies. Nature Methods 17: 279-282.

Feng, C., E. Roitinger, O. Hudecz, M. Cuacos, J. Lorenz *et al.*, 2023 TurboID-based proteomic profiling of meiotic chromosome axes in *Arabidopsis thaliana*. Nat Plants 9: 616-630.

Feng, S., S. J. Cokus, V. Schubert, J. Zhai, M. Pellegrini *et al.*, 2014 Genome-wide Hi-C analyses in wild-type and mutants reveal high-resolution chromatin interactions in *Arabidopsis*. Mol Cell 55: 694-707.

Fransz, P., J. H. de Jong, M. Lysak, M. R. Castiglione and I. Schubert, 2002 Interphase chromosomes in *Arabidopsis* are organized as well defined chromocenters from which euchromatin loops emanate. Proceedings of the National Academy of Sciences of the United States of America 99: 14584-14589.

Frodyma, D. E., T. C. Troia, C. Rao, R. A. Svoboda, J. A. Berg *et al.*, 2022 PGC-1β and ERRα promote glutamine metabolism and colorectal cancer survival via transcriptional upregulation of pck2. Cancers 14: 4879.

Fuchs, J., U. Pich, A. Meister and I. Schubert, 1994a Differentiation of field bean heterochromatin by in situ hybridization with a repeated *Fok*I sequence. Chromosome Res 2: 25-28.

Fuchs, J., U. Pich, A. Meister and I. Schubert, 1994b Differentiation of field bean heterochromatin byin situ hybridization with a repeated *Fok*I sequence. Chromosome Research 2: 25-28.

Fujimoto, S., and S. Matsunaga, 2017 Visualization of chromatin loci with transiently expressed CRISPR/Cas9 in plants. Cytologia 82: 559-562.

Fujimoto, S., S. S. Sugano, K. Kuwata, K. Osakabe and S. Matsunaga, 2016 Visualization of specific repetitive genomic sequences with fluorescent TALEs in *Arabidopsis thaliana*. Journal of Experimental Botany 67: 6101-6110.

Gall, J. G., and M. L. Pardue, 1969 Formation and detection of RNA-DNA hybrid molecules in cytological preparations. Proc Natl Acad Sci U S A 63: 378-383.

Garneau, J. E., M.-È. Dupuis, M. Villion, D. A. Romero, R. Barrangou *et al.*, 2010 The CRISPR/Cas bacterial immune system cleaves bacteriophage and plasmid DNA. Nature 468: 67-71.

Gasiunas, G., R. Barrangou, P. Horvath and V. Siksnys, 2012 Cas9–crRNA ribonucleoprotein complex mediates specific DNA cleavage for adaptive immunity in bacteria. Proceedings of the National Academy of Sciences 109: E2579-E2586.

Geng, Y., and A. Pertsinidis, 2021 Simple and versatile imaging of genomic loci in live mammalian cells and early pre-implantation embryos using CAS-LiveFISH. Scientific Reports 11: 12220.

Ghazizadeh, M., Y. Sasaki, T. Oguro, S. Sato, S. Egawa *et al.*, 2008 A novel technique for observing the internal ultrastructure of human chromosomes with known karyotype. Microscopy and Microanalysis 14: 357-361.

Giorgetti, L., and E. Heard, 2016 Closing the loop: 3C versus DNA FISH. Genome Biol 17: 215.

Grützner, R., P. Martin, C. Horn, S. Mortensen, E. J. Cram *et al.*, 2021 High-efficiency genome editing in plants mediated by a Cas9 gene containing multiple introns. Plant Commun 2: 100135.

Guilinger, J. P., D. B. Thompson and D. R. Liu, 2014 Fusion of catalytically inactive Cas9 to FokI nuclease improves the specificity of genome modification. Nature Biotechnology 32: 577-582.

Gundinger, T., and O. Spadiut, 2017 A comparative approach to recombinantly produce the plant enzyme horseradish peroxidase in *Escherichia coli*. Journal of Biotechnology 248: 15-24.

Guo, J., Z. Cheng, J. Berdychowska, X. Zhu, L. Wang *et al.*, 2021 Effect and mechanism analysis of different linkers on efficient catalysis of subunit-fused nitrile hydratase. International Journal of Biological Macromolecules 181: 444-451.

Hainfeld, J. F., and R. D. Powell, 2000 New frontiers in gold labeling. Journal of Histochemistry & Cytochemistry 48: 471-480.

Harun, A., H. Liu, S. Song, S. Asghar, X. Wen *et al.*, 2023 Oligonucleotide fluorescence *in situ* hybridization: An efficient chromosome painting method in plants. Plants 12: 2816.

Hausmann, M., R. Winkler, G. Hildenbrand, J. Finsterle, A. Weisel *et al.*, 2003 COMBO-FISH: specific labeling of nondenatured chromatin targets by computer-selected DNA oligonucleotide probe combinations. Biotechniques 35: 564-570, 572-567.

Hopman, A. H. N., J. Wiegant, A. K. Raap, J. E. Landegent, M. van der Ploeg *et al.*, 1986 Bi-color detection of two target DNAs by non-radioactive *in situ* hybridization. Histochemistry 85: 1-4.

Horvath, P., and R. Barrangou, 2010 CRISPR/Cas, the immune system of bacteria and archaea. Science 327: 167-170.

Hsu, P. D., E. S. Lander and F. Zhang, 2014 Development and applications of crispr-cas9 for genome engineering. Cell 157: 1262-1278.

Hutchinson, J., R. B. Flavell and J. Jones, 1981 Physical mapping of plant chromosomes by *in situ* hybridization, pp. 207-222 in *Genetic Engineering: Principles and Methods. Volume 3*, edited by J. K. Setlow and A. Hollaender. Springer US, Boston, MA.

Hutchison , N., P. Langer-Safer , D. Ward and B. Hamkalo 1982 *In situ* hybridization at the electron microscope level: hybrid detection by autoradiography and colloidal gold. Journal of Cell Biology 95: 609-618.

Ichikawa, D. M., O. Abdin, N. Alerasool, M. Kogenaru, A. L. Mueller *et al.*, 2023 A universal deep-learning model for zinc finger design enables transcription factor reprogramming. Nature Biotechnology 41: 1117-1129.

Igreja, C., T. Loschko, A. Schäfer, R. Sharma, S. P. Quiobe *et al.*, 2022 Application of ALFA-tagging in the nematode model organisms *Caenorhabditis elegans* and *Pristionchus pacificus*. Cells 11: 3875.

Irifune, K., K. Hirai, J. Zheng, R. Tanaka and H. Morikawa, 1995 Nucleotide sequence of a highly repeated DNA sequence and its chromosomal localization in *Allium fistulosum*. Theoretical and Applied Genetics 90: 312-316.

Ishii, T., V. Schubert, S. Khosravi, S. Dreissig, J. Metje-Sprink *et al.*, 2019 RNA-guided endonuclease – *in situ* labelling (RGEN-ISL): a fast CRISPR/Cas9-based method to label genomic sequences in various species. New Phytologist 222**:** 1652-1661.

Ishino, Y., H. Shinagawa, K. Makino, M. Amemura and A. Nakata, 1987 Nucleotide sequence of the iap gene, responsible for alkaline phosphatase isozyme conversion in *Escherichia coli*, and identification of the gene product. J Bacteriol 169**:** 5429-5433.

Jacobi, A. M., G. R. Rettig, R. Turk, M. A. Collingwood, S. A. Zeiner *et al.*, 2017 Simplified CRISPR tools for efficient genome editing and streamlined protocols for their delivery into mammalian cells and mouse zygotes. Methods 121-122**:** 16-28.

Jayakodi, M., A. A. Golicz, J. Kreplak, L. I. Fechete, D. Angra *et al.*, 2023 The giant diploid faba genome unlocks variation in a global protein crop. Nature 615**:** 652-659.

Jiang, F., and J. A. Doudna, 2017 CRISPR-Cas9 structures and mechanisms. Annu Rev Biophys 46**:** 505-529.

Jiang, F., D. W. Taylor, J. S. Chen, J. E. Kornfeld, K. Zhou *et al.*, 2016 Structures of a CRISPR-Cas9 R-loop complex primed for DNA cleavage. Science 351**:** 867-871.

Jiang, F., K. Zhou, L. Ma, S. Gressel and J. A. Doudna, 2015 A Cas9–guide RNA complex preorganized for target DNA recognition. Science 348**:** 1477-1481.

Jiang, J., and B. S. Gill, 1994 Nonisotopic *in situ* hybridization and plant genome mapping: the first 10 years. Genome 37**:** 717-725.

Jiang, J., and B. S. Gill, 2006 Current status and the future of fluorescence *in situ* hybridization (FISH) in plant genome research. Genome 49**:** 1057-1068.

Jin, L., and R. V. Lloyd, 1997 *In situ* hybridization: methods and applications. J Clin Lab Anal 11**:** 2-9.

Jinek, M., K. Chylinski, I. Fonfara, M. Hauer, J. A. Doudna *et al.*, 2012 A programmable dual-RNA–guided dna endonuclease in adaptive bacterial immunity. Science 337**:** 816-821.

Jinek, M., F. Jiang, D. W. Taylor, S. H. Sternberg, E. Kaya *et al.*, 2014 Structures of Cas9 endonucleases reveal RNA-mediated conformational activation. Science 343**:** 1247997.

John, H. A., M. L. Birnstiel and K. W. Jones, 1969 RNA-DNA hybrids at the cytological level. Nature 223**:** 582-587.

Jung, W. J., S. J. Park, S. Cha and K. Kim, 2024 Factors affecting the cleavage efficiency of the CRISPR-Cas9 system. Anim Cells Syst (Seoul) 28**:** 75-83.

Kato, A., K. Yakura and S. Tanifuji, 1984 Sequence analysis of *Vicia faba* repeated DNA, the *Fok*I repeat element. Nucleic Acids Res 12**:** 6415-6426.

Kato, N., and E. Lam, 2001 Detection of chromosomes tagged with green fluorescent protein in live *Arabidopsis thaliana* plants. Genome Biology 2**:** research0045.0041.

Khosravi, S., T. Ishii, S. Dreissig and A. Houben, 2020a Application and prospects of CRISPR/Cas9-based methods to trace defined genomic sequences in living and fixed plant cells. Chromosome Research 28**:** 7-17.

Khosravi, S., P. Schindele, E. Gladilin, F. Dunemann, T. Rutten *et al.*, 2020b Application of aptamers improves CRISPR-based live imaging of plant telomeres. bioRxiv**:** 2020.2005.2005.078246.

Khosravi, S., P. Schindele, E. Gladilin, F. Dunemann, T. Rutten *et al.*, 2020c Application of aptamers improves CRISPR-based live imaging of plant telomeres. Frontiers in plant science**:** 1254.

Kilisch, M., H. Götzke, M. Gere-Becker, A. Crauel, F. Opazo *et al.*, 2021 Discovery and characterization of an ALFA-tag-specific affinity resin optimized for protein purification at low temperatures in physiological buffer. Biomolecules 11**:** 269.

Kirov, I., M. Divashuk, K. Van Laere, A. Soloviev and L. Khrustaleva, 2014 An easy "SteamDrop" method for high quality plant chromosome preparation. Molecular Cytogenetics 7**:** 21.

Kishi, J. Y., S. W. Lapan, B. J. Beliveau, E. R. West, A. Zhu *et al.*, 2019 SABER amplifies FISH: enhanced multiplexed imaging of RNA and DNA in cells and tissues. Nature Methods 16**:** 533-544.

Kishi, J. Y., T. E. Schaus, N. Gopalkrishnan, F. Xuan and P. Yin, 2018 Programmable autonomous synthesis of single-stranded DNA. Nature Chemistry 10**:** 155-164.

Koblan, L. W., J. L. Doman, C. Wilson, J. M. Levy, T. Tay *et al.*, 2018 Improving cytidine and adenine base editors by expression optimization and ancestral reconstruction. Nat Biotechnol 36**:** 843-846.

Kolodziej, K. E., F. Pourfarzad, E. de Boer, S. Krpic, F. Grosveld *et al.*, 2009 Optimal use of tandem biotin and V5 tags in ChIP assays. BMC Molecular Biology 10**:** 6.

Kubalová, I., A. S. Câmara, P. Cápal, T. Beseda, J. M. Rouillard *et al.*, 2023 Helical coiling of metaphase chromatids. Nucleic Acids Res 51**:** 2641-2654.

Langer-Safer, P. R., M. Levine and D. C. Ward, 1982 Immunological method for mapping genes on *Drosophila* polytene chromosomes. Proceedings of the National Academy of Sciences 79**:** 4381-4385.

Lau, I. F., S. R. Filipe, B. Søballe, O.-A. Økstad, F.-X. Barre *et al.*, 2003 Spatial and temporal organization of replicating *Escherichia coli* chromosomes. Molecular Microbiology 49**:** 731-743.

Li, G., T. C. Hall and R. Holmes-Davis, 2002 Plant chromatin: development and gene control. Bioessays 24**:** 234-243.

Li, G., X. Ruan, R. K. Auerbach, K. S. Sandhu, M. Zheng *et al.*, 2012 Extensive promoter-centered chromatin interactions provide a topological basis for transcription regulation. Cell 148**:** 84-98.

Li, Y., V. Agrawal, R. K. A. Virk, E. Roth, W. S. Li *et al.*, 2022 Analysis of three-dimensional chromatin packing domains by chromatin scanning transmission electron microscopy (ChromSTEM). Scientific Reports 12**:** 12198.

Lieber, M. R., 2010 The mechanism of double-strand DNA break repair by the nonhomologous DNA end-joining pathway. Annual Review of Biochemistry 79**:** 181-211.

Lieberman-Aiden, E., N. L. van Berkum, L. Williams, M. Imakaev, T. Ragoczy *et al.*, 2009 Comprehensive mapping of long-range interactions reveals folding principles of the human genome. Science 326**:** 289-293.

Lindhout, B. I., P. Fransz, F. Tessadori, T. Meckel, P. J. Hooykaas *et al.*, 2007 Live cell imaging of repetitive DNA sequences via GFP-tagged polydactyl zinc finger proteins. Nucleic Acids Res 35**:** e107.

Liu, Y., P. Le, S. J. Lim, L. Ma, S. Sarkar *et al.*, 2018 Enhanced mRNA FISH with compact quantum dots. Nature Communications 9**:** 4461.

Luger, K., A. W. Mäder, R. K. Richmond, D. F. Sargent and T. J. Richmond, 1997 Crystal structure of the nucleosome core particle at 2.8 A resolution. Nature 389**:** 251-260.

Ma, H., A. Naseri, P. Reyes-Gutierrez, S. A. Wolfe, S. Zhang *et al.*, 2015 Multicolor CRISPR labeling of chromosomal loci in human cells. Proceedings of the National Academy of Sciences 112**:** 3002-3007.

Ma, H., P. Reyes-Gutierrez and T. Pederson, 2013 Visualization of repetitive DNA sequences in human chromosomes with transcription activator-like effectors. Proceedings of the National Academy of Sciences 110**:** 21048-21053.

Ma, H., L.-C. Tu, A. Naseri, Y.-C. Chung, D. Grunwald *et al.*, 2018 CRISPR-Sirius: RNA scaffolds for signal amplification in genome imaging. Nature Methods 15**:** 928-931.

Ma, H., L.-C. Tu, A. Naseri, M. Huisman, S. Zhang *et al.*, 2016 Multiplexed labeling of genomic loci with dCas9 and engineered sgRNAs using CRISPRainbow. Nature Biotechnology 34**:** 528-530.

Ma, L., S.-M. Wu, J. Huang, Y. Ding, D.-W. Pang *et al.*, 2008 Fluorescence *in situ* hybridization (FISH) on maize metaphase chromosomes with quantum dot-labeled DNA conjugates. Chromosoma 117**:** 181-187.

Ma, Y., M. Wang, W. Li, Z. Zhang, X. Zhang *et al.*, 2017 Live visualization of HIV-1 proviral DNA using a dual-color-labeled CRISPR system. Anal Chem 89**:** 12896-12901.

Maggio, I., H. A. Zittersteijn, Q. Wang, J. Liu, J. M. Janssen *et al.*, 2020 Integrating gene delivery and gene-editing technologies by adenoviral vector transfer of optimized CRISPR-Cas9 components. Gene Ther 27**:** 209-225.

Mair, A., S. L. Xu, T. C. Branon, A. Y. Ting and D. C. Bergmann, 2019 Proximity labeling of protein complexes and cell-type-specific organellar proteomes in *Arabidopsi*s enabled by TurboID. Elife 8.

Mak, A. N., P. Bradley, R. A. Cernadas, A. J. Bogdanove and B. L. Stoddard, 2012 The crystal structure of TAL effector PthXo1 bound to its DNA target. Science 335**:** 716-719.

Makarova, K. S., Y. I. Wolf, J. Iranzo, S. A. Shmakov, O. S. Alkhnbashi *et al.*, 2020 Evolutionary classification of CRISPR–Cas systems: a burst of class 2 and derived variants. Nature Reviews Microbiology 18: 67-83.

Mandáková, T., and M. A. Lysak, 2016 Chromosome Preparation for Cytogenetic Analyses in *Arabidopsis*. Current Protocols in Plant Biology 1**:** 43-51.

Manuelidis, L., P. R. Langer-Safer and D. C. Ward, 1982 High-resolution mapping of satellite DNA using biotin-labeled DNA probes. J Cell Biol 95**:** 619-625.

Mao, S., Y. Ying, X. Wu, C. J. Krueger and A. K. Chen, 2019 CRISPR/dual-FRET molecular beacon for sensitive live-cell imaging of non-repetitive genomic loci. Nucleic Acids Research 47**:** e131-e131.

Mariamé, B., S. Kappler-Gratias, M. Kappler, S. Balor, F. Gallardo *et al.*, 2018 Real-time visualization and quantification of human cytomegalovirus replication in living cells using the ANCHOR DNA labeling technology. Journal of Virology 92**:** 10.1128/jvi.00571-00518.

Marillonnet, S., and R. Grützner, 2020 Synthetic DNA assembly using golden gate cloning and the hierarchical modular cloning pipeline. Current Protocols in Molecular Biology 130**:** e115.

Markaki, Y., D. Smeets, S. Fiedler, V. J. Schmid, L. Schermelleh *et al.*, 2012 The potential of 3D-FISH and super-resolution structured illumination microscopy for studies of 3D nuclear architecture: 3D structured illumination microscopy of defined chromosomal structures visualized by 3D (immuno)-FISH opens new perspectives for studies of nuclear architecture. Bioessays 34**:** 412-426.

Marraffini, L. A., and E. J. Sontheimer, 2010 CRISPR interference: RNA-directed adaptive immunity in bacteria and archaea. Nature Reviews Genetics 11**:** 181-190.

Matos, D. M., 2021 Steric hindrance: A practical (and frequently forgotten) problem in flow cytometry. Cytometry Part B: Clinical Cytometry 100**:** 397-401.

Matzke, A. J., B. Huettel, J. van der Winden and M. Matzke, 2005 Use of two-color fluorescence-tagged transgenes to study interphase chromosomes in living plants. Plant Physiol 139**:** 1586-1596.

Meschichi, A., M. Ingouff, C. Picart, M. Mirouze, S. Desset *et al.*, 2021 ANCHOR: A technical approach to monitor single-copy locus localization in planta. Frontiers in Plant Science 12.

Milbredt, S., and T. Waldminghaus, 2017 BiFCROS: A low-background fluorescence repressor operator system for labeling of genomic loci. G3 (Bethesda) 7: 1969-1977.

Miller, J., A. D. McLachlan and A. Klug, 1985 Repetitive zinc-binding domains in the protein transcription factor IIIA from *Xenopus* oocytes. Embo j 4: 1609-1614.

Misteli, T., 2020 The self-organizing genome: principles of genome architecture and function. Cell 183: 28-45.

Miyanari, Y., C. Ziegler-Birling and M.-E. Torres-Padilla, 2013 Live visualization of chromatin dynamics with fluorescent TALEs. Nature Structural & Molecular Biology 20: 1321-1324.

Mojica, F. J. M., C. Díez-Villaseñor, J. García-Martínez and C. Almendros, 2009 Short motif sequences determine the targets of the prokaryotic CRISPR defence system. Microbiology 155: 733-740.

Mojica, F. J. M., C. Díez-Villaseñor, E. Soria and G. Juez, 2000 Biological significance of a family of regularly spaced repeats in the genomes of Archaea, Bacteria and mitochondria. Molecular Microbiology 36: 244-246.

Mongelard, F., C. Vourc'h, M. Robert-Nicoud and Y. Usson, 1999 Quantitative assessment of the alteration of chromatin during the course of FISH procedures. Cytometry 36: 96-101.

Murata, M., Y. Ogura and F. Motoyoshi, 1994 Centromeric repetitive sequences in *Arabidopsis thaliana*. The Japanese Journal of Genetics 69: 361-370.

Nagaki, K., and N. Yamaji, 2020 Decrosslinking enables visualization of RNA-guided endonuclease–*in situ* labeling signals for DNA sequences in plant tissues. Journal of Experimental Botany 71: 1792-1800.

Naito, Y., K. Hino, H. Bono and K. Ui-Tei, 2014 CRISPRdirect: software for designing CRISPR/Cas guide RNA with reduced off-target sites. Bioinformatics 31: 1120-1123.

Nederlof, P. M., D. Robinson, R. Abuknesha, J. Wiegant, A. H. N. Hopman *et al.*, 1989 Three-color fluorescence *in situ* hybridization for the simultaneous detection of multiple nucleic acid sequences. Cytometry 10: 20-27.

Neguembor, M. V., R. Sebastian-Perez, F. Aulicino, P. A. Gomez-Garcia, M. P. Cosma *et al.*, 2017 (Po)STAC (Polycistronic SunTAg modified CRISPR) enables live-cell and fixed-cell super-resolution imaging of multiple genes. Nucleic Acids Research 46: e30-e30.

Němečková, A., C. Wäsch, V. Schubert, T. Ishii, E. Hřibová *et al.*, 2019 CRISPR/Cas9-based RGEN-ISL allows the simultaneous and specific visualization of proteins, dna repeats, and sites of dna replication. Cytogenetic and Genome Research 159: 48-53.

Nidhi, S., U. Anand, P. Oleksak, P. Tripathi, J. A. Lal *et al.*, 2021 Novel CRISPR-Cas systems: an updated review of the current achievements, applications, and future research perspectives. Int J Mol Sci 22.

Nishimasu, H., L. Cong, W. X. Yan, F. A. Ran, B. Zetsche *et al.*, 2015 Crystal structure *of Staphylococcus aureus* Cas9. Cell 162: 1113-1126.

Nozawa, K., T. Sogabe, A. Hayashi, J. Motohashi, E. Miura *et al.*, 2022 In vivo nanoscopic landscape of neurexin ligands underlying anterograde synapse specification. Neuron 110: 3168-3185.e3168.

O'Leary, T., C. Fowler, D. Evers and J. Mason, 2009 Protein fixation and antigen retrieval: chemical studies. Biotechnic & Histochemistry 84: 217-221.

Park, S.-J., T. Y. Jeong, S. K. Shin, D. E. Yoon, S.-Y. Lim *et al.*, 2021 Targeted mutagenesis in mouse cells and embryos using an enhanced prime editor. Genome Biology 22: 170.

Peric-Hupkes, D., W. Meuleman, L. Pagie, S. W. Bruggeman, I. Solovei *et al.*, 2010 Molecular maps of the reorganization of genome-nuclear lamina interactions during differentiation. Mol Cell 38**:** 603-613.

Phan, H. T., and U. Conrad, 2016 Plant-based vaccine antigen production. Methods in Molecular Biology (Clifton, N.J.) 1349**:** 35-47.

Pinkel, D., T. Straume and J. W. Gray, 1986 Cytogenetic analysis using quantitative, high-sensitivity, fluorescence hybridization. Proc Natl Acad Sci U S A 83**:** 2934-2938.

Pope, B. D., T. Ryba, V. Dileep, F. Yue, W. Wu *et al.*, 2014 Topologically associating domains are stable units of replication-timing regulation. Nature 515**:** 402-405.

Potlapalli, B. P., V. Schubert, J. Metje-Sprink, T. Liehr and A. Houben, 2020 Application of Tris-HCl allows the specific labeling of regularly prepared chromosomes by CRISPR-FISH. Cytogenetic and Genome Research 160**:** 156-165.

Püllmann, P., C. Ulpinnis, S. Marillonnet, R. Gruetzner, S. Neumann *et al.*, 2019 Golden Mutagenesis: An efficient multi-site-saturation mutagenesis approach by Golden Gate cloning with automated primer design. Scientific Reports 9**:** 10932.

Qi, Lei S., Matthew H. Larson, Luke A. Gilbert, Jennifer A. Doudna, Jonathan S. Weissman *et al.*, 2013 Repurposing CRISPR as an RNA-guided platform for sequence-specific control of gene expression. Cell 152**:** 1173-1183.

Qin, P., M. Parlak, C. Kuscu, J. Bandaria, M. Mir *et al.*, 2017 Live cell imaging of low- and non-repetitive chromosome loci using CRISPR-Cas9. Nature Communications 8**:** 14725.

Raap, A. K., J. G. Marijnen, J. Vrolijk and M. van der Ploeg, 1986 Denaturation, renaturation, and loss of DNA during *in situ* hybridization procedures. Cytometry 7**:** 235-242.

Raap, A. K., M. P. van de Corput, R. A. Vervenne, R. P. van Gijlswijk, H. J. Tanke *et al.*, 1995 Ultra-sensitive FISH using peroxidase-mediated deposition of biotin- or fluorochrome tyramides. Human Molecular Genetics 4**:** 529-534.

Ran, F. A., L. Cong, W. X. Yan, D. A. Scott, J. S. Gootenberg *et al.*, 2015 *In vivo* genome editing using *Staphylococcus aureus* Cas9. Nature 520**:** 186-191.

Ran, F. A., P. D. Hsu, J. Wright, V. Agarwala, D. A. Scott *et al.*, 2013 Genome engineering using the CRISPR-Cas9 system. Nature Protocols 8**:** 2281-2308.

Rayburn, A. L., and B. S. Gill, 1985 Use of biotin-labeled probes to map specific DNA sequences on wheat chromosomes. Journal of Heredity 76**:** 78-81.

Reddy Chichili, V. P., V. Kumar and J. Sivaraman, 2013 Linkers in the structural biology of protein–protein interactions. Protein Science : A Publication of the Protein Society 22**:** 153-167.

Rennke, H. G., and M. A. Venkatachalam, 1979 Chemical modification of horseradish peroxidase. Preparation and characterization of tracer enzymes with different isoelectric points. Journal of Histochemistry & Cytochemistry 27**:** 1352-1353.

Resch-Genger, U., M. Grabolle, S. Cavaliere-Jaricot, R. Nitschke and T. Nann, 2008 Quantum dots versus organic dyes as fluorescent labels. Nature Methods 5**:** 763-775.

Robinett, C. C., A. Straight, G. Li, C. Willhelm, G. Sudlow *et al.*, 1996 *In vivo* localization of DNA sequences and visualization of large-scale chromatin organization using lac operator/repressor recognition. J Cell Biol 135**:** 1685-1700.

Ross, K. J., P. Fransz and G. H. Jones, 1996 A light microscopic atlas of meiosis in *Arabidopsis thaliana*. Chromosome Research 4**:** 507-516.

Rudkin, G. T., and B. D. Stollar, 1977 High resolution detection of DNA–RNA hybrids in situ by indirect immunofluorescence. Nature 265**:** 472-473.

Saito, M., P. Xu, G. Faure, S. Maguire, S. Kannan *et al.*, 2023 Fanzor is a eukaryotic programmable RNA-guided endonuclease. Nature 620**:** 660-668.

Sapranauskas, R., G. Gasiunas, C. Fremaux, R. Barrangou, P. Horvath *et al.*, 2011 The *Streptococcus thermophilus* CRISPR/Cas system provides immunity in *Escherichia coli*. Nucleic Acids Research 39**:** 9275-9282.

Schellenberger, V., C.-w. Wang, N. C. Geething, B. J. Spink, A. Campbell *et al.*, 2009 A recombinant polypeptide extends the in vivo half-life of peptides and proteins in a tunable manner. Nature Biotechnology 27**:** 1186-1190.

SCHWARZACHER, T., A. R. LEITCH, M. D. BENNETT and J. S. HESLOP-HARRISON, 1989 *In situ* localization of parental genomes in a wide hybrid. Annals of Botany 64**:** 315-324.

Sewell, B. T., C. Bouloukos and C. von Holt, 1984 Formaldehyde and glutaraldehyde in the fixation of chromatin for electron microscopy. Journal of Microscopy 136**:** 103-112.

Sexton, T., and G. Cavalli, 2015 The role of chromosome domains in shaping the functional genome. Cell 160**:** 1049-1059.

Shah, S. A., S. Erdmann, F. J. M. Mojica and R. A. Garrett, 2013 Protospacer recognition motifs. RNA Biology 10**:** 891-899.

Shim, A. R., J. Frederick, E. M. Pujadas, T. Kuo, I. C. Ye *et al.*, 2024 Formamide denaturation of double-stranded DNA for fluorescence *in situ* hybridization (FISH) distorts nanoscale chromatin structure. bioRxiv**:** 2024.2003.2001.582995.

Silva, G. S., and M. M. Souza, 2013 Genomic *in situ* hybridization in plants. Genet Mol Res 12**:** 2953-2965.

Simon, L., M. Voisin, C. Tatout and A. V. Probst, 2015 Structure and function of centromeric and pericentromeric heterochromatin in *Arabidopsis thaliana*. Frontiers in Plant Science 6.

Singer, R. H., and D. C. Ward, 1982 Actin gene expression visualized in chicken muscle tissue culture by using in situ hybridization with a biotinated nucleotide analog. Proc Natl Acad Sci U S A 79**:** 7331-7335.

Smith, A. T., N. Santama, S. Dacey, M. Edwards, R. C. Bray *et al.*, 1990 Expression of a synthetic gene for horseradish peroxidase C in *Escherichia coli* and folding and activation of the recombinant enzyme with Ca2+ and heme. J Biol Chem 265**:** 13335-13343.

Solovei, I., A. Cavallo, L. Schermelleh, F. Jaunin, C. Scasselati *et al.*, 2002 Spatial preservation of nuclear chromatin architecture during three-dimensional fluorescence *in situ* hybridization (3D-FISH). Exp Cell Res 276**:** 10-23.

Sternberg, S. H., B. LaFrance, M. Kaplan and J. A. Doudna, 2015 Conformational control of DNA target cleavage by CRISPR-Cas9. Nature 527**:** 110-113.

Tanenbaum, M. E., L. A. Gilbert, L. S. Qi, J. S. Weissman and R. D. Vale, 2014 A protein-tagging system for signal amplification in gene expression and fluorescence imaging. Cell 159**:** 635-646.

Thyme, S. B., L. Akhmetova, T. G. Montague, E. Valen and A. F. Schier, 2016 Internal guide RNA interactions interfere with Cas9-mediated cleavage. Nature Communications 7**:** 11750.

Trzaskoma, P., B. Ruszczycki, B. Lee, K. K. Pels, K. Krawczyk *et al.*, 2020 Ultrastructural visualization of 3D chromatin folding using volume electron microscopy and DNA *in situ* hybridization. Nature Communications 11**:** 2120.

Urbanek, M. O., P. Galka-Marciniak, M. Olejniczak and W. J. Krzyzosiak, 2014 RNA imaging in living cells - methods and applications. RNA Biol 11**:** 1083-1095.

Van Tricht, C., T. Voet, J. Lammertyn and D. Spasic, 2023 Imaging the unimaginable: leveraging signal generation of CRISPR-Cas for sensitive genome imaging. Trends Biotechnol 41**:** 769-784.

Vergara, Z., and C. Gutierrez, 2017 Emerging roles of chromatin in the maintenance of genome organization and function in plants. Genome Biology 18**:** 96.

Veselinyová, D., J. Mašlanková, K. Kalinová, H. Mičková, M. Mareková *et al.*, 2021 Selected *in situ* hybridization methods: Principles and application. Molecules 26.

Virant, D., B. Traenkle, J. Maier, P. D. Kaiser, M. Bodenhöfer *et al.*, 2018 A peptide tag-specific nanobody enables high-quality labeling for dSTORM imaging. Nature Communications 9: 930.

Wang, H., M. La Russa and L. S. Qi, 2016 CRISPR/Cas9 in Genome Editing and Beyond. Annu Rev Biochem 85: 227-264.

Wang, H., M. Nakamura, T. R. Abbott, D. Zhao, K. Luo *et al.*, 2019 CRISPR-mediated live imaging of genome editing and transcription. Science 365: 1301-1305.

Wang, J. Y., and J. A. Doudna, 2023 CRISPR technology: A decade of genome editing is only the beginning. Science 379: eadd8643.

Wang, Y., W. T. Cottle, H. Wang, X. A. Feng, J. Mallon *et al.*, 2021 Genome oligopaint via local denaturation fluorescence *in situ* hybridization. Molecular Cell 81: 1566-1577.e1568.

Weber, E., C. Engler, R. Gruetzner, S. Werner and S. Marillonnet, 2011 A modular cloning system for standardized assembly of multigene constructs. PloS One 6: e16765.

Werner, S., C. Engler, E. Weber, R. Gruetzner and S. Marillonnet, 2012 Fast track assembly of multigene constructs using Golden Gate cloning and the MoClo system. Bioeng Bugs 3: 38-43.

Wu, X., S. Mao, Y. Yang, M. N. Rushdi, C. J. Krueger *et al.*, 2018 A CRISPR/molecular beacon hybrid system for live-cell genomic imaging. Nucleic Acids Research 46: e80-e80.

Wu, Z., Y. Zhang, H. Yu, D. Pan, Y. Wang *et al.*, 2021 Programmed genome editing by a miniature CRISPR-Cas12f nuclease. Nature Chemical Biology 17: 1132-1138.

Xu, S. L., R. Shrestha, S. S. Karunadasa and P. Q. Xie, 2023 Proximity labeling in plants. Annu Rev Plant Biol 74: 285-312.

Ye, H., Z. Rong and Y. Lin, 2017 Live cell imaging of genomic loci using dCas9-SunTag system and a bright fluorescent protein. Protein & Cell 8: 853-855.

Yi, E., A. D. Gujar, M. Guthrie, H. Kim, D. Zhao *et al.*, 2022 Live-cell imaging shows uneven segregation of extrachromosomal DNA elements and transcriptionally active extrachromosomal DNA hubs in cancer. Cancer Discovery 12: 468-483.

Zhang, Q., Z. Wen, X. Zhang, J. She, X. Wang *et al.*, 2023 RETICULON-LIKE PROTEIN B2 is a proviral factor co-opted for the biogenesis of viral replication organelles in plants. Plant Cell 35: 3127-3151.

Zhang, Y., G. Song, N. K. Lal, U. Nagalakshmi, Y. Li *et al.*, 2019 TurboID-based proximity labeling reveals that UBR7 is a regulator of N NLR immune receptor-mediated immunity. Nat Commun 10: 3252.

Zhang, Z., X. Rong, T. Xie, Z. Li, H. Song *et al.*, 2024 Fluorogenic CRISPR for genomic DNA imaging. Nature Communications 15: 934.

Zhou, J., J. Ma, C. Yang, X. Zhu, J. Li *et al.*, 2023 A non-canonical role of ATG8 in Golgi recovery from heat stress in plants. Nat Plants 9: 749-765.

Zhou, Y., P. Wang, F. Tian, G. Gao, L. Huang *et al.*, 2017 Painting a specific chromosome with CRISPR/Cas9 for live-cell imaging. Cell Research 27: 298-301.

Zhu, M., P. Du, L. Zhuang, C. Chu, H. Zhao *et al.*, 2017 A simple and efficient non-denaturing FISH method for maize chromosome differentiation using single-strand oligonucleotide probes. Genome 60: 657-664.

Zwyrtková, J., H. Šimková and J. Doležel, 2021 Chromosome genomics uncovers plant genome organization and function. Biotechnology Advances 46: 107659.

10. *Curriculum vitae*

Bhanu Prakash Potlapalli

Leibniz Institute of Plant Genetics and Crop Plant Research (IPK), Gatersleben, Germany
https://orcid.org/0000-0002-9148-8384

Education

Ph.D. Student   Research group: **"Chromosome Structure and Function"**
Leibniz Institute of Plant Genetics and Crop Plant Research (IPK), Germany
(2021.05 ~ Expected 2024.12)
Thesis title: Extending the CRISPR-Cas9-based imaging toolbox to improve the detection of chromosomal DNA
Supervisor: Prof. Dr. Andreas Houben

MS.c.   Crop Sciences
University of Hohenheim, Germany
(2017.10 ~ 2020. 09)
Thesis title: Development of RGEN-ISL, a CRISPR-Cas9 based genome labeling tool for metaphase chromosomes of plants and mammalian cells
Advisor: Prof. Dr Uwe Ludwig and Prof. Dr. Andreas Houben (IPK, Gatersleben)
Final Grade: 1.3

B.Sc.   Horticultural sciences
Dr. Y.S.R Horticultural University, India
(2011.08 ~ 2015.06)
Final Grade: 7.6 / 10

Research and work experience

- *Research visiting scientist*   2023.01 ~ 2023.03
  Prof. Dr. Nobuko Ohmido, Kobe University, Japan
  Focus on the development of CRISPR-ISH for electron microscope

- *Research associate*   2020.10 ~ 2021.05
  Chromosome Structure and Function
  Leibniz Institute of Plant Genetics and Crop Plant Research (IPK), Germany
  Focus on the development of CRISPR-based DNA labeling methods

Journal Articles

1. **Potlapalli BP**, Ishii T, Nagaki K, Somasundaram S, Houben A. "CRISPR-FISH: A CRISPR/Cas9-based *in situ* labeling method". Plant Cytogenetics and Cytogenomics. Methods in Molecular Biology, vol 2672. Humana, New York, NY. https://doi.org/10.1007/978-1-0716-3226-0_20

2. **Potlapalli BP**, Schubert V, Metje-Sprink J, Liehr T, Houben A. "Application of Tris-HCl allows the specific labeling of regularly prepared chromosomes by CRISPR-FISH". Cytogenet Genome Res 24 April 2020; 160 (3): 156–165. https://doi.org/10.1159/000506720

3. **Potlapalli BP**, J Fuchs, T Rutten, A Meister, Houben A. Application of ALFA-tag and tyramide-based fluorescence signal amplification expands the CRISPR-based DNA imaging toolkit (manuscript submitted)

4. **Potlapalli BP**, Fuchs J, Dassau F, Sushmoy DR, Houben A. CRISPR-CID - an in situ chromogenic DNA repeat detection system for research and life science education (manuscript prepared)

5. Houben A, **Potlapalli BP**, Khosravi S. Anwendung von CRISPR/dCas9-basierten Methoden in lebenden und fixierten Pflanzenzellen Genomische Sequenzen sichtbar machen. https://www.biuz.de/ (manuscript submitted)

Conference contribution

1. **Potlapalli BP**, Fuchs J, Ohmido N, Houben A. "Improved CRISPR imaging techniques for target-specific DNA sequences" 8th Asia-Pacific Chromosome Colloquium (APCC8), Turkey, (September 18 - 21, 2023) – Oral presentation

2. **Potlapalli BP**, Dassau F, Fuchs J, Ohmido N, Houben A. "Development of novel CRISPR/Cas9-based tools for visualizing genomic sequences" Plant Chromosome Biology Cytogenetics Conference, Brno (September 11 - 13, 2023) – Poster presentation

3. **Potlapalli BP**, Dassau F, Sushmoy DR, Fuchs J, Houben A. "Novel CRISPR/Cas9-based tools for the visualization of genomic DNA in fixed samples" Plant Science Student Conference (PSSC), IPK, Germany (June 3 – 4, 2023) – Poster presentation

4. **Potlapalli BP,** Dassau F, Sushmoy DR, Fuchs J, Houben A. "Development of a novel CRISPR/Cas9-based genome labelling tools for fixed nuclei and chromosomes" Molecular Cytogenetic Techniques and plant breeding workshop (Virtual), Turkey, (June 27 – 28, 2022) - Oral presentation

Other oral presentations
1. Presentation at Kobe University, Japan (2023)
2. Presentation at Tottori University, Japan (2023)
3. Presentations include PhD and department seminars at IPK
4. Presentations in Chromosome Biology retreat (2022)

Supervision experience
- Supervising undergraduate, graduate, and international visiting students, IPK Gatersleben, Germany (2020 - 2024)

1. Deboprio Roy Sushmoy, master student, Kiel University
2. Anton Ulbricht, batchelor student, Hochschule Mittweida
3. Fatemeh Orooji, PhD student, University of Kurdistan, Iran
4. Aurélien Devillars, PhD student, University of Padova, Italy

Gatersleben, 10.05.24   Bhanu Prakash Potlapalli

11. Eidesstattliche Erklärung / Declaration under Oath

Ich erkläre an Eides statt, dass ich die Arbeit selbstständig und ohne fremde Hilfe verfasst, keine anderen als die von mir angegebenen Quellen und Hilfsmittel benutzt und die den benutzten Werken wörtlich oder inhaltlich entnommenen Stellen als solche kenntlich gemacht habe.

I declare under penalty of perjury that this thesis is my own work entirely and has been written without any help from other people. I used only the sources mentioned and included all the citations correctly both in word or content.

_____   _____

Datum / Date   Unterschrift des Antragstellers / *Signature of the applicant*

12. Appendix

Appendix Table 1: List of primer sequences used in this thesis

Name of primer	Sequence (5`-3`)	Purpose
dCas9-NcoI-F	CATGCCATGGATAAGAAGTACTCTATCGGACTC	F and R primers are required to amplify the Sp.dCas9 sequence from dCas9:3xPP7: GFP for cloning onto the pET22b+ vector
dCas9-HindIII-F	CCCAAGCTTAACCTTCCTCTTCTTCTTAGGATCAG	
HRP-HindIII-F	AAGCTTTCGAGCGGTGGAGCTGCAGCC	F and R primers are required to amplify the HRP sequence from pOCC30-dCas9-linker-HRP for cloning onto the C-terminus of the pET22b-dCas9 vector
HRP-NotI-R	GCGGCCGCAGAGTTGCTGTTGACCACTCTACAGTTC	
1x ALFA-N ter-F	CCAGCCGGCGATGGCAATGCCATCACGTTTGGAAGAGGAACTGAGACGCCGCTTAACTGAACCT	F and R primers are required to amplify a single copy of the ALFA tag from the ALFA synthetic fragment for cloning onto the N-terminus of the pET22b+-dCas9 vector
1x ALFA-N ter-R	GTCCGATAGAGTACTTCTTATCAGGTTCAGTTAAGCGGCGTCTCAGTTCCTCTTCCAAACGTGATGG	
1x ALFA-C ter-F	AAGCTTGGCTCTCCATCACGTTTGGAAGAGGAACTGAGACGCCGCTTAACTGAACCT	F and R primers are required to amplify a single copy of the ALFA tag from the ALFA synthetic fragment for cloning onto the C-terminus of the pET22b+-dCas9 vector
1x ALFA-C ter-R	GGGCCGCAGGTTCAGTTAAGCGGCGTCTCAGTTCCTCTTCCAAACGTGATGG	
3x ALFA-N ter-F	CATGCCATGGCCCCCTCACGATTAGAAGAGGAACT	F and R primers are required to amplify a three copies of the ALFA tags from the 3x ALFA synthetic fragment for cloning onto the N-terminus of the pET22b+-dCas9 vector
3x ALFA-N ter-R	CATGCCATGGGCGGCTCGGTCAAACGACG	
3x ALFA-C ter-F	AAGCTTCCCTCACGATTAGAAGAGGAACT	F and R primers are required to amplify a three copies of the ALFA tags from the 3x ALFA synthetic fragment for cloning onto the C-terminus of the pET22b+-dCas9-3xALFA tag (N-ter) vector (3+3x)
3x ALFA-C ter-R	GCGGCCGCCGGCTCGGTCAAACGACG	
6x ALFA-N ter-F	CATGCCATGGCCCCCTCACGATTAGAAGAGGAACT	F and R primers are required to amplify a six copies of the ALFA tags from the 6xALFA synthetic fragment for cloning onto the N-terminus of the pET22b+-dCas9 vector
6x ALFA-N ter-R	CATGCCATGGGAGGTTCGGTCAGACGCCT	
12x ALFA-N ter-F	CATGCCATGGCCCCCTCACGATTAGAAGAGGAACT	F and R primers are required to amplify a twelve copies of the ALFA tags from the 12xALFA synthetic fragment for cloning onto the N-terminus of the pET22b+-dCas9 vector
12x ALFA-N ter-R	CATGCCATGGCCGGCGGCTCGGTTAAACGCCTAC	
12x ALFA-C ter-F	CCCAAGCTTCCCTCACGATTAGAAGAGGAACT	F and R primers are required to amplify a twelve copies of the ALFA tags from the 12xALFA synthetic fragment for cloning onto the N-terminus of the pET22b+-dCas9-12xALFA tag (N-ter) vector (12+12x)
12x ALFA-C ter-R	AAATAGCGGCCGCGGACGGCTCGGTTAAACGCCTAC	
6x GS ALFA-N ter-F	CATGCCATGGccGGTGGCGGAGGGTCTCC	F and R primers are required to amplify a six copies of the ALFA tags from the 6xALFA (GGGGS linker) synthetic fragment for cloning onto the N-terminus of the pET22b+-dCas9 vector
6x GS ALFA-N ter-R	CATGCCATGGGAGGTTCGGTCAGACGCCT	
6x GS ALFA-C ter-F	CCCAAGCTTGGTGGCGGAGGGTCTCC	F and R primers are required to amplify a six copies of the ALFA tags from the 6xALFA (GGGGS linker) synthetic fragment for cloning onto the N-terminus of the pET22b+-dCas9-6xALFA GS (N-ter) vector
6x GS ALFA-C ter-R	AAATAGCGGCCGCGGAAGGTTCGGTCAGACGCCT	
NbALFA-F	TTGAAGACAAAGGTGAAGTGCAGCTTCAGGAGAGTG	F and R primers are required to amplify NbALFA from pET51b(+)_eGFP NbALFA, (Addgene 136626) for cloning onto pAGM1299
NbALFA-R	TTGAAGACAACGAATTATGACGACACAGTGACCTG	
mRuby-F	TTGAAGACAAAGGTGGCTCTGGATCGGGGTCGGGCTCAATGGTGTCTAAGGGCGAAGAGCTG	F and R primers are required to amplify mRuby from Sp-dCas9-mRuby (DREISSIG et al. 2017), for cloning onto pICH41258
mRuby-R	TTGAAGACTTCGAAAAGCTTACTTGTACAGCTCGTCCATCCCACC	
RPS5A Pro-F	TTGAAGACAAGGAGCTCAACTTTTGATTCGC	F and R primers are required to amplify RPS5A promoter for cloning onto pICH41295
RPS5A Pro-R	TTGAAGACAACATTGCTGTGGTGAGAGAAACAGAGC	
rbcSE9 ter-F	TTGAAGACATCTCATTCGTAGTAATTATGGCATTGGGAAAACTG	F and R primers are required to amplify rbcSE9 terminator for cloning onto pICH9121
rbcSE9 ter-R	TTGAAGACAACTCGAGCGTGTTTTACTCCTCATATTAACTTCGGTC	
Pea3A ter-F	TTGAAGACAAGCTTCAGGCCTCCCAGCTTTCGT	F and R primers are required to amplify Pea3A promoter from Sp-dCas9-eGFP (DREISSIG et al. 2017), for cloning onto pICH41276
Pea3A ter-R	TTGAAGACAAAGCGAAGCCTATACTGTACTTAACTTGATTGCATAATTACTTGA	
3x eGFP-F	TTGAAGACAAAGGTGGCTCTGGATCGGGGTCG	F and R primers are required to amplify 3x eGFP from Sp-dCas9-eGFP (DREISSIG et al. 2017), for cloning onto pAGM1299
3x eGFP-R	TTGAAGACTTCGAATTCAGGCGTAGCGCTCTCG	

Name of primer	Sequence (5`-3`)	Purpose
Sp.dCas9-F	TTGAAGACAAAATGGATAAGAAGTACTCTATCGGACTCGC	F and R primers are required to amplify Sp.dCas9 from Sp-dCas9-eGFP (DREISSIG et al. 2017), for cloning onto pICH41258
Sp.dCas9-R	TTGAAGACATACCTTTTGAGCCCGACCCCGAT	
Ubi4 pro-F	TTGAAGACAAGGAGAAAAATTACGGGATATGAATATAGGCATATCCG	F and R primers are required to amplify Ubi4 promoter from Sp-dCas9-eGFP (DREISSIG et al. 2017), for cloning onto pICH41295
Ubi4 pro-R	TTGAAGACAACATTGCTGCACATACATAACATATCAAGATCAG	
6x ALFA (GS)-F	TTGAAGACAATTCGGTAGCATCGATGGTAGCCCATC	F and R primers are required to amplify 6x ALFA GS (linker) from pET22b+-dCas9-6xALFA GS, for cloning onto pAGM1301
6x ALFA (GS)-R	TTGAAGACAAAAGCTTATTCGGTCAGACGCCTACGG	
Telomere sgRNA-F	TGTGGTCTCAATTGGGGTTTAGGGTTTAGGGTTTGTTTTAGAGCT AGAAATAGCAAG	F and R primers are required to amplify Arabidopsis Telomere sgRNA from dCas9:3xPP7:GFP, for cloning onto pICH47742 along with pICH41295-U6 (At-26) promoter to make level 1 vector
sgRNA scaffold-R	TGTGGTCTCAAGCGTAATGCCAACTTTGTAC	
At-U6(26)-Pro-F	TGTGAAGACAAGGAGCTTTTTTTCTTCTTCTTCGTTCATACAGTTTT TTTTTGTTTAT	F and R primers are required to amplify U6 (At-26) promoter from dCas9:3xPP7:GFP, for cloning onto pICH41295
U6(At-26)-Pro-R	TTGAAGACAACATTCACTACTTCGACTCTAGCTGTATATAAACTCA G	
z.dCas9i-F1	TTGAAGACAAAATGGCTTCTAGCCCACCGAAGAAGAAGCGGAAGG TCAGCTGGAAAATGGACAAGAAGTACAGCATTGGACTTGCGATTG GTACGAACTCAGTTGGGTGGGC	F and R primers are required to amplify the fragment-1 from z.dCas9i sequence from pAGM47523, The resulting fragment contain point mutation in the RuvC1 for cloning onto pICH41258
z.dCas9i-R2	TTGAAGACCCTCGCATCCACATCATAGTCGGAGAGTCTGTTAAT	
z.dCas9i-F2	TTGAAGACAGGCGATTGTCCCTCAATCTTTCCTGAAGGAC	F and R primers are required to amplify the fragment-2 from z.dCas9i sequence from pAGM47523, The resulting fragment contain point mutation in the HNH for cloning onto pICH41258
z.dCas9i-R2	TTGAAGACTTACCTGAGCCCGACCCCGATCCAGAGCCTGCGACTT TACGCTTCTTCTTTGGG	
Sp.dCas9-2xNLS-F	TTGAAGACAAAATGCCTAAGAAGAAGAGGAAGGTTTCAAGGGCTG ATGATAAGAAGTACTCTATCGGACTCGCTATCG	F and R primers are required to amplify Sp.dCas9 sequence containing 2x NLS from Sp-dCas9-eGFP, for cloning onto pICH41295
Sp.dCas9-2xNLS-R	TTGAAGACATACCTTTTGAGCCCGACCCCGAT	
6x ALFA-2x NLS-F	TTGAAGACAATTCGAACCTAAGAAGAAGAGGAAGGTTTCAAGGGC TGATGGTAGCATCGATGGTAGCCCA	F and R primers are required to amplify 6x ALFA GS (linker) sequence containing 2x NLS from pET22b+-dCas9-6xALFA GS, for cloning onto pAGM1301
6x ALFA-2x NLS-R	TTGAAGACAAAAGCTTAAACCTTCCTCTTCTTCTTAGGATCAGCCC TTGATTCGGTCAGACGCCTACGG	

Appendix Fig 1: Comparison of His-tag affinity-purified (A) dCas9-HRP and (B) dCas9 proteins respectively on a Coomassie-stained SDS-PAGE gel. Elution fractions from both gels show clear differences in protein amounts purified, indicating that most of the dCas9-HRP could be lost as inclusion bodies, whereas high amounts of dCas9 protein were observed in the elution fractions as shown in right gel (B). The size of both proteins was marked with a black arrow. PR, BB, NB, and W represent PAGE ruler, before binding of lysate with agarose resin, non-binding, and wash fractions, respectively. Elution 1-7 represents 1 mL fractions of eluted protein.

Appendix Fig 2: Labeling of *Fok*I repeats in 3:1 fixed *V. faba* nuclei with dCas9-ALFA tag using biotinylated tracrRNA and detection with streptavidin conjugated FITC and Cy3, and as a control *Fok*I repeats were labeled with standard CRISPR-FISH using dCas9-ALFA tag and tracrRNA Atto550. FokI-specific signals were not observed in indirect approach with streptavidin-FITC and Cy3, but labeled with standard CRISPR-FISH.